Alma Mater Studiorum · Università di Bologna

School of Universe Sciences
Department of Physics and Astronomy
Master's degree in Astrophysics and Cosmology

Probing modified Gravitational Wave propagation using Standard Sirens with future observational data

Candidate:
Manfred Fiebig

Supervisor:
Prof. Michele Ennio Maria Moresco

Co-supervisors:
Dr. Matteo Tagliazucchi
Dr. Nicola Borghi

Academic Year 2023/2024

Abstract

Gravitational waves (GWs) are writing a new chapter in cosmology as novel and independent probes to measure the expansion history and test the foundations of gravitational physics. In particular, GWs directly provide the luminosity distance to their source, bypassing the uncertainties of traditional distance ladders. However, this distance may differ from the electromagnetic one, due to modified GW propagation predicted by various modified gravity (MG) theories.

This thesis explores the potential of future GW observations to constrain modified GW propagation and potential biases on H_0. We use CHIMERA, a pipeline for joint inference of cosmological and astrophysical population parameters that we extended to include MG effects with the (Ξ_0, n), parametrization. We generate GW catalogs assuming MG cosmologies and simulate their observation with the configuration of the future LIGO Virgo KAGRA observing run (O5). After exploring potential systematics in one-dimensional posteriors, we run full Markov chain Monte Carlo (MCMC) analyses including a galaxy catalog with spectroscopic redshift measurements, and derive constraints on both cosmological and MG parameters.

We find a significant correlation between H_0 and Ξ_0 due to their relationship with luminosity distance at fixed z. By fixing H_0 to the fiducial value, we recover Ξ_0 with an uncertainty of 3%. On the other hand, if Ξ_0 is fixed, H_0 is constrained at 1% in a GR universe ($\Xi_0 = 1$), 1.2%, and 2% in different MG universe with $\Xi_0 = 1.8$ and 0.6, respectively. In a full MCMC analysis, when both H_0 and Ξ_0 vary, their inherent degeneracy leads to weaker constraints, finding 2.3%, 6% and 7% for H_0 while 10% 17% and 20% for Ξ_0, respectively for the different cosmologies. This work provides a first assessment of the constraints that can be achieved on those parameters with future GW data, paving the way to properly model them to derive unbiased and precise determinations of cosmological parameters.

Contents

Chapter 1

Introduction

The Lambda Cold Dark Matter (ΛCDM) model currently stands as the landmark of our understanding of the Universe. It postulates that ordinary baryonic matter comprises only a small fraction of the total content of the Universe, while the energy budget is dominated by cold dark matter (CDM) and dark energy (DE) (Peebles and Ratra 2003, Dodelson and Schmidt 2020). Despite the success of the ΛCDM model in explaining various cosmic phenomena such as large-scale structure formation and the dynamics of galaxies, it relies on two components, DM and DE, which remain enigmatic. Dark matter, which interacts only through gravity, is essential to explain the mass content of the Universe. Dark energy, often associated with the cosmological constant (Λ), is thought to be responsible for the accelerated expansion of the Universe. However, neither dark matter nor dark energy has been directly detected, and their nature remains one of the greatest mysteries (Abdalla et al. 2022). Since the first groundbreaking discovery of the accelerated expansion of the universe observed through Type Ia supernovae (Riess, Filippenko, et al. 1998, Perlmutter et al. 1999), many observations have provided more precise constraints to the ΛCDM model using multiple probes.

However, emerging observational data are pointing out potential limitations. Among them, the Hubble constant (H_0) tension is one of the most debated. This parameter, which defines the present rate of cosmic expansion, has been measured with high precision using two distinct probes: one based on the cosmic microwave background (CMB) under the assumption of the ΛCDM model, and another based on measurements of nearby Type Ia supernovae (Riess, Casertano, et al. 2019). Intriguingly, the values obtained by these methods show discrepancies well beyond their error margins, suggesting possible new physics beyond ΛCDM.

In 2015, the groundbreaking detection of gravitational waves (GWs) has opened up a new avenue to address these questions (B. Abbott et al. 2016). Since then, the interferometers of the LIGO-Virgo-KAGRA (LVK) collaborations have observed more than 90 events (R. Abbott et al. 2023) produced by mergers of Binary Black Holes (BBH), Binary Neutron Stars (BNS), or Neutron Star-Black Holes (NSBH), with BBH comprising the majority ($\sim 90\%$) of the detections. To assess the performance of these detectors and track the number of detected and expected GWs, both from past and future advancements of the LVK configuration, the observations have been structured into successive observing runs. The completed O1-O3 runs established the foundation for GW astronomy and cosmology (B. P. Abbott 2023, Cahillane and Mansell 2022). The improved sensitivity of ongoing O4 run, extending through 2024 and partially in 2025, will reveal more well-localized events, such as BBHs and NSBHs systems. Looking ahead to the upcoming O5 run (Kiendrebeogo et al. 2023, B. P. Abbott et al. 2020) featuring enhanced detector sensitivity allowing the detection of a broader range of sources.

From the cosmological perspective, gravitational waves produced by compact binary mergers can be used as "standard sirens". Their signal, calibrated by General Relativity (GR), provides a direct measurement of the luminosity distance to the source without relying on intermediate calibrators. By complementing this measurement with the source redshift z, it is possible to constrain cosmological parameters through the distance-redshift relation. Unfortunately, the measurement of z is hindered by an intrinsic degeneracy with binary masses, i.e. more massive systems at larger z produce the same signal as lower mass systems at lower z. For this reason, various approaches have been proposed to obtain external information on z and enable cosmological analyses.

When the electromagnetic (EM) counterpart of a GW event is detected and its host galaxy identified, the redshift can be directly measured (Holz and Hughes 2005; Schutz 1986). These events are known as "bright sirens". The binary neutron star (BNS) merger event GW170817 B. P. Abbott 2017a is the first and only known example so far, leading to a measurement of $H_0 = 70.0^{+12.0}_{-8.0}\ \mathrm{km\,s^{-1}\,Mpc^{-1}}$. However, EM counterparts are rare, as they typically require mergers involving at least one neutron star.

When the counterpart is either too faint to be detected or absent, the information on z can still be statistically inferred from the distribution of potential hosts within the GW localization volume (Del Pozzo 2012; M. Fishbach et al. 2019; Schutz 1986). Combining the redshift of each potential host with the d_L measured with GWs, provides separate constraints to the cosmological parameters. In this way, by stacking together the information from multiple events, the true cosmology will statistically prevail. This is known as the "dark sirens" method and becomes more effective as the GW localization volumes become smaller, up to the limit when only a single galaxy is present, resembling the situation of bright sirens. The latest analysis by the LVK collaboration using the 47 dark sirens events with SNR > 11 from the GWTC-3 catalog yields $H_0 = 67^{+13}_{-12}$ km/s/Mpc (excluding GW170817, B. P. Abbott 2023).

Alternatively, the degeneracy between mass and redshift can be broken by modeling intrinsic astrophysical properties as the source-frame mass distribution (Chernoff and Finn 1993; S. R. Taylor and Jonathan R. Gair 2012). This is known as the "spectral sirens" method and is more effective when the source-frame mass distribution contains features such as breaks, peaks, or changes in slope that act as standard properties.

In addition to cosmological constraints, GWs and standard sirens have emerged as powerful tools for testing GR (Yunes, Yagi, and Pretorius 2016, B. Abbott et al. 2016, B. P. Abbott 2017a, Goldstein et al. 2017, Savchenko et al. 2017).

Investigations of GR can be studied by comparing the GW waveform predicted by GR with the observed one.

Recently, new modified gravity (MG) theories have been developed (Belgacem et al. 2018a, Dvali, Gabadadze, and Porrati 2000) and some of them predict a friction term that modifies the GW propagation (Deffayet and Menou 2007, Brandenburg et al. 2021). For example, the observation of GW170817 constrained the propagation velocity of GWs to an impressive limit of $\frac{|c_{\rm gw}-c|}{c} < \mathcal{O}(10^{-15})$ (B. P. Abbott 2016, B. P. Abbott 2017a,Goldstein et al. 2017, Savchenko et al. 2017). Beyond velocity constraints, several MG theories parameterize the source distance, that differ from the EM one due to the modified GW propagation, using two parameters, Ξ_0 and n (Mancarella, Genoud-Prachex, and Michele Maggiore 2022). Standard sirens method can be thus used to infer MG paramaters along with cosmological ones.

In this context, innovative methods have been developed to combine galaxy catalog and the spectral sirens methods, allowing for joint parameter inference integrating all these approaches. Tools like `CHIMERA` (Borghi et al. 2024), `icarogw` (Simone Mastrogiovanni et al. 2023), and `gwcosmo` (Gray et al. 2023) have implemented these techniques, offering a powerful framework for exploring the constraining power of future observing runs.

These methods and pipelines have played a key role in obtaining first results, particularly in constraining modified GW propagation. By correlating galaxy catalog methods with the GWTC-3 catalog, results show that these parameterizations are currently consistent with GR (Mancarella, Finke, et al. 2022). However, as detectors improve, it's crucial to forecast their ability to refine these constraints. To achieve this, mock GW catalogs are simulated. While Leyde et al. 2022 applied the spectral siren method to forecast constraints on MG parameters, this thesis uses galaxy catalog information to predict for the first time constraints on MG propagation using the combined galaxy catalog and spectral siren method.

For this study, we modify the `CHIMERA` Pipeline, which implements the Bayesian hierarchical likelihood to jointly infer cosmological and astrophysical parameters using standard sirens, to include modified GW propagation. In particular, a new module MG_FLRW, was developed and integrated into the `CHIMERA` pipeline. This module incorporates modified GW propagation effects into the computation of luminosity distance of GWs (d_L^{GW}), enabling analyses of MG scenarios. Additionally, changes in the luminosity distance required adjustments in likelihood calculations, this was applied to the integration grid, which is constructed adaptively in `CHIMERA` and required modifications to accommodate a new parametrization of luminosity distance. To evaluate the potential of O5, one of the main features of this work is simulating mock GW catalogs. Currently, there are no comprehensive catalogs that incorporate information on GW events under modified GW propagation scenarios, so two new catalogs of this kind will be generated and investigated using existing tools (`GWFAST` Iacovelli et al. 2022a). Two new mock GW event catalogs are simulated considering different MG regimes, compatible with current constraints (Leyde et al. 2022). The `CHIMERA` code is then used to forecast the constraining capabilities of the dark siren method and an LVK network in the O5 configuration on cosmological and MG parameters considering both GR and modifications to the GW propagation. Through a one-dimensional posterior analysis, we demonstrate that the correct value of Ξ_0 can be recovered by fixing H_0 and other relevant parameters to the fiducial values of the cosmological model. We also find that when an incorrect cosmology is assumed, a bias in Ξ_0 is observed. Extending this analysis through a full Markov chain Monte Carlo (MCMC) approach, it becomes possible to sample the posterior and constrain both Ξ_0 and H_0 jointly, allowing for a comprehensive inference of cosmological parameters (including modified GW propagation) and astrophysical parameters.

This analysis is crucial in assessing whether future observational runs will be capable of measuring Ξ_0, ultimately aiming to provide precise constraints on H_0 in both GR and modified GW propagation scenarios.

The Thesis is structured as follows

- Chapter 2 introduces the theoretical background, focusing on the standard cosmological model, the standard siren method, and modified GW propagation. The chapter concludes with an overview of the statistical framework necessary to understand the workflow of the standard sirens analysis implemented in `CHIMERA` that is extended in this Thesis.

- Chapter 3 describes the methodology, outlining how modified GW propagation parameters are included in the pipeline. Then a comprehensive description of the generation of mock GW catalogs with modified GW propagation effects is provided. Furthermore, the GW catalogs simulated for this Thesis are analyzed and discussed.
- Chapter 4 presents the results, separated into two statistical analysis methodologies: the one-dimensional posteriors method and the MCMC method. The findings will then be explored, highlighting the constraints derived for three distinct catalog analyses: one in a GR scenario and two with modified GW propagation. Particular emphasis is placed on the biases that may impact the measurement of H_0 and the precision on Ξ_0 that can be reached in about one year of the LVK O5 observational run.

Chapter 2

Cosmological background

This chapter presents an overview of the cosmological model and its main equations and parameters (Section 2.1). Then, it presents the fundamentals of gravitational wave (GW) theory (Section 2.2), the methodologies that allow constraining cosmology using GWs as "standard sirens" (Section 2.3), and an overview of modified GW propagation theories as well as a possible parametrization (Section 2.4). In the end, Section 2.5 introduces the statistical framework and pipeline used in this work to provide future constraints on modified GW propagation.

2.1 The main cosmological model

The ΛCDM (Lambda Cold Dark Matter) model is the prevailing cosmological framework describing the evolution of the universe (Dodelson and Schmidt 2020). It introduces a universe dominated by dark energy (Λ) and cold dark matter (CDM), along with ordinary baryonic matter. At its core, the model relies on the principles of GR to describe the gravitational interaction that shapes the evolution of the universe. Its geometry is described by the Friedmann-Lemaitre-Robertson-Walker (FLRW) metric, given in polar coordinates by:

$$ds^2 = -c^2 dt^2 + a(t)^2 \left(\frac{dr^2}{1 - kr^2} + r^2 (d\theta^2 + \sin^2\theta d\phi^2) \right), \tag{2.1}$$

where $a(t)$ denotes the scale factor, k represents the curvature parameter (indicating the spatial geometry as flat ($k = 0$), positively curved ($k > 0$), or negatively curved ($k < 0$)). This is obtained only under assumptions that the universe is homogeneous and isotropic

(Weinberg 1976). The FLRW metric tensor components are given by:

$$g_{\mu\nu} = \begin{pmatrix} -1 & 0 & 0 & 0 \\ 0 & a(t)^2\frac{1}{1-kr^2} & 0 & 0 \\ 0 & 0 & a(t)^2r^2 & 0 \\ 0 & 0 & 0 & a(t)^2r^2\sin^2\theta \end{pmatrix}. \tag{2.2}$$

2.1.1 Distances in cosmology

In cosmology, because of the scale factor, it is not possible to measure the distance in a canonical way (Coles and Lucchin 2003), so new descriptions are used to quantify the spatial separation between objects. The key distance measures include:
Proper Distance (d_{pr}): It represents the distance between two points in the universe at a given time, accounting for the time expansion of the universe. It is defined as:

$$d_{pr} = a(t)\int \frac{dr}{\sqrt{1-kr^2}}, \tag{2.3}$$

where $\int \frac{dr}{\sqrt{1-kr^2}}$ is called curvature function $f_k(r)$ which for a flat universe becomes $f_0(k) = r$.
So the d_{pr} becomes :

$$d_{pr}(t) = a(t)r \tag{2.4}$$

Differentiating this equation, by imposing that there is no proper motion of the observed point, it is possible to obtain the Hubble-Lemaitre law:

$$v(t) = \frac{\dot{a(t)}}{a(t)}d_{pr}(t) \tag{2.5}$$

defining the famous Hubble parameter $H(t)$ and its present-day value at $t = t_0$ (time of the expansion history of the universe today), called Hubble constant H_0:

$$H(t) = \frac{\dot{a(t)}}{a(t)} \qquad H_0 = \frac{\dot{a(t_0)}}{a(t_0)} \tag{2.6}$$

Given this information, it is possible to define a new quantity called redshift z, that quantifies the expansion of the universe, as the fractional change in the wavelength of light observed from distant objects compared to the wavelength emitted:

$$1 + z = \frac{\lambda_{\text{obs}}}{\lambda_{\text{em}}}. \tag{2.7}$$

It serves as a crucial observational tool in cosmology, allowing us to probe the universe's history. It is related to the expansion factor $a(t)$ as follows:

$$a(t) = \frac{1}{1+z} \tag{2.8}$$

Comoving Distance (d_c): The comoving distance represents the spatial separation between two points that are not moving relative to the expansion of the Universe. It is defined as:

$$d_c = c\int_t^{t_0} \frac{dt'}{a(t')} \tag{2.9}$$

or by exploiting the relation between $a(t)$ and z:

$$d_c = c\int_0^{z} \frac{dz'}{H(t')} \tag{2.10}$$

And for a massless particle with $ds^2 = 0$ the comoving distance simplifies as $d_c = d_{pr}/a(t)$ These quantities cannot be measured directly in cosmology because they depend on time through the expansion factor. To solve this problem several astronomical quantities can be introduced:

Angular Distance (d_A): The distance obtained by measuring the angular size of the object $\Delta\theta$ and relating to the actual size L:

$$d_A = \frac{L}{\Delta\theta} : \tag{2.11}$$

In the comoving frame the size becomes $\frac{L}{a}$ and $\Delta\theta = L\frac{1}{d_c}$, so that by exploiting equation 2.9 the angular distance becomes

$$d_A = \frac{1}{1+z} d_c : \tag{2.12}$$

Luminosity Distance (d_L): It is a measure of distance to an astronomical object based on the observed flux it emits. It is defined by considering the intrinsic luminosity L of a bright source and the flux F observed from it, and relates them through the following formula:

$$F = \frac{L}{4\pi d_L^2}. \tag{2.13}$$

In an expanding universe, a photon emitted at some time in the past will undergo a redshift due to the expansion of the universe, which causes it to lose energy proportional to the scale factor a. Consequently, the observed flux decreases by an additional factor of a because of the time dilation, for which the arrival rate of photons at the observer's location is decreased by the aforementioned factor, since time appears to pass more slowly for events at high redshift from our perspective. This effect leads to a modification of the flux, decreasing it by a factor a^2 or $(1+z)^2$, while for these reasons, the luminosity distance can be expressed in terms of the comoving distance d_c as follows:

$$d_L = (1+z)d_c. \tag{2.14}$$

where z is the redshift, and $(1+z)$ accounts for both the photon energy loss and the arrival rate reduction. The cosmological luminosity distance-redshift relation in complete form is expressed as:

$$d_L = c(1+z)\frac{1}{H_0}\int_0^z \frac{dz'}{E(z')}, \tag{2.15}$$

where c is the speed of light, H_0 is the Hubble constant, and $E(z)$ describes the redshift-dependent expansion rate of the universe.

2.1.2 Components of the Universe

The Universe consists of several components, each with distinct properties characterized by the **Equation of State (EoS) parameter**: $w = \frac{P}{\rho}$, which defines the relation between pressure and energy density for each component. From the adiabatic condition,

$$d(a^3\rho c^2) = -P da^3, \tag{2.16}$$

we obtain the density evolution as:

$$\rho_i(z) = \rho_{i,0}(1+z)^{3(1+w_i)}. \tag{2.17}$$

where w_i is the EoS parameter for each component, which are:

- **Baryonic Matter**: Non-relativistic matter with $w_{\mathrm{b}} = 0$, evolving as

$$\rho_{\mathrm{b}}(z) = \rho_{\mathrm{b},0}(1+z)^3. \tag{2.18}$$

- **Cold Dark Matter (CDM)**: Non-interacting, pressureless matter ($w_{\mathrm{cdm}} = 0$), evolving as

$$\rho_{\mathrm{CDM}}(z) = \rho_{\mathrm{CDM},0}(1+z)^3. \tag{2.19}$$

- **Dark Energy**: Drives accelerated expansion, with $w_\Lambda = -1$. Its density remains constant:

$$\rho_\Lambda(z) = \rho_{\Lambda,0}. \tag{2.20}$$

  Although for dynamical models, $w_{\mathrm{DE}}(z)$ may vary, e.g., by the CPL parameterization:

$$w(z) = w_0 + w_a \frac{z}{1+z}. \tag{2.21}$$

- **Radiation**: Relativistic particles with $w_{\mathrm{rad}} = \frac{1}{3}$, evolving as

$$\rho_{\mathrm{rad}}(z) = \rho_{\mathrm{rad}0}(1+z)^4. \tag{2.22}$$

It is possible to define the **adimensional density parameter** (Ω), which expresses each component's contribution to the **critical density** ρ_{crit}, needed for a flat universe:

$$\rho_{\mathrm{crit}} = \frac{3H_0^2}{8\pi G}. \tag{2.23}$$

where G is the gravitational constant. The adimensional density parameter is defined as $\Omega_i = \frac{\rho_i}{\rho_{\mathrm{crit}}}$, and the sum over all components gives $\Omega_{\mathrm{tot}} = 1$, implying flatness.

2.1.3 Einstein field equations

It is understood that the Universe is expanding, so an evolutionary description of its dynamics and knowledge of its components are needed.

This is all well described by the Einstein field equations, that considering a cosmological constant $\Lambda_{\mu\nu}$ are:

$$G_{\mu\nu} + \Lambda g_{\mu\nu} = \frac{8\pi G}{c^4} T_{\mu\nu}, \tag{2.24}$$

where $G_{\mu\nu}$ is the Einstein tensor describing the curvature of spacetime, G is Newton's gravitational constant, c is the speed of light in vacuum, and $T_{\mu\nu}$ is the stress-energy tensor, representing the distribution and flow of energy and momentum. The Einstein tensor can be expressed in terms of the Ricci tensor ($R_{\mu\nu}$) and the Ricci scalar (R) as:

$$G_{\mu\nu} = R_{\mu\nu} - \frac{1}{2} g_{\mu\nu} R \tag{2.25}$$

where $g_{\mu\nu}$ is the metric tensor. In the perfect fluid approximation the time-time components of the stress-energy tensor $T^{\mu\nu}$ is the energy density of the source, ρc^2, while the spatial-spatial components represent the source pressure P. By exploiting the equation 2.25 it is possible to derive the Friedmann equations in the most general case with components just mentioned before:

$$\left(\frac{\dot{a}(t)}{a(t)}\right)^2 = \frac{8\pi G}{3}\rho - \frac{k}{a^2} + \frac{\Lambda}{3}c^2 \tag{2.26}$$

$$\frac{\ddot{a}(t)}{a(t)} = -\frac{4\pi G}{3}(\rho + 3P) + \frac{\Lambda}{3}c^2 \tag{2.27}$$

In this thesis, we will consider a flat universe assuming $k = 0$ and $\Lambda = 0$, to describe the theoretical aspects of GWs.

Then, by combining these equations with the adimensional density parameter, it is possible to write the Hubble parameter in this very interesting way:

$$H(z) = H_0 \left[\Omega_r(1+z)^4 + \Omega_m(1+z)^3 + \Omega_\Lambda\right]^{1/2} \tag{2.28}$$

2.2 Gravitational wave theory

Gravitational waves (GW) are distortions in the space-time continuum. These waves are a fundamental prediction of Einstein's theory of GR, representing a solution to the linearized Einstein field equations.
The field equations of GR dictate how matter and energy bend spacetime, which in turn leads to the formation of GWs.

In the linearized approximation of GR, the field equations are simplified by expanding around the flat Minkowski spacetime. This involves perturbing the flat metric by a weak field $h_{\mu\nu}$, assuming $h_{\mu\nu}$ much less than 1. By writing out the full expressions for the linearized Ricci tensor and scalar and choosing the correct Lorentz gauge, the wave equation is derived (M. Maggiore 2008):

$$\Box h_{\mu\nu} = -16\pi G T_{\mu\nu}, \quad \partial_\nu h^{\mu\nu} = 0, \tag{2.29}$$

where $\Box = \partial_\mu \partial^\mu$ is the d'Alembertian operator.

To solve these equations, the compact source approximation is typically used, which assumes the gravitational wave source is located near the observer. The point where the field is measured is at a distance $r = \|x\|$, which is much larger than the size of the source. For an isolated system, the GW solution is:

$$h_{ij}(ct, x) = -\frac{2G}{c^6}\frac{1}{r}\left[\frac{d^2 I_{ij}(ct')}{dt'^2}\right]_{ct'=ct-r}, \tag{2.30}$$

where i, j denote spatial components, and $I_{ij}(ct)$ is the quadrupole moment tensor of the source. It is important to highlight that the only way to generate GWs the quadrupole term needs to change with time. So any a-symmetrical system that has this term different from zero can generate GWs, the most simple ones are the compact coalescing binary systems (CBCs). Note that h_{ij} is small due to the $\frac{1}{c^6}$ factor. In vacuum ($\Box h_{\mu\nu} = 0$), the solution reads as:

$$h_{\mu\nu}(ct, x) = \int A_{\mu\nu}(k) e^{ik_\rho x^\rho} \frac{d^3k}{(2\pi)^3}, \tag{2.31}$$

representing a superposition of plane-wave solutions with $A_{\mu\nu}$ as a 4×4 matrix defining the wave amplitude. The physical solutions for propagating gravitational waves require taking the real part of $h_{\mu\nu}$. The wavevector $k = (\omega_c, \mathbf{k}) = (\omega_c, k_1, k_2, k_3)$ must satisfy $|\mathbf{k}| = 0$, indicating that both the phase and group velocities of gravitational waves equal c.

2.2.1 Transverse-Traceless gauge and GW propagation

To analyze the propagation of GWs, we consider a vacuum environment. The solution to equation 2.29 in vacuum is 2.31.

Beyond the Lorentz gauge, an additional gauge transformation can be used (Hobson, Efstathiou, and Lasenby 2006): $h'_{\mu\nu} = h_{\mu\nu} - \partial_\mu \xi_\nu - \partial_\nu \xi_\mu$, where ξ^μ satisfies the wave condition $\Box \xi^\mu = 0$. Incorporating this new gauge condition with the Lorentz gauge and considering the symmetry of the amplitude matrix, the independent components of a GW are reduced to two, representing the two possible GW polarizations. This gauge is also known as the transverse-traceless gauge (TT gauge). For a GW propagating along the x^3 or z direction, applying these considerations, the solution in the TT gauge is:

$$A^{TT}_{\mu\nu} = \begin{pmatrix} 0 & 0 & 0 & 0 \\ 0 & h_+ & h_\times & 0 \\ 0 & h_\times & -h_+ & 0 \\ 0 & 0 & 0 & 0 \end{pmatrix}, \tag{2.32}$$

$$A^{TT}_{\mu\nu} = h_+ e^+_{\mu\nu} + h_\times e^\times_{\mu\nu}, \tag{2.33}$$

with:

$$e^+_{\mu\nu} = \begin{pmatrix} 0 & 0 & 0 & 0 \\ 0 & 1 & 0 & 0 \\ 0 & 0 & -1 & 0 \\ 0 & 0 & 0 & 0 \end{pmatrix} \quad e^\times_{\mu\nu} = \begin{pmatrix} 0 & 0 & 0 & 0 \\ 0 & 0 & 1 & 0 \\ 0 & 1 & 0 & 0 \\ 0 & 0 & 0 & 0 \end{pmatrix} \tag{2.34}$$

with h_+ and $h_\times$ called plus and cross polarizations. As the name of the gauge suggests, the trace is zero and the non-transverse components vanish.

2.2.2 Generation of gravitational waves

The generation of gravitational waves is derived directly from equation 2.30. Assuming the compact-source approximation and a slow-moving particle regime, the quadrupole moment tensor of the matter density distribution is:

$$I_{ij} = c^2 \int \rho(ct, \mathbf{x}) x_i x_j \, d^3x. \tag{2.35}$$

For a binary system with two objects in circular orbit, the two polarization signals measured by an observer behave as:

$$h_+ = \frac{4}{r} \left(\frac{GMc}{c^2} \right)^{\frac{5}{3}} \left(\frac{\pi f_{GW}}{c} \right)^2 \frac{1 + \cos^2(i)}{2} \cos(2\pi f_{GW} t), \tag{2.36}$$

$$h_\times = \frac{4}{r} \left(\frac{GMc}{c^2} \right)^{\frac{5}{3}} \left(\frac{\pi f_{GW}}{c} \right)^2 \cos(i) \sin(2\pi f_{GW} t), \tag{2.37}$$

where i is the inclination angle between the observer's line-of-sight and the orbital plane's normal; f_{GW} is the GW frequency which is twice the binary system's frequency, M_c is the chirp mass, defined as $\mu^{3/5} m_{\text{tot}}^{2/5}$ with μ and m_{tot} being the reduced and total masses of the system.

Considering also that the energy loss due to GW emission happens through the quasi-circular orbit approximation, meaning that the separation and angular frequency of the system do not vary with time, and introducing the quantity:

$$\Phi(t) = 2\pi \int_{t_0}^{t} f_{GW}(t) \, dt, \tag{2.38}$$

the equations 2.36 and 2.37 become:

$$h_+ = \frac{4}{r} \left(\frac{GM_c}{c^2} \right)^{\frac{5}{3}} \left(\frac{\pi f_{GW}(t)}{c} \right)^{\frac{2}{3}} \frac{1 + \cos^2(i)}{2} \cos(\Phi(t)), \tag{2.39}$$

$$h_\times = \frac{4}{r} \left(\frac{GM_c}{c^2} \right)^{\frac{5}{3}} \left(\frac{\pi f_{GW}(t)}{c} \right)^{\frac{2}{3}} \cos(i) \sin(\Phi(t)). \tag{2.40}$$

To observe the characteristic shape of a GW from an inspiraling binary, we use the time to coalescence $\tau = t_{\text{coal}} - t$. Rewriting equations 2.39 and 2.40 with τ, we see both frequency and amplitude increase as t_{coal} approaches.

To include GWs from a compact binary system at cosmological distance, Eqs. 2.39 and 2.40 need to be adjusted accounting for universe's expansion. The distance r is replaced with $a(t_0)r$ and the frequency is adjusted for redshift ($f_{\rm obs}^{GW} = \frac{f_{\rm em}^{GW}}{1+z}$). Despite the potential coupling of h_+ and $h_\times$ due to the expanding universe, they remain distinct. With these adjustments, the expressions for GWs in a ΛCDM universe are:

$$\begin{aligned} h_+ &= \frac{4}{d_L}\left(\frac{G\mathcal{M}_c}{c^2}\right)^{\frac{5}{3}}\left(\frac{\pi f_{\rm obs}^{GW}(t)}{c}\right)^{\frac{2}{3}}\frac{1+\cos^2(i)}{2}\cos(\Phi(t)), \\ h_\times &= \frac{4}{d_L}\left(\frac{G\mathcal{M}_c}{c^2}\right)^{\frac{5}{3}}\left(\frac{\pi f_{\rm obs}^{GW}(t)}{c}\right)^{\frac{2}{3}}\cos(i)\sin(\Phi(t)), \end{aligned} \tag{2.41}$$

With $\mathcal{M}_c = M_c(1+z)$ the redshifted chirp mass. Which is also given by:

$$\mathcal{M}_c = (1+z)\frac{(m_1 m_2)^{\frac{3}{5}}}{(m_1+m_2)^{\frac{1}{5}}}, \tag{2.42}$$

where m_1 and m_2 are the component masses in the source frame.
The overlap of GW polarizations in Eq. 2.41, combined with the antenna receptor gain of the interferometer, produces the GW strain observed for a detected event. Crucially, by analyzing both the amplitude and frequency evolution of the GW signal, the luminosity distance can be determined directly, without the need for distance calibrators. All quantities in Eq. 2.41, except for the redshift, are directly measurable by the interferometer.

However, if the redshift of the emitting system can be measured independently, the redshift degeneracy described in Eq. 2.42 can be resolved. This, in turn, enables the extraction of cosmological information via Eq.2.15. Note that the amplitude is also dependent on different quantities: position, inclination, and polarization with respect to the detector, which is a big part of doing cosmology with GWs. This peculiar property of directly measuring the luminosity distance, with previous knowledge of redshift, is the main reason for using GWs as standard sirens.

2.3 Standard siren cosmology

Merger of black holes and neutron stars provides a robust framework to use GWs as cosmological probes (Holz and Hughes 2005 and Dalal et al. 2006). These astrophysical events generate GW signals that inherently encode the luminosity distance d_L to the binary systems as seen in Eq.2.41, which allows to obtain information on the components of the universe through Eqs.2.15 and 2.28. However, the GW signal alone is insufficient to infer the redshift due to the degeneracy between the source-frame mass and redshift within the GW waveform as seen in Eq.2.42. This degeneracy needs to be broken to allow the use of GWs for cosmology. There are three primary methodologies to break this degeneracy, referred to as standard sirens, and divided into the following:

- Bright Sirens are GWs that can be associated with an electromagnetic counter-part signal to retrieve redshift measurements (B. P. Abbott 2016)
- Dark Sirens have no counter-part, so they rely on a galaxy catalog to identify a possible galaxy host and obtain redshift (MacLeod and Hogan 2008, Oguri 2016, Mukherjee and Wandelt 2018, Vijaykumar et al. 2023, Bera et al. 2020, Mukherjee, Wandelt, et al. 2021)
- Spectral Sirens are a sub-category of Dark Sirens, with an empty galaxy catalog using features in the source masses population to directly extract the redshift. (Ezquiaga and Holz 2022)

Bright Sirens are the best method to assign redshift with low uncertainty, in fact, Multi-messenger observations, such as neutron star mergers with electromagnetic counterparts, offer the most straightforward redshift measurements (Dalal et al. 2006; Holz and Hughes 2005), revealing amazing results just with a single event detected. However, this method is statistically inconsistent since multiple detections are needed to have good constraints on cosmological quantities. Because of the rarity of these types of events dark sirens and spectral sirens have been used. Statistical methods as proposed by Schutz 1986 and developed in a Bayesian context by Del Pozzo 2012, allow for redshift estimation by cross-correlating GW localization volumes with galaxy distributions (Chen, Maya Fishbach, and Holz 2018). In the absence of counterparts or comprehensive galaxy catalogs, known features in the source population such as gaps or peaks, will be affected by redshift. This can be used to directly extract z from the CBC populations; one example is the lower edge of the pair-instability mass gap, which can provide redshift information directly from knowledge on the whole population(Will M. Farr et al. 2019; S. R. Taylor and Jonathan R. Gair 2012). This approach is the spectral siren method, which seeks to estimate the redshift of GW sources based on the relationship between source-frame masses and detector-frame masses, that fitting the population distribution of source-frame masses, allows to place constraints on cosmology. Similar to the mass method, the potential redshift information of GW events can also be derived from the CBC merger rate as a function of redshift. A noteworthy piece of information is that these two final methods, dark and spectral sirens are related. The dark siren method is essentially an extension of the spectral sirens, which can be considered a method that cross-correlates GW detections with an empty catalog. For this reason, it makes sense to merge these two methods and use them in a single joint analysis employing them both, describing it as a single unified framework called dark sirens. By incorporating prior knowledge about the population into a comprehensive joint analysis of GW sources (S. Mastrogiovanni et al. 2021, Moresco et al. 2022) it is possible to obtain information about the entire population rather than focusing solely on individual cases. These methods however are not free of problems or biases; first of all the galaxy catalog method crucially relies on the theoretical assumptions regarding the population model for the GW sources. This includes aspects such as the source-frame mass, redshift, and spin distribution (S. Mastrogiovanni et al. 2021; Finke et al. 2021; B. P. Abbott 2023). Incorrect population modeling must be carefully taken care of, to avoid biases in the estimation of any parameter. Secondly, the detectors' limits on the localization of a GW event must be considered. Without electromagnetic counterparts, GW events are often poorly localized, making unique host galaxy identification difficult (B. P. Abbott 2018). Since these methods exploit the derivation of localization volumes, which usually encompasses $\mathcal{O}(10^4 - 10^5)$ possible host galaxies, the limiting horizon of detectors reduces the accuracy on parameters. Hence this dark siren technique would provide significantly less information, even having exhaustive galaxy catalogs with accurately measured redshifts. Finally, an assumption must be made to address the completeness of the galaxy catalog. Failing to consider these would lead to a biased measurement when analyzing a population. The dark siren approach involves using galaxy catalogs to statistically determine a host galaxy, and thus a redshift, for the GW event. Incompleteness of these catalogs especially at high redshifts, renders them unable to provide relevant information on the source redshift, so accounting for these selection effects, is essential for robust cosmological constraints (Chen, Maya Fishbach, and Holz 2018; Mandel, Will M Farr, and Jonathan R Gair 2019; Mortlock et al. 2019). For certain cosmological observables, like bright sirens, GWs complement electromagnetic observations. This is particularly relevant for the Hubble parameter H_0, where GWs can provide measurements with different systematic uncertainties, potentially helping to address the discrepancy between early-universe (Aghanim et al. 2020) and late-universe (Wong et al. 2019) measurements of H_0. The first standard siren measurement of the Hubble constant was derived from the binary neutron star detection GW170817, which provided a luminosity distance and identified a unique host galaxy, NGC4993 (L. S. C. Abbott B. P. et al. 2017). This event enabled a measurement of the Hubble constant of $H_0 = 70^{+13}_{-7}$ km s^{-1} Mpc^{-1} (B. P. Abbott 2019). All subsequent analyses, because of the rarity of these events, have utilized galaxy catalogs and spectral sirens to derive statistical Hubble constant measurements for events without electromagnetic counterparts (M. Fishbach et al. 2019; Palmese et al. 2020). These have focused on nearby sources, typically within $d_L < 400$ Mpc, thus examining the local distance-redshift relation via the Hubble constant H_0. However, advances in gravitational wave detectors, such as LIGO and Virgo, have extended this observational range to $d_L \approx 5$ Gpc, with future enhancements expected to surpass 10 Gpc (Moresco et al. 2022). This extended range facilitates measurements of the expansion history up to $z \approx 1$, offering not only insights into the Hubble constant but also potential deviations in GW propagation predicted by various cosmological theories and Modified Gravity (MG) theories.

2.4 Modified gravity and GWs

Since gravitational waves are predicted as space-time perturbations propagating in a GR scenario, they can be employed to test deviation from GR. One test that has been performed is testing the propagation velocity of GWs, though observations of GW170817 have put strong limits on it at a level of $\frac{|c_{\rm gw}-c|}{c} < \mathcal{O}(10^{-15})$ (B. P. Abbott 2016, B. P. Abbott 2017a,Goldstein et al. 2017, Savchenko et al. 2017). Even though this constrain has been put there are other ways to test alterations of GR; in particular in recent years, it has been recognized that all modified gravity models that adhere to the constraint defined before on the propagation speed, still predict a different evolution of the amplitude of GWs during their propagation over cosmological distances (Mancarella, Genoud-Prachex, and Michele Maggiore 2022). Moreover it has been found that deviations from GR can be also studied through tensor perturbation theory of a FLRW metric and these can be found only investigating GWs (Brandenburg et al. 2021). These studies consider a modified GW propagation which is the starting point of this thesis work. For this reason, is important to describe a mathematical framework that can predict these alterations. Generally, on cosmological scales, it is beneficial to differentiate between a homogeneous background described by FLRW metric and the scalar, vector, and tensor (SVT) perturbations superimposed on it. The SVT decomposition is a mathematical framework used to analyze perturbations in cosmological models (Amarasinghe et al. 2022). Starting from this SVT framework it is possible to study deviations from GR. So it is still necessary to study these perturbations through their amplitude. In general, in GR this is determined by the equation for tensor perturbations over the FLRW background, which takes the form:

$$\tilde{h}''_A + 2\mathcal{H}\tilde{h}'_A + c^2k^2\tilde{h}_A = 0, \tag{2.43}$$

where $\tilde{h}_A$ is the gravitational wave amplitude for the two polarizations in Fourier space. The prime denotes the derivative with respect to conformal time η and $\mathcal{H} = \frac{a'}{a}$. In current cosmic epoch, $\frac{a''}{a} \sim \frac{1}{\eta^2}$ and η is very large so the term $\frac{a''}{a}$ can be neglected compared to k^2. This approximation holds with great accuracy for GW observed by ground- or space-based interferometers. The amplitude of the GW turns to be proportional to the luminosity distance $\tilde{h}_A(\eta, k) \propto \frac{1}{d_L(z)}$. Different MG theories predict that GW propagates differently than the GR case and a modified version of Eq.2.43 must be considered. With modification of the term $2\mathcal{H}$ the Eq.2.43 becomes (Saltas et al. 2014):

$$\tilde{h}''_A + 2\mathcal{H}[1 - \delta(\eta)]\tilde{h}'_A + k^2\tilde{h}_A = 0. \tag{2.44}$$

This holds for some time-dependent function $\delta(\eta)$ that represents the deviation from GR. In this case, introducing $\tilde{\chi}_A(\eta, k)$ as

$$\tilde{h}_A(\eta, k) = \frac{1}{\tilde{a}(\eta)}\tilde{\chi}_A(\eta, k), \tag{2.45}$$

where

$$\frac{\tilde{a}'}{\tilde{a}} = H[1 - \delta(\eta)], \tag{2.46}$$

yields to

$$\tilde{\chi}''_A + (k^2 - \frac{\tilde{a}''}{\tilde{a}})\tilde{\chi}_A = 0. \tag{2.47}$$

Once again, inside the horizon, the term $\frac{\tilde{a}''}{\tilde{a}}$ is completely negligible, so GWs propagate at the speed of light. However, across cosmological distances, $\tilde{h}_A$ now decreases as $\frac{1}{\tilde{a}}$ rather than $\frac{1}{a}$. Therefore, in such a modified gravity model, a distinction between the electromagnetic luminosity distance $d_L^{\mathrm{EM}}(z)$ and the GW luminosity distance $d_L^{GW}(z)$ needs to be done (Belgacem et al. 2018b). The GW amplitude of a measured CBC at redshift z will now be proportional to $\frac{1}{d_L^{GW}(z)}$, where

$$d_L^{GW}(z) = \frac{a(z)}{\tilde{a}(z)}d_L^{EM}(z) = \frac{1}{(1+z)\tilde{a}(z)}d_L^{EM}(z). \tag{2.48}$$

For this reason, while in GR the signal from a merging binary allows for the extraction of the luminosity distance of the source, in the context of modified gravity it provides a measure of a different quantity, $d_L^{\mathrm{GW}}(z)$, known as the "GW luminosity distance" (Belgacem et al. 2018b).

In this context, the standard luminosity distance, referred to as the 'electromagnetic luminosity distance' and denoted as $d_L(z)$, is related to $d_L^{\mathrm{GW}}(z)$ as follows:

$$d_L^{GW}(z) = d_L(z) \exp\left(-\int_0^z \frac{dz'}{1+z'}\delta(z')\right), \tag{2.49}$$

where $\delta(z) \equiv \delta[\eta(z)]$. It is understood that a change in the coefficient of the k^2 term in Eq. 2.43 gives a friction term to the GWs propagation and changes the luminosity distance. Assuming that all these MG theories leave the evolution of the cosmic background unchanged, Friedmann's equations still describe the expansion of the universe with H_0 and Ω_m as parameters for a flat ΛCDM model. In these MG theories, both the coefficient of the k^2 term and that of the $2\mathcal{H}$ term can differ (Belgacem et al. 2018a). This variation has been predicted in several explicit models. For instance, in the Dvali Gabadadze Porrati (DGP) model (Dvali, Gabadadze, and Porrati 2000), gravity leaks into extra dimensions on cosmological scales, affecting the $\frac{1}{d_L(z)}$ behavior of a gravitational signal (Deffayet and Menou 2007). A similar effect has been found in Einstein-Aether models, scalar-tensor theories of the Horndeski class, and even in models affected by a time-dependent Planck mass in terms of dark energy content. They are called c_M-parametrization (Saltas et al. 2014, Lombriser and A. Taylor 2016) in which the parameter c_M (which vanishes in GR) affects the luminosity distance. These are different ways to influence the friction term that affects d_L^{GW} but in the context of this thesis the Eq.2.49 will be parametrized with simplest MG parametrization accordingly to the introduction of two quantities that will affect the GW propagation, Ξ_0 and n (Leyde et al. 2022), defining the following term:

$$\Xi(z) = \Xi_0 + \frac{1-\Xi_0}{(1+z)^n}. \tag{2.50}$$

The luminosity distance formula can thus be written as:

$$d_L^{GW} = d_L \Xi(z) \tag{2.51}$$

By combining this with redshift data, it becomes possible to simultaneously measure the Universe's expansion history and test GR on cosmological scales.

2.5 The statistical framework

As explained in the previous sections, the introduction of dark sirens cosmology allows us to derive cosmological information with the combination of GWs and galaxy catalogs; this needs a theoretical introduction on the statistical techniques to be used. The statistical background is achieved by employing a hierarchical Bayesian inference approach, which enables the simultaneous estimation of parameters and model selection (Adams, Cornish, and Littenberg 2012; Thrane and Talbot 2019). Generically, given $\{d_{GW}\}$ the measured data and λ the model's parameter, a definitive and unique value for these λ cannot be obtained; instead, the posterior distribution of λ can be obtained from Bayes theorem as:

$$p(\lambda|\{d_{GW}\}) = \frac{\mathcal{L}(\{d_{GW}\}|\lambda)\pi(\lambda)}{p(\{d_{GW}\})}, \tag{2.52}$$

where $\pi(\lambda)$ encodes the prior information on λ which is supposedly already known, $\mathcal{L}(\{d_{GW}\}|\lambda)$ is the likelihood function quantifying how well a particular set of model parameters explain the observed data, playing as central role in statistical inference and in parameter estimation. While $p(\{d_{GW}\})$ is called evidence and is the likelihood marginalized over all parameters.

More specifically, according to `CHIMERA`'s description the general problem for this work, involves a population of events described by a set of event-level parameters θ, from which we aim to determine a set of hyper-parameters λ that characterize the source population. In GW cosmology, the event-level parameters are $\theta = \{d_L, \hat{\Omega}, m_1, m_2\}$, where d_L is the luminosity distance of the source, $\hat{\Omega}$ is the sky localization (RA,Dec), and m_1, m_2 are the binary masses. Instead, the population level parameter describing the distributions of θ, are divided into three sets: cosmological parameters λ_c; mass function parameters λ_m, and rate parameters λ_z. These specifically correspond to:

- $\lambda_c = \{H_0, \Omega_{0,m}, w_0, w_a, \Xi_0, n\}$ (cosmological parameters),
- $\lambda_m = \{\alpha, \beta, \delta_m, m_{\text{low}}, m_{\text{high}}, \mu_g, \sigma_g, \lambda_g\}$ (mass parameters),
- $\lambda_z = \{\gamma, \kappa, z_p\}$ (rate parameters).

2.5.1 The `CHIMERA` code

The core of statistical analysis with `CHIMERA` involves constructing and evaluating the likelihood function from multiple events. Assuming a set of N_{ev} independent GW events $d_{\text{GW}} = \{d^i_{\text{GW}}\}$ from which we can measure the luminosity distance, the total likelihood is proportional to the product of the individual event likelihoods multiplied by the population function:

$$\mathcal{L}(d_{\rm GW}|\lambda) = p(d_{\rm GW}|\lambda) \propto \frac{1}{\xi(\lambda)} \prod_{i=1}^{N_{\rm ev}} \int p(d^i_{\rm GW}|\theta_i, \lambda_c) p_{\rm pop}(\theta_i|\lambda) d\theta_i, \tag{2.53}$$

The first term is $\xi(\lambda)$, which accounts for selection bias; current interferometers are sensitive only to specific ranges of GW signal frequencies, and this bias must be considered when inferring population distributions. In any dataset of GW events, detectability is considered deterministic, meaning that an event is detectable if the data exceeds a certain threshold $r_{\rm thr}$. In this context, the threshold is the signal-to-noise ratio (SNR) of the event. Therefore, $p_{\rm det}$ is essentially the likelihood distribution of observed SNRs, expressed as:

$$p_{\rm det}(\theta_i, \lambda_c) = \int_{{\rm SNR}(d_{\rm GW})>r_{\rm thr}} p(d_{\rm GW}|\theta_i, \lambda_c) dd_{\rm GW}. \tag{2.54}$$

A GW event has an intrinsic SNR due to the properties of the emitting system, such as the signal amplitude, which strongly depends on the compact objects' masses, inclination, and sky localization. Additionally, stochastic fluctuations in the interferometers may alter the intrinsic SNR, making it different from the observed one.

Then the term $p(d^i_{\rm GW}|\theta_i, \lambda_c)$ is the single-event likelihood, which can be expressed following Bayes' theorem as:

$$p(d^i_{\rm GW}|\theta_i, \lambda_c) \propto \frac{p(\theta_i|d^i_{\rm GW}, \lambda_c)}{\pi(\theta_i)} \tag{2.55}$$

Here, $p(\theta_i|d^i_{\rm GW}, \lambda_c)$ is obtained from $p(\theta_i^{\rm det}|d^i_{\rm GW}, \lambda_c)$, the posterior distribution of the event-level parameters in detector-frame, and $\pi(\theta_i)$ is the prior probability. Returning now to Eq.2.53, note that the single-event probability depends on the cosmological hyper-parameters, as the data contain information on the detector frame parameters $\theta_{\rm det}$, so they necessitate of a conversion to the source frame. The luminosity distance d_L and the detector frame masses $m_1^{\rm det}, m_2^{\rm det}$ are related to the source frame masses by $m_1^{\rm det} = m_1(1+z)$ and $m_2^{\rm det} = m_2(1+z)$. The population function $p_{\rm pop}$ can be further decomposed as the product of two distributions:

$$p_{\rm pop} = p(m_1, m_2|\lambda_m) p(z, \hat{\Omega}|\lambda_z, \lambda_c), \tag{2.56}$$

assuming that $p(m_1, m_2|\lambda_m)$ does not evolve in redshift. This distribution represents the masses m_1 and m_2 given a well-defined mass function of the sources. The other term can be expressed as:

$$p(z,\hat{\Omega}|\lambda_z,\lambda_c) \propto p_{\rm gal}(z,\hat{\Omega}|\lambda_c)p_{\rm rate}(z|\lambda_z), \tag{2.57}$$

where $p_{\rm gal}(z,\hat{\Omega}|\lambda_c)$ is the distribution of potential hosts that may include corrections for completeness effects, expressed as:

$$p_{\rm gal}(z,\hat{\Omega}|\lambda_c) = f_R p_{\rm cat}(z,\hat{\Omega}|\lambda_c) + (1-f_R)p_{\rm miss}(z,\hat{\Omega}|\lambda_c), \tag{2.58}$$

with $p_{\rm cat}$ being the probability distribution from galaxy catalogs and $p_{\rm miss}$ accounting for the completeness of these catalogs as explained by Jonathan R. Gair et al. 2023 and Borghi et al. 2024. The quantity f_R is defined as:

$$f_R = \frac{\int P_{\rm comp}(z,\hat{\Omega})\ {\rm d}V_c}{V_c(\lambda_{\rm c})} \tag{2.59}$$

Here $P_{\rm comp}(z,\hat{\Omega})$ is the completeness fraction of the catalog given sky localization and redshift range, and $V_c(\lambda_{\rm c})$ the comoving volume. The probability $p_{\rm rate}(z|\lambda_z)$ represents the probability of a galaxy hosting a GW event at redshift z, given by:

$$p_{\rm rate}(z|\lambda_z) \propto \frac{\psi(z,\lambda_z)}{1+z}, \tag{2.60}$$

where the denominator accounts for the conversion between source and detector frames, and $\psi(z,\lambda_z)$ describes the merger rate evolution of compact objects with redshift (Madau and Dickinson 2014).

Combining all components from all the previous equations, the full likelihood is described as:

$$\mathcal{L}(d_{\rm GW}|\lambda) \propto \frac{1}{\xi(\lambda)}\prod_{i=1}^{N_{\rm ev}}\int dz d\hat{\Omega}\mathcal{K}_{\rm GW,i}(z,\hat{\Omega}|\lambda_c,\lambda_m)p_{\rm gal}(z,\hat{\Omega}|\lambda_c)\frac{\psi(z,\lambda_z)}{1+z}, \tag{2.61}$$

This equation is a specific implementation for `CHIMERA` that relies on this $\mathcal{K}_{\rm GW}$:

$$\mathcal{K}_{\rm GW,i}(z,\hat{\Omega}|\lambda_c,\lambda_m) \equiv \int dm_1 dm_2 \frac{p(z,m_1,m_2,\hat{\Omega}|d^i_{GW},\lambda_c)}{\pi(d_L)\pi(m_{1,det})\pi(m_{2,det})}\frac{p(m_1,m_2|\lambda_m)}{\frac{dd_L}{dz}(z;\lambda_c)(1+z)^2} \tag{2.62}$$

This quantity is the marginalization of the event posterior over m_1 and m_2, containing information on the localization volume (RA, Dec, z) of the GW and computed for each

set of λ_m and λ_c. The terms $(1+z)^2$ and $\frac{dd_L}{dz}(z;\lambda_c) = \frac{d_L}{1+z} + \frac{c(1+z)}{H(z,\lambda_c)}$ are the Jacobian factors arising from the conversion from detector frame to source frame. In general, the prior probabilities for the astrophysical population are assumed to be flat for m_1 and m_2, $\pi(m_{1,2}) = 1$, whereas for luminosity distance it is imposed to be $\pi(d_L) \propto d_L^2$. Additionally, it is essential to understand the bias factor $\xi(\lambda)$, as it is crucial for obtaining a proper posterior distribution since some events are more likely to be observed than others due to intrinsic properties or instrument limitations. Ignoring this bias would result in incorrect uncertainty assessments and posterior distributions.
The selection effect is incorporated by introducing a detection probability $p_{\rm det}$, such that the selection function is expressed as (Mandel, Will M Farr, and Jonathan R Gair 2019):

$$\xi(\lambda) = \int p_{\rm det}(\theta_i, \lambda_c) p(m_1, m_2|\lambda_m) p_{\rm gal}(z, \hat{\Omega}|\lambda_c) \frac{\psi(z;\lambda_z)}{1+z} d\theta_i. \tag{2.63}$$

The final integral in Eq. 2.61 is computed in `CHIMERA` using adaptive redshift grids. These grids are constructed based on the GW data and span the range of redshifts covered by the allowed cosmologies. For well-localized events, the grid becomes relatively small, which improves computational efficiency. These implementations and features will be explored in the next chapter with an overview of the effects of MG on the `CHIMERA` pipeline as the introductory work of this thesis.

Chapter 3

Developing methods and catalogs for modified GW propagation

This chapter presents the methods and data developed in this thesis to study cosmological constraints on modified GW propagation. Section 3.1 describes the implementation of modified GW propagation functions in `CHIMERA`, including adequate measurements taken to avoid potential biases in the inference. The developed modules are used to provide a preliminary study of the modified propagation effects on GW observations, which will be then extended in Section 3.1.1. The motivation for this is related to the link between hyper-parameters and luminosity distance, this quantity changes in a modified propagation scenario and at the same time contains cosmological information depending so from λ_c. These preliminary studies are done to better understand which parameters have a deeper impact, in order to decide which one will be fixed in the cosmological model in future analyses. Section 3.2 instead describes the generation of mock events catalog. Starting from a parent galaxy catalog, the methodology to generate realistic GW catalogs will be given to simulate population of GW emitters, considering specific mass population distribution and merger rate. Moreover in Section 3.2.3 will be presented the techniques used in this work to simulate GW detections highlighting the importance of simulating how future detectors will be able to localize gravitational wave signals. Concluding the chapter in Section 3.3 with a significant emphasis on generating a catalog under both GR and modified GR scenarios with resulting study of their properties.

3.1 Implementation of modified GW propagation in CHIMERA

This section focuses on explaining how the CHIMERA code calculates the luminosity distance for gravitational waves and the corresponding likelihood, providing insight into the impact of modified gravitational wave propagation on these quantities. To extend the code to deal with these effects, some changes were needed. The first difference is related to the computation of luminosity distance, which is changed according to the concept of "friction" in the GW propagation as seen in Chapter 2. Following Eq.2.51 this modification affects both d_L^{GW} and its derivative $\frac{d}{dz}d_L^{GW}$, which I implemented in a new CHIMERA module named MG_FLRW. These modifications enter at different steps during the code execution. At the beginning of the pipeline, the code loads:

- A data set containing the posteriors of observed GW events defined as GW catalog. This data-set encompasses the distribution samples related to the detected parameters for the specific GW event in detector-frame.
- A catalog of potential host galaxies each characterized by z, RA, Dec values.

The reason why the data-set are in detector-frame is that these are observables measured by the interferometers obtained in a detector-frame, which is different from the source-frame through the redshift-mass degeneracy relation. In practice, CHIMERA cross-correlates the GW catalog with the galaxy catalog to compute Eq.2.61. A thorough discussion of each term is essential to understand how CHIMERA computes each term and how the impact of modified GW propagation parameters influences the full likelihood computation. The likelihood is obtained through different quantities:

- $p_{GW}(\theta|\theta_{det})$ the probability function related to the detector-frame parameters. This quantity contains all the information of the GW events, also its localization.
- $p_{gal}(z)$ which is the distribution of all the potential hosts pre-computed from the galaxy catalog, as a function of redshift, dividing in pixels the GW localization area and summing the contribution of every galaxy probability in the pixels.
- $\xi(\lambda)$ the selection bias.

For each GW event in the catalog, a p_{GW} is given, containing various distribution samples related to the detected parameters. Among these distribution samples the d_L^{GW} distribution is present, which is converted to a z_{sample} distribution. To each z_{sample} depending on the mass population distribution a weight is associated, in order to marginalize p_{GW} over the correct mass-population parameters. This results in: $\mathcal{K}_{\rm GW}(z, \Omega|\lambda_c, \lambda_m)$ which is the final distribution of the GW event for a specific set of cosmological and astrophysical parameter. Additionally this quantity has to be converted from a detector-frame to source-frame distribution through mass-redshift degeneracy relation in order to correctly compute the integration. Note that both the re-weight and frame-shift are done on the numerator of the likelihood because the denominator does not need it. This denominator is the selection bias 2.63, this term is computed through a Monte Carlo integral (Tiwari 2018, Will M. Farr et al. 2019) using only detector-frame quantities since it is related to the detectability of a GW event ($p_{\rm det} = p_{\rm det}(\theta_{\rm det})$). This allows to compute this function only once. To do it, `CHIMERA` takes a set of simulated injections' events and multiplies the detector-frame distribution by the mass distribution and merging rate, summing at the end over all the detected injections. Considering all these quantities and conversions the final posterior is computed and can be used to infer population hyper-parameters λ. All the quantities described above are multiplied and integrated on an adaptive redshift grid called z_{grid}. This grid which depends on all the possible combinations of hyper-parameters is fundamental to correctly integrate the likelihood. This is needed because during the step of re-weighting the likelihood numerator is shifted and reshaped, so if the grid is not wide enough the integration is wrongly computed.

The z_{grid} mentioned beforehand is significantly influenced by modified GW propagation parameters and needs to be investigated. From d_L^{min} and d_L^{max} of each GW event, considering the hyper-parameter priors presented in table 3.2 it is possible to generate the z_{grid}. This allows to find appropriate limit values ($z_{\rm min}, z_{\rm max}$) which encompass the $\mathcal{K}_{\rm GW}$ range considering the additional parameters (Ξ_0, n).
The d_L^{GW} formula in 2.51 can be written as:

$$1 + z = \frac{1}{c} \frac{d_L^{GW} H_0}{\Xi(z) \int_0^z \frac{dz}{E(z)}} \tag{3.1}$$

Studying this relation, it is clear that to estimate z_{max} it is necessary to maximize $\frac{H_0}{\int_0^z \frac{dz}{E(z)}}$ and minimize $\Xi(z)$, while for for z_{min} it is the opposite. Therefore, we have:

$$z_{max} \iff (d_L^{GW})^{max}, (H_0)^{max}, (\Xi(z))^{min}, \left(\int_0^z \frac{dz}{E(z)}\right)^{min} \tag{3.2}$$

$$z_{min} \iff (d_L^{GW})^{min}, (H_0)^{min}, \Big(\Xi(z))^{max}, (\int_0^z \frac{dz}{E(z)}\Big)^{max} \tag{3.3}$$

In this thesis work, the relations 3.2, 3.3 were implemented in the MG_FLRW module. This implementation in `CHIMERA` pipeline was of great importance, allowing us to compute the final hyper-likelihood (as in Eq.2.61) also in a MG scenario. As it will be seen in the next section, this function is primarily influenced by the Ξ_0 prior assumed, which has a huge effect on the z_{grid}.

3.1.1 Effects of modified GW propagation on the luminosity distance

Now that the numerical computation of likelihood was introduced, the effects of Ξ_0 and n can be explored. It is of great importance to investigate how luminosity distance and final hyper-likelihood are influenced by modified GW propagation parameters. Figures 3.1, 3.2a, and 3.2b show the dependence of d_L^{GW} on various cosmological parameters (namely $\Omega_{m,0}, H_0, w_0, w_a$) and on modified GW propagation parameters (Ξ_0, n). These figures indicate that the significant quantities affecting the values of d_L^{GW} at identical redshifts are Ξ_0 and H_0. More quantitatively, if the redshift is fixed at $z = 1$, a 10% increase in H_0 generates a $\sim$ 10% decrease in d_L^{GW}, whereas a 10% increase in Ξ_0 leads to a 5% increase in the luminosity distance. This clearly shows a correlation between H_0 and Ξ_0 since they have opposite effect on luminosity distance Additionally, a 10% increase in $\Omega_{0,m}$ causes a 1.8% decrease, while the parameter n, which only affects d_L^{GW} when $\Xi_0 \neq 1$, shows that for $n = 1.5$, the relative increase is just 1%. Furthermore, the gradient variation observed in figure 3.2b emerges from the form of $\Xi(z)$ (see Eq.2.50) and its relationship with n varies depending on whether Ξ_0 is less than or greater than 1. Nevertheless, n's influence on luminosity distance is not as impacting as the other two parameters, especially at low redshift, and it will be clear that this will have an influence on determining a constraint on this particular parameter since the analyzed events are below $z < 1.3$ as it will be seen in Section 3.3. With the exception of H_0 and Ξ_0, the remaining parameters exhibited minimal impact on d_L^{GW} and therefore will be fixed.

It is possible now to explore the effects of the additional parameters on the z_{grid} in a modified GW propagation scenario as explained in the previous section. To validate this approach, figures 3.3 and 3.4 are chosen as an illustrative case. They have been used as a preliminary test to visually understand how to derive the z_{grid} integration grid needed for the likelihood computation. These figures represent a three-dimensional space computing the extension of the redshift grid for different combination of parameters, (H_0 vs. $\Omega_{0,m}$) and (Ξ_0 vs n). These highlight the maximum values at which the z_{grid} extends

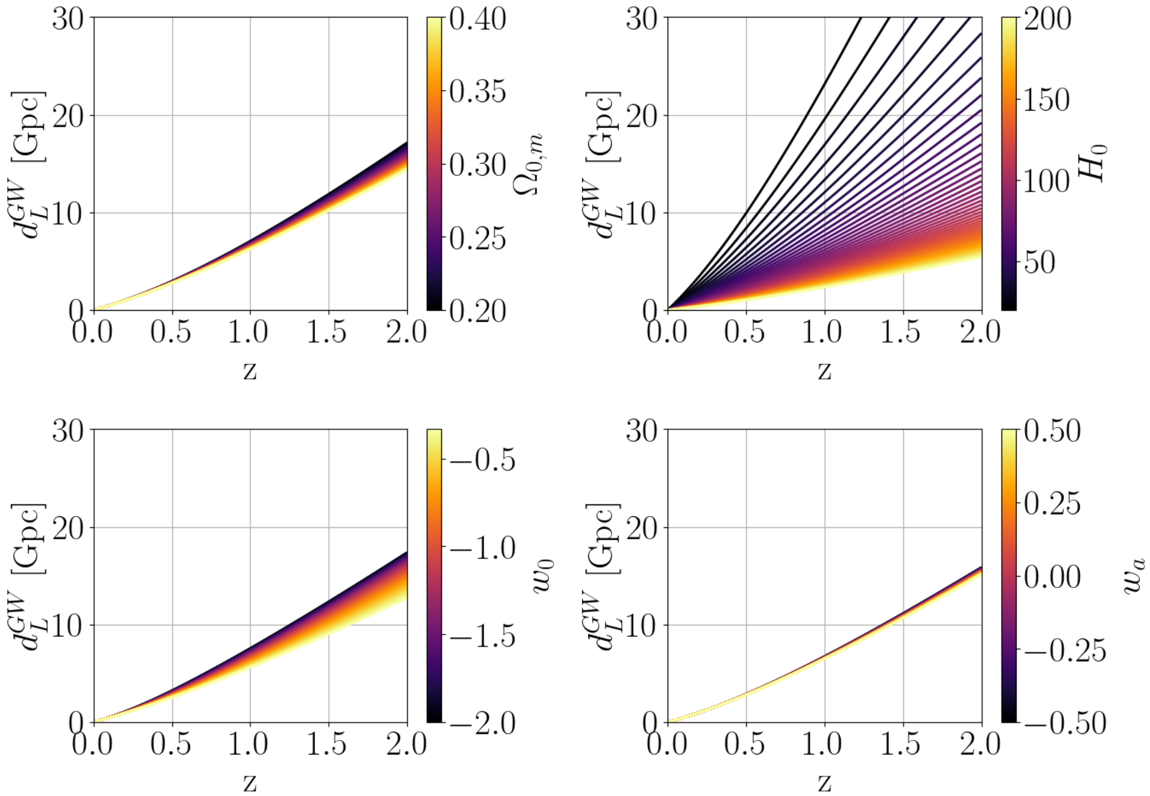

Figure 3.1: d_L^{GW} as function of z with color-bar on varying H_0, $\Omega_{0,m}$, w_0, w_a. Upper left corner: Variation of luminosity distance from matter's critical density showing mild effects on it. Upper right corner: Variation with cosmic expansion revealing huge effects on luminosity distance Lower side: Minor influence of w_0 and w_a parameters over luminosity distance

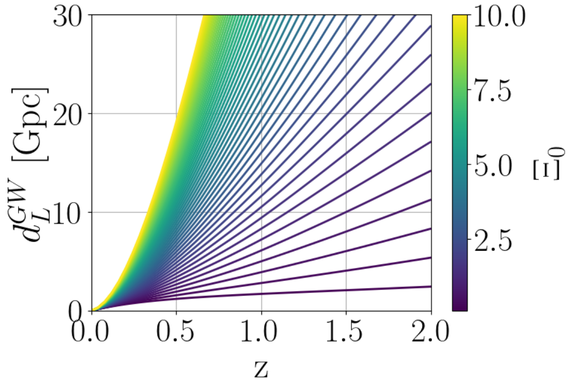

(a) d_L^{GW} as function of z with color-bar varying on Ξ_0. This parameter has huge effects on luminosity distance, showing also showing also a change in the derivative of the function revealed by change of concavity passing from $\Xi_0 < 1$ to $\Xi_0 > 1$

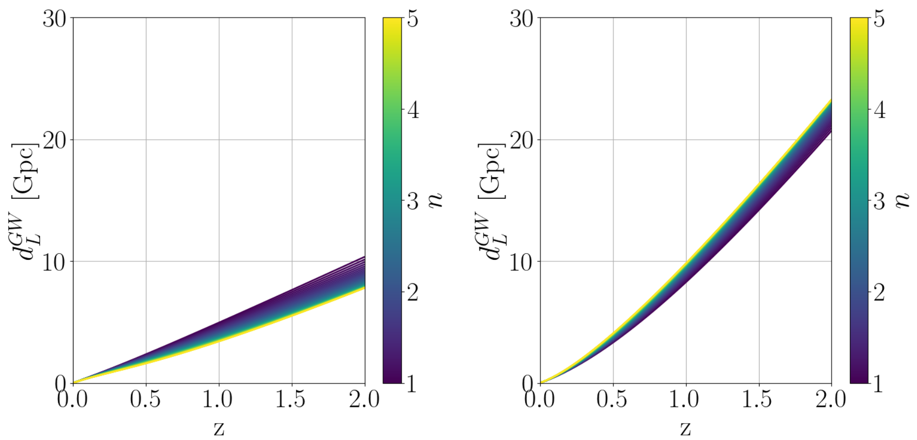

(b) d_L^{GW} as function of z with varying n to highlight the effect of convexity change. Left: Luminosity distance calculated fixing $\Xi_0 = 0.5$ showing lower increase rate of d_L^{GW} function. Right: Luminosity distance fixing $\Xi_0 = 1.5$ resulting in higher increase rate of the d_L^{GW} function.

supporting what said in Eqs.3.2 and 3.3. The chosen d_L^{GW} are typical values of luminosity distance for GW events and from the results, it emerges that the parameters with the larger impact are H_0 and Ξ_0. Firstly, a generic trend is found when the parameters pairs are fixed, in fact the redshift grid is dilated for higher values of luminosity distance since z is directly proportional to d_L^{GW}, as expected from Eq.3.1, when the cosmological parameters are fixed. Secondly at fixed luminosity distance the redshift extension is determined by the cosmological parameters in a way that the maximum redshift value is achieved with maximum H_0 and minimum Ξ_0, while the minimum redshift corresponds to the minimum H_0 and maximum Ξ_0 proving the relations 3.2 and 3.3. Nevertheless, one must interpret these results with caution, as the impact of $\Omega_{0,m}$ amplifies at greater distances, but since the events in the catalogs are not significantly far away, this effect has not been explored. This feature might be interesting to analyze in future analyses to investigate its effect on events at greater distances. Moreover, because of the predominant influence of H_0 and Ξ_0, this analysis supports the decision to work fixing $\Omega_{0,m} = 0.25$, $w_0 = -1$ and $w_a = 0$ since they have a subdominant effect; for this reason, they will not be considered anymore in the following analysis.

3.1.2 Effects of modified GW propagation on the likelihood

In Section 3.1, the quantities on which likelihood is built upon are processed and defined with a deeper focus on the $\mathcal{K}_{\text{GW}}$ representing the p_{GW} marginalized over the mass-population distribution integrated over the pre-computed z_{grid}. Moreover in Section 3.1.1 the predominant parameters modifying the integration grid are discussed. In the context of these modification, this section will focus on the effect that these predominant parameters have on the p_{GW} illustrating Figs. 3.5 and 3.6 as an example. Fig. 3.5, collects the different p_{GW} as function of redshift with respect to the cosmological parameters. The left figure focuses on the effect of H_0 alone, while the right figure on the effects Ξ_0. This last one shows how Ξ_0 strongly influences the integration grid by extending redshift to a $z_{max} \sim 6$ compared to the $z \sim 0.8$ of the left figure. In Fig 3.6 instead, the importance of re-weighting is depicted for the two cases, with and without considering the effects of Ξ_0 as in Fig.3.5. The pictures are generated by choosing the same event, to validate that the integration of the p_{GW} is performed in the same redshift ranges. Focusing on the right-side, the green histogram represents the p_{GW} as function of redshift before weighting on the population parameters and shift to the source frame. It is possible to see that if these features are not considered, the localization would happen at around $z \sim 3$. If instead they are considered, the shape and position of the p_{GW} are

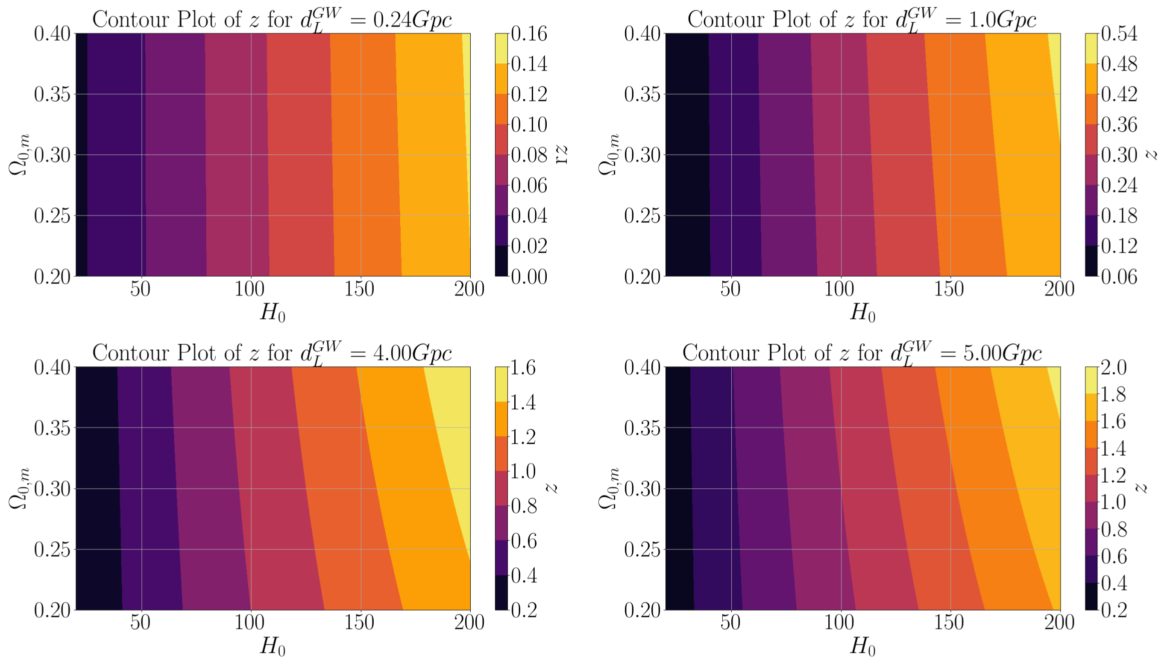

Figure 3.3: Three dimensional space depicting, the redshift obtained for different combination of $\Omega_{0,m}$ and H_0, all the quadrants are at different fixed luminosity distances. These show that redshift is mainly affected by H_0, which means that at fixed d_L^{GW} the redshift extension changes proportionally to H_0. Recovering the maximum redshift for high values of H_0, the opposite for low values of H_0. However, with an overall small dependency on $\Omega_{0,m}$ which is amplified at higher redshifts

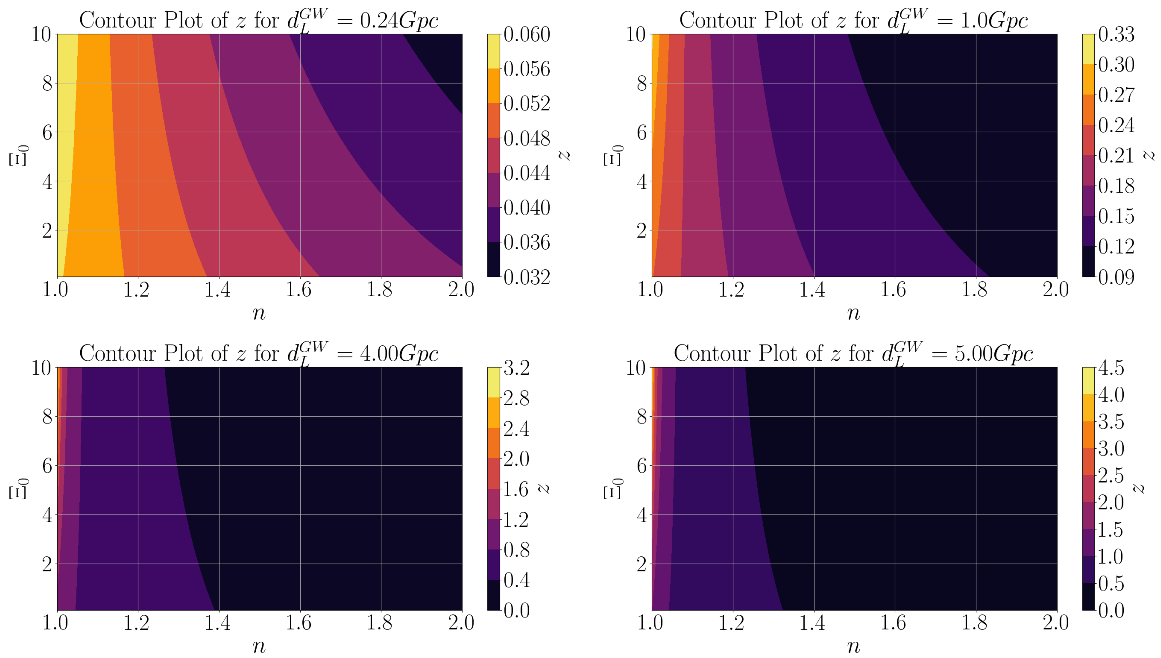

Figure 3.4: Three dimensional space depicting, the redshift obtained for different combination of Ξ_0 and n, at different fixed d_L^{GW}. These show that the major driving modifications of z_{grid} are from Ξ_0. To better visualize the results a zoom for n in range $[1, 2]$ was taken. The redshift extends for lower Ξ_0 values. While the minimum z is revealed for greater Ξ_0.

changed as depicted in blue, showing a z localization $\tilde{0}.5$. Finally, in red is presented a smoothed version of the histogram which is the effective $\mathcal{K}_{\mathrm{GW}}$ used by `CHIMERA` to compute the final likelihood.

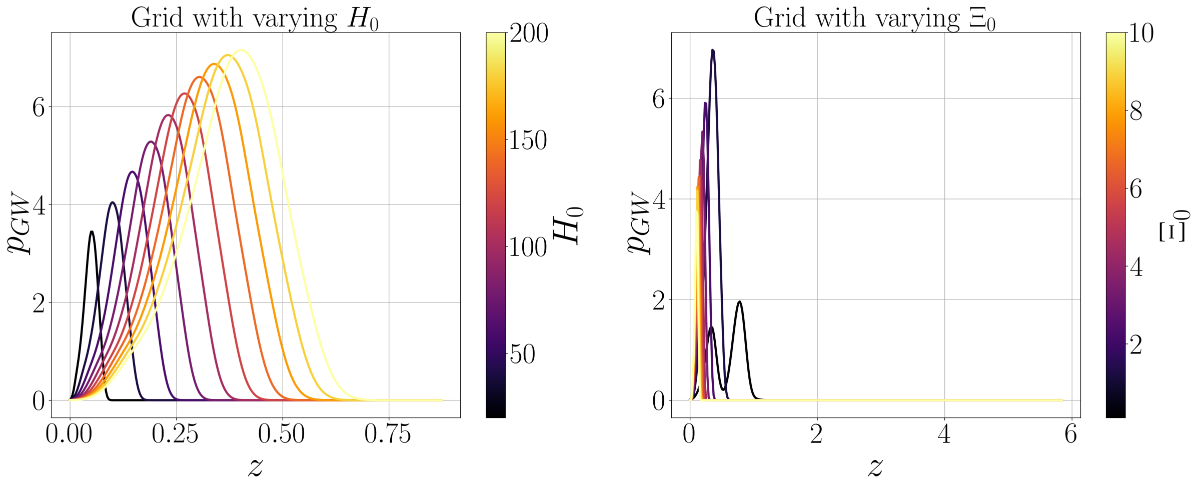

Figure 3.5: Different p_{GW} as function of redshift for different parameters H_0 and Ξ_0 revealed through a color-map. Left: Revealing the effects of H_0 fixing all the other parameters, its major influence is a shift at bigger redshifts on the p_{GW} with an additional increase of its normalization. Right: Showing the effects of Ξ_0 explicitly extending the redshift range with an enlarging that is stronger than H_0 effect, of pushing the posterior towards lower values of redshift.

As seen by the previous figures, the p_{GW} is strongly influenced by the cosmological parameters. To broadly visualize this, Figure 3.7 is generated by fixing all the astrophysical parameters as in Tab. 3.1 and considering a variation of λ_c in the ranges given by Tab.3.2. These are all the probabilities of the GW events, fixing two parameters and leaving either H_0 or Ξ_0 free with its influence shown with a color-bar, finally highlighting in green the p_{GW} for $H_0 = 70$. The first two rows show the effect of varying H_0 fixing different combinations of Ξ_0 and n, the interesting result is that for low values of both fixed quantities, the p_{GW} moves toward higher z because of the direct proportionality between H_0 and z (see Eq.3.1). Although as the fixed Ξ_0 increases the effect is dumped, forcing the p_{GW} toward the left. In the other two rows, the effect of varying Ξ_0 are investigated at fixed H_0 and n. The results are the opposite as varying H_0, stating that because of a negative correlation with redshift, high Ξ_0 results in a p_{GW} placed at lower redshift values. Moreover features like broadening and bi-modality appear as H_0 increases, but

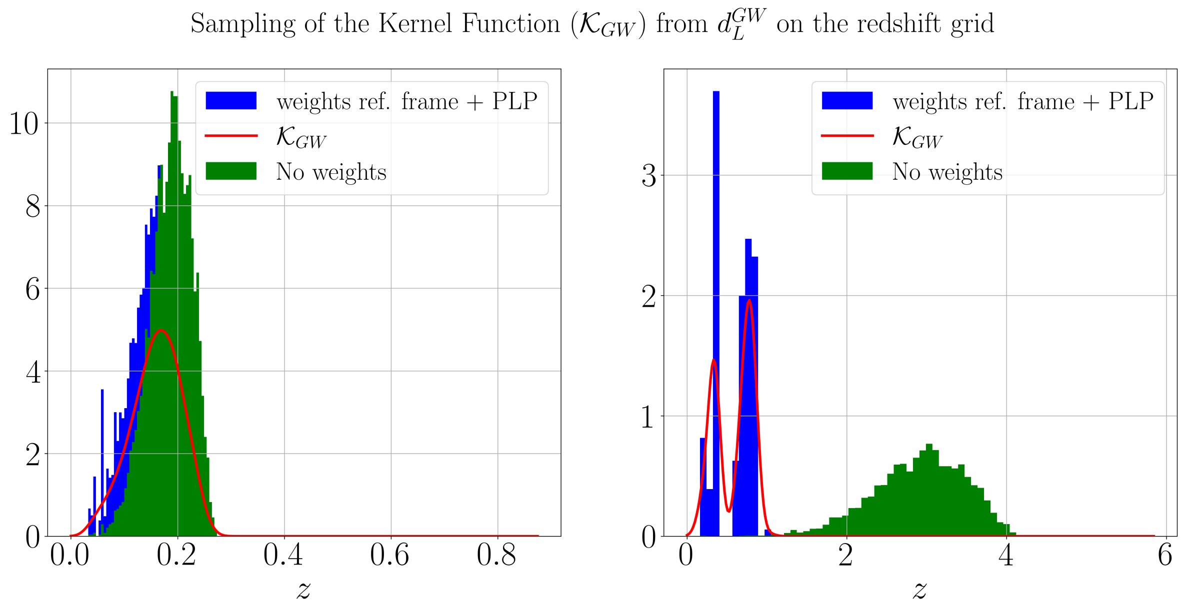

Figure 3.6: Histograms showing how the computation of the $\mathcal{K}_{\mathrm{GW}}$ happens and the clear importance of weights. In green is the depicted the p_{GW} for the same event in both pictures before the aforementioned weighting on the population parameters and shift to source frame. In blue what happens afterwards those considerations. In red the final $\mathcal{K}_{\mathrm{GW}}$ used for likelihood computation. This shows that the localization of the GW event is wrongly placed at higher redshifts if the re-weight is not considered. Left: The distributions without considering Ξ_0's effects are visualized, revealing the magnitude of influence on the redshift grid by only considering H_0. Right: The distribution also considers Ξ_0 effects. Clearly stating a predominant influence from Ξ_0 extending the redshift grid up to $z_{max} \sim 6$

this effect is again dumped by a large value of Ξ_0. Finally it is clear that the effect of n on shifting the posterior result very mild as previously said in Section 3.1.1 even at the highest allowed value of $n = 5$. Consequently to this analysis, n will be fixed to a single value consistent with the prior range, since it does not have notable effects in the posterior computation.

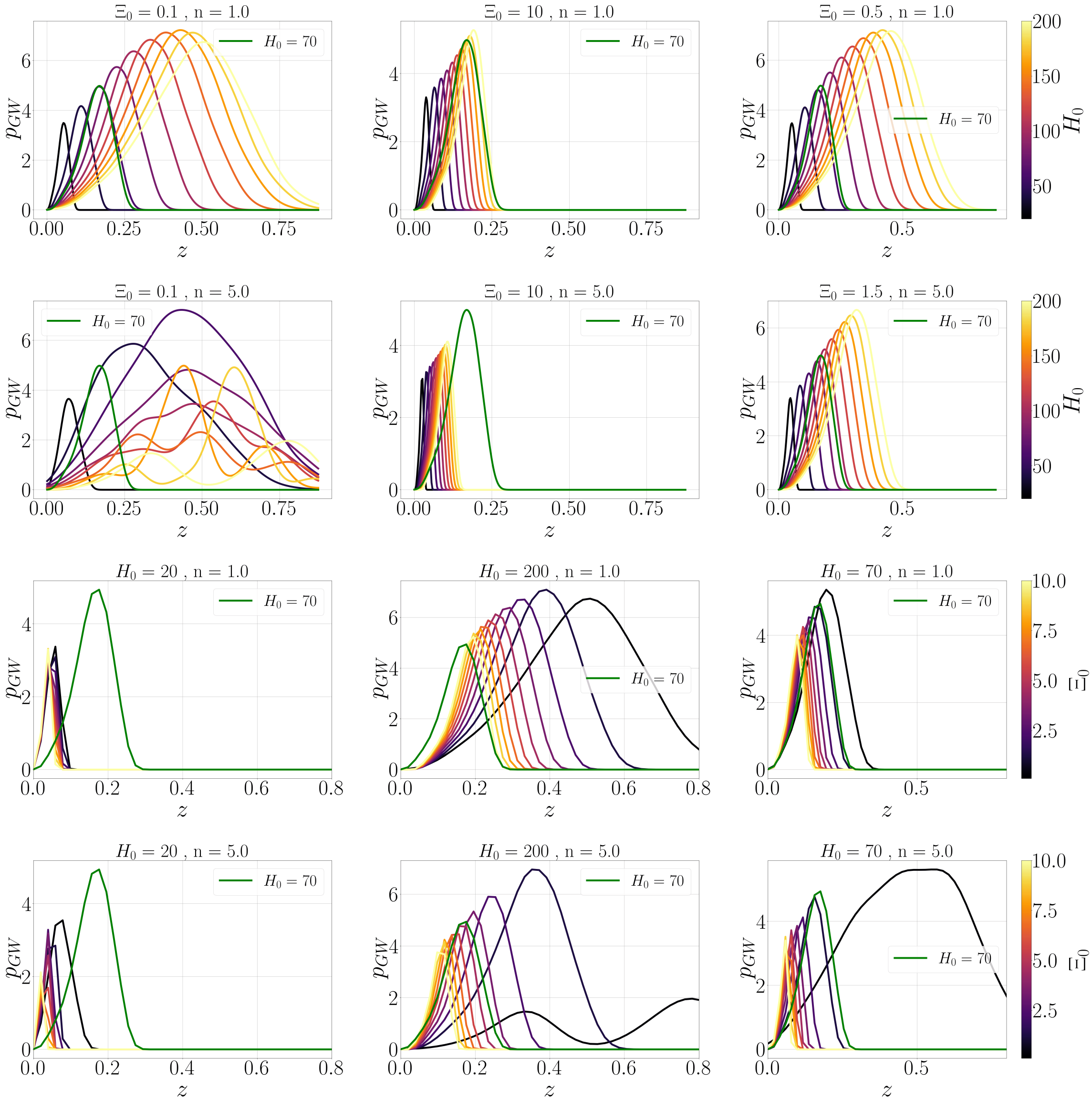

Figure 3.7: The figure represents the p_{GW} as function of z with either H_0 or Ξ_0 free and consequent fixed combination of parameters. First two rows: Effect of changing H_0 fixing different combinations of Ξ_0 and n. Revealing the positive correlation between H_0 with z, pushing p_{GW} to higher values of the z range. Second two rows: Effect of variations on Ξ_0 fixing H_0 and n revealing instead the negative correspondence between Ξ_0 and z with consequent shift of the p_{GW} to lower values.

3.2 Mock catalogs generation

The previous sections have described all the effects of the cosmological parameters on the localization of a GW to allow the correct computation of likelihood from the `CHIMERA` code. The likelihood computation is the core quantity for parameter inference which is nowadays done jointly with cosmological and astrophysical parameters for improved statistical accuracy. This feature, also implemented in `CHIMERA`, has been reached only recently for a better statistical representation of the results. Although this is better performed with higher accuracy with a larger number of events and stronger Signal-to-Noise ratio (SNR). For these reasons the constraints on parameters like Ξ_0 have been obtained with very large error-bars with relative error of the order of $\sim$ 20% of the constraint value (Mancarella, Finke, et al. 2022). Current and future GW analysis fortunately have increased the sensitivity of the LIGO-Virgo-KAGRA detector network from which are expected a large number of events at higher SNR, this will be able to improve the constraints on Ξ_0. For these reason it is interesting to forecast the detectability of modified GW propagation parameters using a future O5 observing run sensitivity. In order to do that mock GW observations are needed to describe said constraints. The generation of a mock GW event needs a specific workflow based on the following features:

- A mock parent galaxy catalog containing raw information about galaxies like sky-position referred to (RA, Dec), associated redshift, masses, Star Formation Rate (SFR) and other main quantities related to millions of galaxies.

- An associated GW event catalog encompassing a series of GW events at a high SNR value, for accurate localization. Each event related to a posterior which contains the probability of detecting GWs in a localization volume (RA, Dec, z).

- A code like `CHIMERA` for cross-correlating the galaxy catalog and the GW catalog.

This following section so, explores in details these features, additionally describing the workflow needed to generate and simulate these catalogs. The whole generation starts from a mock parent galaxy catalog associated to the GW events. This galaxy catalog initially contains millions of galaxies spanning a wide range of galaxy properties which is usually sub-sampled to contain a final catalog with plausible hosts of GW events. This is done through a mass cut ($M_{gal} > 10^{10} M_\odot$) and reshaped through re-weighting with a modeled merging rate of compact binaries so that the distribution of galaxies is transformed to one presenting possible GW emitters. The reason of this cut comes from the idea that more BBHs are expected in more massive galaxies as done by Borghi et al.

2024. This catalog obviously does not have yet the GW properties, so after selecting hosts, it is important to associate these to parameters related to gravitational waves, extracted from an assumed fiducial population distribution. From this, detections can now be simulated. They are generated with GWFAST (Iacovelli et al. 2022a), a code that uses event-like parameters and additional information on theoretical GW wave-forms to derive GW detections. This particular code simulates them through the computation of the Fisher Information Matrix (FIM). After this step the final mock GW catalog is generated, resulting in distributions called p_{GW} that will be cross-correlated to the parent galaxy catalog by `CHIMERA` to finally calculate the likelihood and perform joint inference for both cosmological and astrophysical parameters, deducting their constraints. In the following two sub-sections the parent and the GW events catalogs' properties will be described with a more extensive focus on explaining in depth how they can be generated and then employed for statistical analysis with `CHIMERA`.

3.2.1 The parent galaxy catalog

The parent catalog used for this work is based on the MICE Grand Challenge-light-cone galaxy simulation, covering one octant of the full sky and including galaxies with observed magnitudes in i-band $i < 24$ up to redshift $z < 1.4$. MICE has been generated assuming a ΛCDM cosmology with $H_0 = 70\ km/s/Mpc$, $\Omega_{m,0} = 0.25$, and $\Omega_{\Lambda,0} = 0.75$. The MICE galaxy catalog is then subsampled as explained above, to match the number density of galaxies with masses $M_{gal} > 10^{10.5} M_{\odot}$. This cut, also assumed in previous standard sirens studies (e.g., B. P. Abbott 2023; Borghi et al. 2024; M. Fishbach et al. 2019; S. Mastrogiovanni et al. 2021), is based on the idea that the compact binary merger rate is traced by stellar mass, i.e. more massive galaxies have higher probability of forming these systems, as also shown in synthetic population studies (e.g., Artale et al. 2020). With these prescriptions, the parent sample includes 1.6 millions massive galaxies.

Each galaxy is assigned a corresponding redshift uncertainty σ_z, to represent two typical regimes of current and future galaxy surveys: the photometric uncertainty obtained through future small areas surveys (e.g., Euclid Desprez et al. 2020, Schirmer et al. 2022) which can go to a depth of magnitude in H-band of 24, with an expected uncertainty of $\sigma_z/(1+z) \leq 0.05$ and spectroscopic uncertainty (e.g., Dark Energy Spectroscopic Instrument DESI Collaboration et al. 2016) planning to observe $\sim 14000 deg^2$ in a redshift range $[0.4; 2.1]$. So the two errors regimes that will be considered are:

$$\sigma_z = \begin{cases} 0.001(1+z) & \text{referred to as "}z_{\text{spec}}\text{"} \\ 0.05(1+z) & \text{referred to as "}z_{\text{phot}}\text{"} \end{cases} \tag{3.4}$$

3.2.2 The GW catalog

The GW events catalog is derived from the parent galaxy catalog under the assumption of GW population models with hyper-parameters $\lambda_c, \lambda_m, \lambda_z$

Because $\Omega_{0,m}$ does not have strong effects on luminosity distance it will be fixed to the fiducial value used for generating the parent galaxy catalog so $\Omega_{0,m} = 0.25$. The source frame merger rate is parametrized (Madau and Dickinson 2014) by :

$$\psi(z; \lambda_z) = \frac{(1+z)^\gamma}{\left(1 + \frac{1+z}{1+z_p}\right)^{\gamma+\kappa}} \tag{3.5}$$

assuming the following set of fiducial values: $\gamma = 2.7$, $\kappa = 2$ and $z_p = 3$, consistent with galaxy's star formation rate density parameters (R. Abbott et al. 2023). This rate will be used to re-weight the distributions of the parent catalog multiplying it with the detector-frame merger rate which is $\psi(z; \lambda_z)(1+z)$. This is fundamental to create a realistic GW detections catalog, since if it was not multiplied by that $1+z$ term it would result in biased detections.

The mass distribution is another important factor, used to describe the population probability p_{pop} (see Eq.2.56), for the terms that captures information about the mass distribution of compact objects: $p(m_1, m_2 \mid \lambda_m)$. Since this work is focused on analysis with dark sirens the best model for this distribution is the one found for BBHs. Initially it was thought to be a simple power law but recently this distribution was parametrized (B. P. Abbott 2023) as a Power Law + Gaussian Peak (PLP). This parametrization represents an extension of a truncated mass function, incorporating a Gaussian peak feature to account for the observed clustering of binary black hole (BBH) events with primary mass m_1 around $\approx 35 M_\odot$. This accumulation of events may arise due to the mass gap associated with pair-instability supernovae, which is expected to occur at slightly higher masses, just beyond this peak (Talbot and Thrane 2018).
The distribution of m_1 takes the form of :

$$p(m_1 \mid \lambda_p, \alpha, \delta_m, m_{low}, m_{high}, \mu_g, \sigma_g) = [(1-\lambda_p)P(m_1 \mid -\alpha, m_{high}) + \lambda_p G(m_1 \mid \mu_g, \sigma_g)]\, S(m_1 \mid m_{low}, \delta_m) \tag{3.6}$$

where P is a normalized truncated power-law distribution G is a Gaussian distribution with mean μ_g and standard deviation σ_g, and S is the smoothing function $S(m \mid m_{low}, \delta_m)$, which is a function that smoothly tapers to zero when m approaches m_{low} or m_{high} over a scale defined by δ_m (B. P. Abbott 2017b). While the distribution for the secondary mass m_2 is:

$$p(m_2 \mid \beta, m_{low}, m_1) \propto \begin{cases} m_2^{\beta} S(m_2 \mid m_{low}, \delta_m) & \text{if } m_{low} < m_2 < m_1 \\ 0 & \text{otherwise.} \end{cases} \tag{3.7}$$

The fiducial values for the hyperparameters λ_m for the Power Law + Peak (PLP) model are shown in table 3.1 as well as the fiducial for λ_c and λ_z. In Fig.3.8 are presented both example of mass distribution and rate that will be used in the GW event catalog generation.

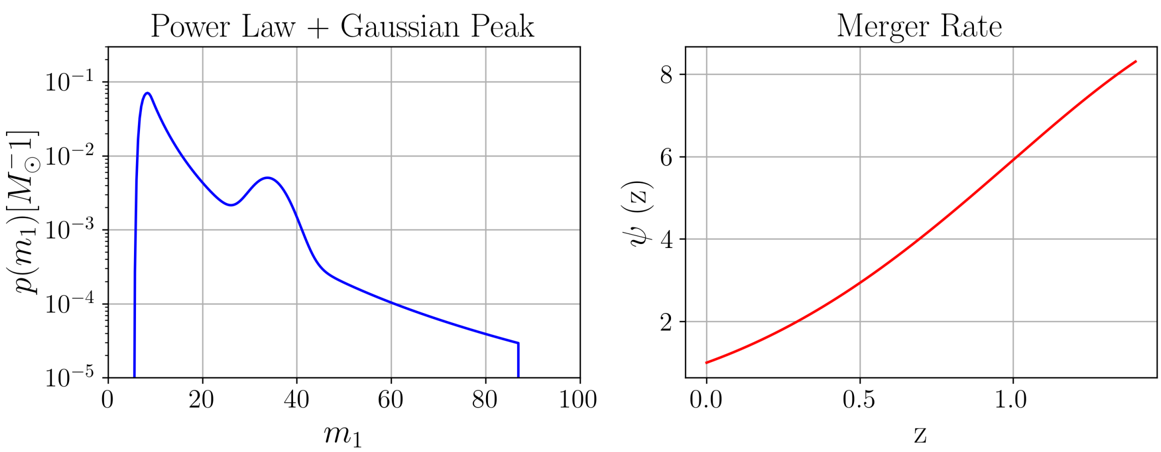

Figure 3.8: Left: Modeled PLP distribution of mass in range [0, 100], Right: Merger rate as function of redshift in range [0, 1.4]

3.2.3 Simulating GW detections

This subsection aims to present an overall description of how to simulate detections for the final GW event catalog. The catalog described before in the previous section is not enough to describe accurately a mock GW catalog, because it lacks of simulated GW detections. The whole point is to simulate how and if these events can be observed by a network of detectors. An interferometer detects a signal called h, which was already introduced in Chapter 2, called strain, representing a signal over frequency. It is depicted as a waveform from which astrophysicists can obtain information on a lot of parameters (like m_1, m_2, RA, Dec, ι, χ_1, χ_2), representing how and where this event happened. For a mock catalog this part is what is related to the simulation of detections, which accounts for errors on measurements deriving from the sensitivities of detectors. To have realistic data, the code needs to simulate errors from detectors, which are going to propagate over all the hyper-parameters. It needs combining initial event-like parameter's distribution, galaxies information and a simulated strain from a general mock wave-form, to obtain the errors on the detections parameters. These are represented as $\theta_{det} \pm \Delta\theta_{det}$ and are parameter with related uncertainty. The waveform of the events generated from CBSs systems are characterized by these detector-frame parameters:

$$\theta_{\text{det}} = \{\mathcal{M}_c, \eta, \chi_{1,z}, \chi_{2,z}, d_L, \theta, \varphi, \iota, \psi, t_c, \Phi_c\}, \tag{3.8}$$

where $\mathcal{M}_c$ is the detector-frame chirp mass, η is the symmetric mass ratio, $\chi_{1,z}$ and $\chi_{2,z}$ are the dimensionless spin parameters along the direction of the orbital angular momentum, d_L is the luminosity distance, $\theta = \pi/2 - \text{Dec}$ and $\varphi = \text{RA}$ are the sky position angles, ι refers to the inclination angle of the binary's orbital angular momentum with respect to the line of sight, ψ is the polarization angle, t_c is the coalescence time, and Φ_c is the phase at coalescence. Now, assuming the initial population distribution and rates described in Section 3.2.2, for quasi circular non precessing BBH systems, the distribution of the detector-frame parameters are generated using the pipeline GWFAST (Iacovelli et al. 2022a, Iacovelli et al. 2022b). This pipeline generates the FIM that defines the correlations among all these detector-frame parameters. For each event the distributions with the same covariance of the FIM are drawn by sampling the parameters space with a Monte Carlo Markov Chain (MCMC) with 5000 samples. This can be performed by GWFAST taking in input a series of specific settings:

- The subsampled galaxies file: MICEv2.
- A wave-form model: IMRPhenomHM.
- A Signal-over-Noise treshold: 20.
- Range of frequency: [10 ; ∞]Hz.

The choices of a waveform and the SNR threshold are crucial to generate a realistic mock catalog computing correct detectability of the GW. Considering a theoretical wave-form coming from BBHs merger, in this case the IMRPhenomHM, gravitational wave signals are generated in the given frequency domain for merging BBHs including the inspiral, merger and ringdown parts for the dominant mode of the signal (Husa et al. 2016, Khan et al. 2016). This is employed to derive the errors in a simulated detected signal through the sensitivity of the LVK detectors. The final strain is then computed, by integrating the GW signal in the ranges given by the input frequencies and correlating it with the responses of the detectors.

As detectors, for this thesis work, the O5 run is considered with a future LVK configuration. The network includes the following detectors with their maximum recoverable distance ranges for BBHs (30 $M_\odot$ + 30 $M_\odot$) and burst ranges assuming an emitted energy GW at $140Hz$ from $E_{\rm GW} = 10^2 Mc^2$ (B. P. Abbott et al. 2020). The network considered is:

- aLIGO: Advanced Ligo including an instrument in India that will join in 2025 corrisponding to a distance of 2500 Mpc with burst range to 210 Mpc
- adV: Advanced Virgo corresponding to distance in range between 1300-2500 Mpc with burst up to 100-155 Mpc
- Kagra: corresponding to a distance range of 1200 Mpc and more, and with burst range of 95 Mpc and more

Accounting for their sensitivities and considering their noise budget (in Fig.3.9) assuming a 100% duty cycle.

Among all the detections only a sub-sample of these will be considered: 100 events with SNR$>$ 25, to select the 100 best events for each configuration with 1 year of observation. The reason for this choice resides in the fact that the GW posterior probabilities are approximated with the FIM approximation so that they are assumed as multi-variate Gaussian distributions and this is valid only for high SNR events (Iacovelli et al. 2022a). This will allow to simulate the GW detections associating to each detection a set of distributions with θ_{det} and relative errors used then to calculate the likelihood. Additionally for a complete GWs catalog generation it is important to pre-compute the so called injections, they are sets of GW detections for O5-like events which are also generated using GWFAST, applying the same selection criteria described above. These injections are employed to calculate the selection bias in a pre-defined range of redshift which can also be represented as the maximum localization volumes that the detectors can achieve extending up to the detector horizon given the SNR thresholds. This means

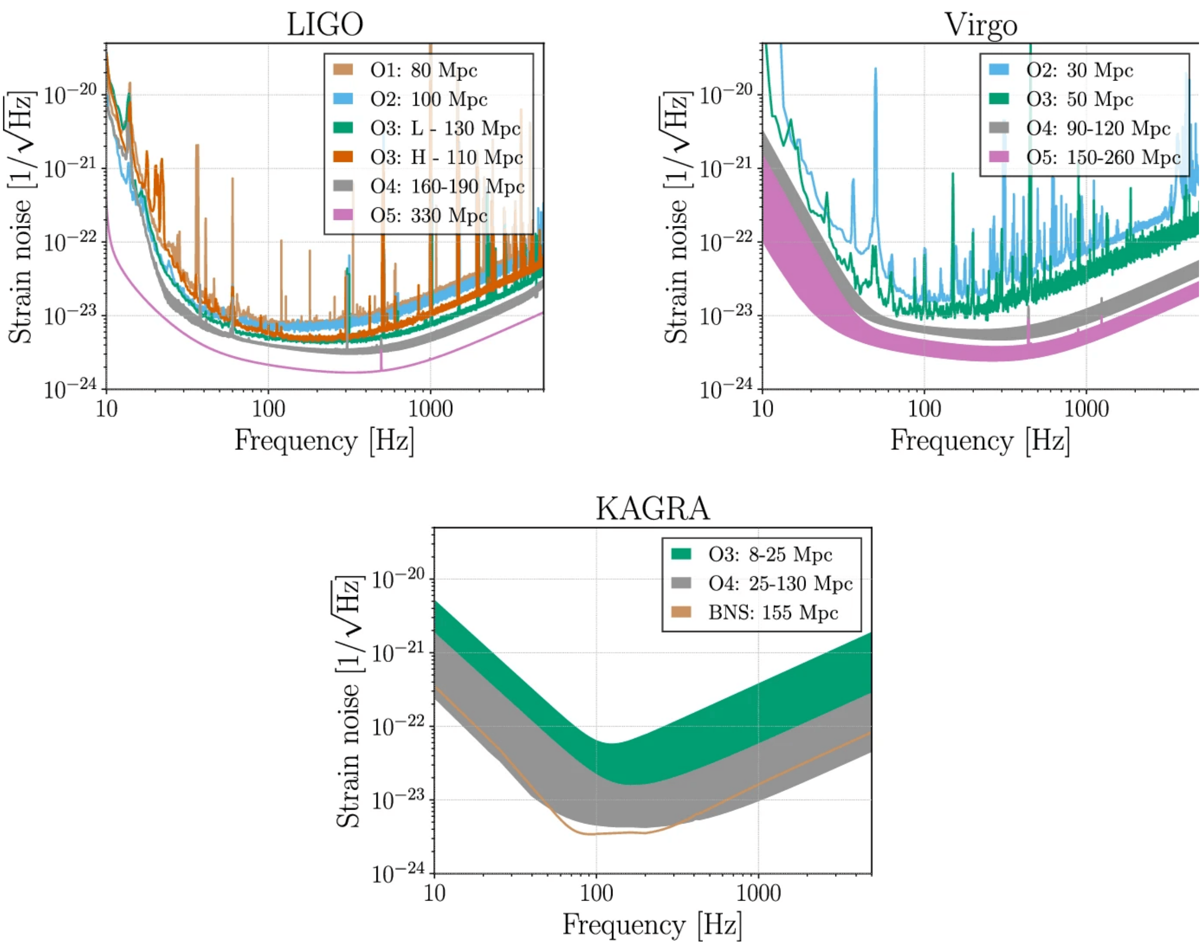

Figure 3.9: Strain noise for all the different observing runs O1-O5 for the three LVK detectors. The image was taken from B. P. Abbott et al. 2020 link: https://link.springer.com/article/10.1007/s41114-020-00026-9/figures/1

that the selection bias is pre-computed in a specific range of redshift containing also the 100 events employed in the analysis, otherwise the bias will be wrongly computed giving biased results. The injection set consists of $N_{\mathrm{inj}} = 4 \times 10^7$ events, resulting in approximately in 10^6 detected events, used to estimate the selection bias.

3.3 Properties of the catalogs

After describing how the event catalog can be generated and how the feature of the parent galaxy catalogs is employed to be be cross-correlated by `CHIMERA`, this section aims to

Table 3.1: List of initialized parameters for the catalogs building

	H_0	Ξ_0	n	λ_p	α	β	δ_m	$m_{\rm low}$	$m_{\rm high}$	μ_g	σ_g	γ	κ	z_p
GR	70.0	1.0	0.0	0.039	3.4	1.1	4.8	5.1	87.0	34.0	3.6	2.7	3.0	2.0
MG_1	70.0	1.8	1.91	0.039	3.4	1.1	4.8	5.1	87.0	34.0	3.6	2.7	3.0	2.0
MG_2	70.0	0.6	1.91	0.039	3.4	1.1	4.8	5.1	87.0	34.0	3.6	2.7	3.0	2.0

describe the main mock event catalogs analyzed in this work with an overview over its properties and use. The motivation for generating new catalogs comes from the necessity of exploring the constraining power of O5 future runs in deviating models from GR. The work done by Mancarella, Finke, et al. 2022 shows promising results in the possibility of constraining deviations from MG theories. Additionally, Leyde et al. 2022, forecasting the O5 configuration constraining power for modified GW propagation with spectral sirens, highlights the fact that the constraining errors on all the hyper-parameters will be influenced by the cosmological model itself, which means from the initialized values of Ξ_0 and n with which the GW detections are generated. Therefore, considering these works we generate two new catalogs in a modified GW propagation scenarios with specific combinations of Ξ_0 and n in order to derive the O5 configuration constraining power, in particular MG frameworks, which will be done for the first time, using a combined galaxy catalog and spectral siren method. The choices for the parameters are taken accordingly to the priors ranges presented in Tab. 3.2 and chosen from the observational constrain with dark sirens found of $\Xi_0 = 1.2^{+0.7}_{-0.7}$ (Mancarella, Finke, et al. 2022). Ξ_0 is initialized to the limit values of the constrain, while n resulting statistically unconstrained was fixed to $n = 1.91$ which is the values that Leyde et al. 2022 uses.

For this work the following catalogs will be considered:

- `GR`: ΛCDM catalog with $\Xi_0 = 1$ and $n = 0$ borrowed from the work of Borghi et al. 2024 generated for basic analysis to reveal the constrains for O5 runs in a GR scenario.

- $\mathtt{MG}_{1.8}$: Modified GW propagation catalog initialized with $\Xi_0 = 1.8$ and $n = 1.91$ generated for this work to understand the constrains for O5 runs from modified GW propagation scenario with $\Xi_0 > 1$ to be compared with the results of Mancarella, Finke, et al. 2022 and Leyde et al. 2022.

- $\mathtt{MG}_{0.6}$: Modified GW propagation catalog initialized with $\Xi_0 = 0.6$ and $n = 1.91$ generated for this work to reveal for the first time the constrains for O5 runs from modified GW propagation scenario with $\Xi_0 < 1$.

Before using these catalogs for any analysis they needed to undergo a small process of revision. Since GWFAST generates simulated distributions for parameters which might contain outliers or problematic distributions these catalogs go through a series of conditions checks:

- Presence of un-physical events ($d_L^{GW} > 0$)
- Presence of too low number of sampling for the events ($N_{samples} \geq 5000$)

The total number of detectable source were, in the GR case ≈ 7000, while ≈ 3000 in both the MG cases. This was all selected in the same range of redshift for all the catalogs as shown in Fig.3.10 to perform correctly the analyses and not overestimate the selection bias. The number of detections though was not as expected. Because of deviations from GR, the signal that arrives from fixed redshift results at a higher or lower distance, respectively to the $\mathtt{MG}_{1.8}$ and $\mathtt{MG}_{0.6}$ catalogs, meaning that in the first case they will be less detectable than GR scenario, while in the second case they would be more detectable. Looking at the luminosity distance distributions in Fig.3.10 the change of Ξ_0 generates a variation of the ranges of d_L^{GW} because of its cosmology dependency easily deducted from the Eq.2.50. If $\Xi_0 > 1$ the luminosity distance for that scenario would be higher, meaning that, for the same redshift range the detectability would be lower showing less detections. The opposite for $\Xi_0 < 1$. This was also expected and recognized in Leyde et al. 2022. This happened for $\mathtt{MG}_{1.8}$ but not for $\mathtt{MG}_{0.6}$. One reason for this might be that the computational time was different from the GR case. Although, this result must be explored in the future with an extensive simulation of GW detections in modified GW propagation so that the expected results can be matched from what is simulated. Fortunately, this will not affect our analyses because the number of considered events will be much lower than the total number of detections. To support this, the detections' SNR are also shown in Fig.3.10. It is possible to observe that the majority of the events are with SNRs much lower than 25, but since the high-SNR approximation is needed, the final event catalog will encompass only 100 detections with SNR> 25. Moreover, it is important to note that the final GW catalogs will contain every event-like parameter initial distribution samples which are related to the modeled population distributions, for this reason all the samples will be the same for all three catalogs except luminosity distance, which depends on cosmology. For simplicity, only the redshift one has been depicted here in Fig.3.10. The reason why redshift is fixed, comes from two necessities;

firstly in order to allow the high-SNR approximation to hold and secondly because the same injections are used for all three catalogs, and if the redshift changed then we would expect biased results.

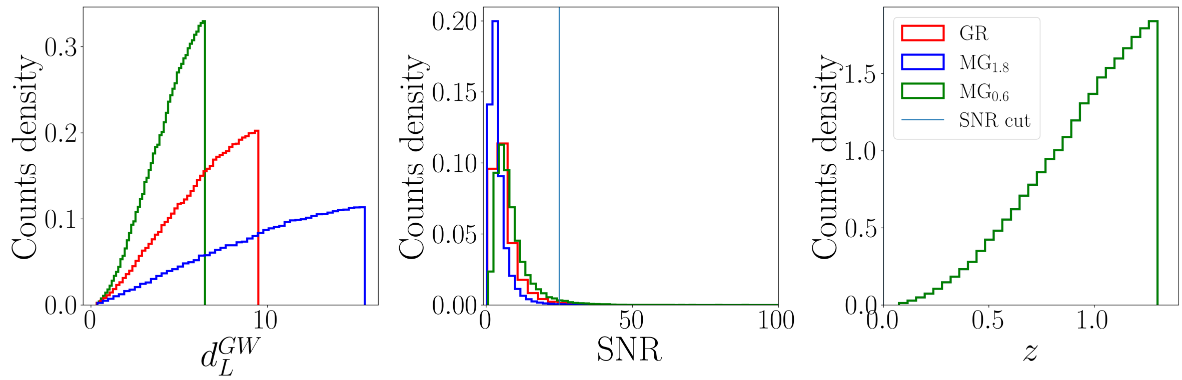

Figure 3.10: Sampled distribution of multiple GW observables for all the considered catalogs. Left: Distribution of luminosity distance which is influenced by the chosen λ_c. Center: SNR distribution of all the events with a vertical line representing the limit at which the GW catalog is subsampled (SNR $>$ 25). Right: Redshift distribution fixed for every catalog. The counts were normalized over the total number of data points and the width of each bin.

In Fig 3.11 are presented the localization and d_L^{GW} uncertainties for the new catalogs, on a redshift color-map, and the highlighted sub-sampled 100 events that will be used in the statistical analysis with `CHIMERA`. Fig.3.12 instead is similar but with a different color-map on SNR. These two figure combined show the effects of modified GW propagation on the detection of GWs. Comparing left and right, higher Ξ_0 reveals lower reachable redshift so lower d_L^{GW}, which means that these sources are the ones that most likely are going to be detected. While lower Ξ_0 shows the opposite. Through this section, the analysis of the catalogs' properties has been explored to support the choices for the modified GW propagation values with which the catalog has been generated. After defining all the generation processes and revealing features of the GW catalog, in the next chapter, their statistical analyses will be described, to reveal how these deviations of GR will have huge consequences on the constraints of the parameters.

Table 3.2: Priors and definition of all the parameters used in the analysis, $\mathcal{U}$ represent a label for a uniform prior, which means that the prior is considered uniform, so it is the same value of probability, for the entirety of the range. These priors are considered constant in redshift.

Parameter	**Definition**	**Prior**
H_0	Hubble constant	$\mathcal{U}(20.0, 200.0)$
Ξ_0	Modified gravity parameter controlling high-z limit of distance ratio in Eq. (2.7)	$\mathcal{U}(0.10, 10.0)$
n	Modified gravity parameter controlling steepness of distance ratio in Eq. (2.7)	$\mathcal{U}(1.00, 5.00)$
λ_p	Fraction of the model in the Gaussian component	$\mathcal{U}(0.01, 0.99)$
α	The power of the power law component in the primary mass distribution	$\mathcal{U}(1.50, 12.0)$
β	The power of the power law component in the mass ratio distribution	$\mathcal{U}(-4.0, 12.0)$
δm	Range of mass tapering at the lower end of the mass distribution	$\mathcal{U}(0.01, 10.0)$
m_{low} [M$_\odot$]	The minimum mass of the mass distribution	$\mathcal{U}(0.01, 50.0)$
m_{high} [M$_\odot$]	The maximum mass of the mass distribution	$\mathcal{U}(50.0, 200.0)$
μ_g	Mean of the Gaussian component in the primary mass distribution	$\mathcal{U}(2.00, 50.0)$
σ_g	Width of the Gaussian component in the primary mass distribution	$\mathcal{U}(0.40, 10.0)$
γ	The power of the power law distribution of the rate evolution before redshift z_p	$\mathcal{U}(0.00, 12.0)$
κ	The power of the power law distribution of the rate evolution after redshift z_p	$\mathcal{U}(0.0, 6.0)$
ζ_p	The redshift turning point between two power law distributions	$\mathcal{U}(0.0, 4.0)$

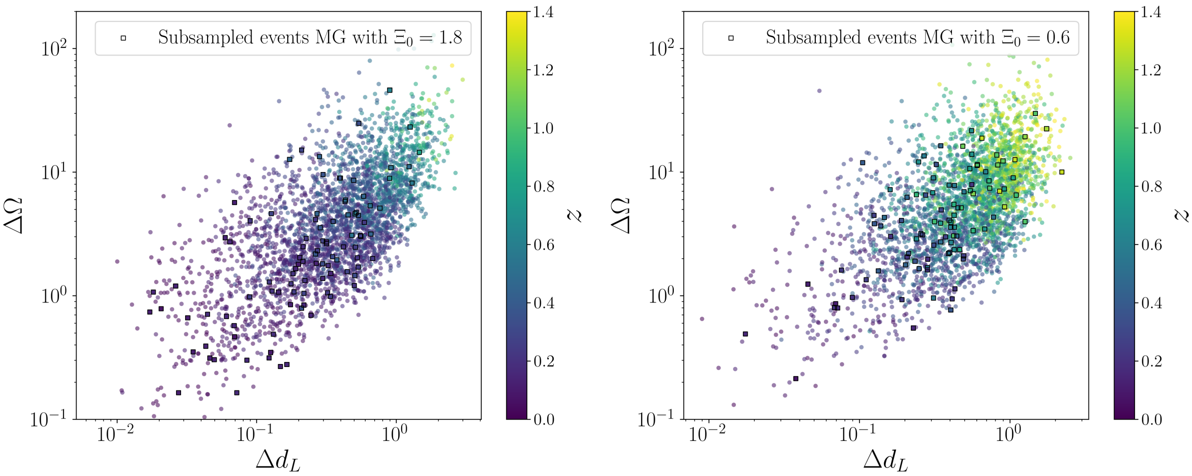

Figure 3.11: Figure showing the errors on localization and luminosity distance for the two new catalogs catalogs, on a redshift color-map, highlighting the 100 events chosen from the total number of detected source. Left: The MG scenario with $\Xi_0 = 1.8$ showing that the majority of detected events' redshifts are lower than 1, supporting the results for which these detections will have a lower value of d_L^{GW} . Right: MG scenario with $\Xi_0 = 0.6$ the majority of the events has a redshift around 1 and more, saying that the d_L^{GW} result higher

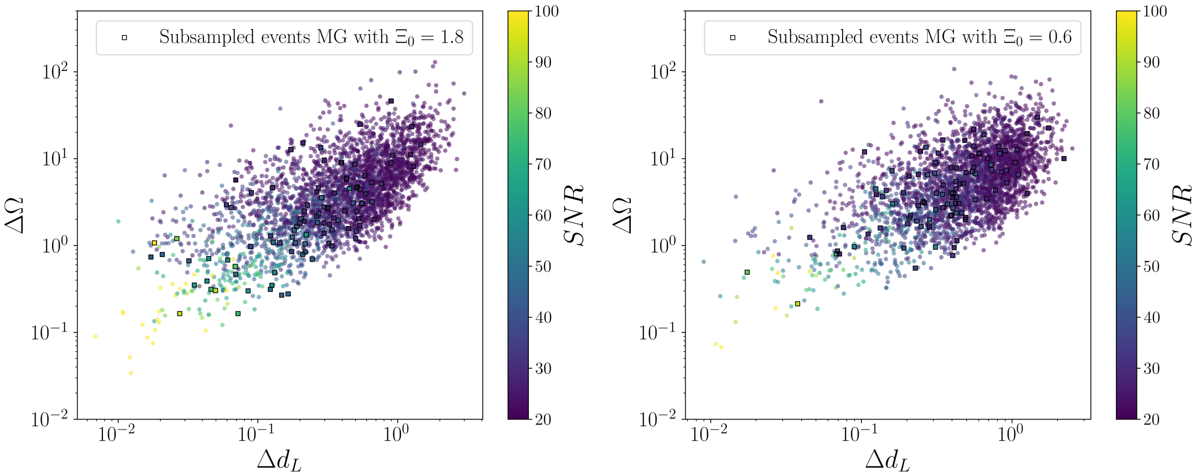

Figure 3.12: Figures showing the errors on localization and luminosity distance for the two catalogs, on an SNR color-map, Left: MG scenario with $\Xi_0 = 1.8$. Right: MG scenario with $\Xi_0 = 0.6$

Chapter 4

Forecasts on modified GW propagation constraints

This chapter presents the constraints on modified GW propagation expected from the fifth LVK observing run (O5). The analysis builds upon the catalogs generated in Chapter 3.2, each including 100 BBH events with SNR > 25 to represent about one year of observations. For the first time, these constraints are obtained through a joint cosmological and astrophysical dark siren analysis, combining information from GW detections and a catalog of potential host galaxies. This is done using `CHIMERA` (Borghi et al. 2024) extended with MG propagation functions (see Chapter 3.1)

The analyses are carried out in two stages. Initially, we compute one-dimensional posteriors for all hyperparameters by fixing all parameters except one. A more comprehensive analysis is then done by exploring the full likelihood in a 14-dimensional parameter space using an MCMC approach. These will be used to investigate the forecasts of determining cosmological parameters and the degeneracies among these, done to derive the constraining power of the future LVK observing runs in different scenarios with modified GW propagation.

4.1 Analysis in one-dimensional parameter space

This section presents preliminary results in one-dimensional parameter space, i.e. for individual hyper-parameters fixing the remaining ones to their fiducial values. This provides a first assessment of O5 capabilities, as well as a first benchmark to identify potential biases in both catalog generation and likelihood implementation. This is generally carried out by cross-correlating gravitational wave data with galaxy catalogs, which can include spectroscopic or photometric information on redshift uncertainty, or alternatively the spectral siren method can be used. As explained in Section 3.2, the setup for these three cases is diversified by the uncertainty on the redshift, which means that a galaxy is localized differently so that the resulting probability of hosting one specific event will be influenced by the redshift's uncertainty. The errors are: spectroscopic $\sigma_{spec} = 0.001$, photometric $\sigma_{phot} = 0.05$. This will affect the analysis seen in the next sections, carrying out the first parameter constraint with a GW catalog that considers modified GR scenarios and then modified GW propagation scenarios.

Cosmological parameters in GR

We start by considering one-dimensional posteriors of the MG parameter Ξ_0 and the Hubble constant H_0. The analysis is carried out by adopting the modified GW model functions presented in Section 2.4 and the GW catalog with `GR` propagation. To be more sensitive to potential biases, the GW data is cross-correlated with the spectroscopic galaxy catalog (see Section 3.3). The upper panels of Figure 4.1 show the results for H_0 and Ξ_0 when assuming the fiducial cosmological model used to generate the catalog. The upper-left figure shows the posterior for H_0, with $\Xi_0 = 1$ fixed at its fiducial values in `GR`, when this happens, no bias on H_0 is observed since the posterior peaks at its fiducial value, standing as validation of correctly implementing Eq.2.49 inside module MG_FLRW allowing to recover the true H_0 when $\Xi_0 = 1$. The uncertainty found fixing the rest of the parameters is $\sim 1\%$ this is comparable with the uncertainty found by Borghi et al. 2024 carefully noting that they found this constraint with an MCMC approach. In parallel, the upper-right figure shows the posterior for Ξ_0 at fixed $H_0 = 70$, both with the rest of the parameters set to their fiducial values (as seen in 3.1). The same happens for Ξ_0, by fixing the rest of the parameters to the fiducials, the final posterior centers the fiducial value belonging to `GR`. The value found for Ξ_0 in this one-dimensional posterior approach is $0.98^{+0.12}_{-0.8}$ with a relative error of $\sim 10\%$. This is obtained in the best case scenario, assuming correct knowledge on the other parameters related to the GW population with 1 year of O5 observations for 100 GW events with SNR> 25. It is interesting so to compare these findings with the ones of an MCMC approach which are more statistically accurate. These could be later compared to the results found by Leyde et al. 2022, they used the spectral sirens approach simulating detections in an O5 scenario detecting 400 simulated events for an SNR cut > 11.

Figure 4.1 (lower panels) shows instead the H_0 posteriors when fixing Ξ_0 incorrectly at 0.5 (lower left) and 1.5 (upper left). The choices for the different values of Ξ_0 here were completely arbitrary and do not rely on any prior assumptions. In this case, the wrong assumption on Ξ_0 are considered, showing a bias on the retrieved H_0 of $\sim 9\%$ for both. This is the first proof of what is revealed in Section 3.1, showing a positive correlation between H_0 and Ξ_0. In fact from Eq.2.49, fixing redshift, $\Xi_0 > 1$ means that the GW's luminosity distance results less than the electromagnetic one 2.48, forcing the cosmological model to compensate for this discrepancy with an increase in H_0. The opposite happens for $\Xi_0 < 1$.

Full population parameters in GR

This subsection aims to verify the impact of wrongly assuming a modified GW model on every parameter considering both astrophysical and cosmological parameter not discussed in the previous subsection. Figure 4.2 presents the `GR` catalog results for all the population parameters considered in this work (for their definition see table 3.1).

It has been produced setting the same catalog setup and depicting a posterior by fixing Ξ_0 in three different versions, the correct GR case with $\Xi_0 = 1$ and modified GW propagation case wrongly assuming $\Xi_0 > 1$ and $\Xi_0 < 1$. First of all, as expected, if $\Xi_0 \neq 1$ it imposes a bias on the posterior, with some ulterior modification in its shape for some of them. For H_0 the bias presented here is equal to Fig.4.1. However for the rest of the parameters the posterior will shift differently according to their positive or negative correlation with Ξ_0. Most of them are positively correlated except α and m_{low} that suffer the opposite shift being negatively correlated to Ξ_0. Meanwhile, parameters like κ and z_p are still unconstrained. Parallel to the known effect resulting from the wrong cosmological model, it appears that even considering the correct value for Ξ_0 using a spectroscopic redshift catalog, the astrophysical parameters' posteriors, do not center all the fiducials. The reason why, resides in the generation of the initial samples. Which are randomly chosen among all detections and so a little inaccuracy is expected. The only crucial factor is that these posteriors reside at least at 1σ from the fiducial.

Cosmological parameters in modified GW propagation

The explored results in the previous section have revealed the possibility to constraint Ξ_0 and H_0 in a `GR` scenario with one-dimensional posteriors. Following the same setup: the spectroscopic galaxy catalog is cross-correlated with the GW catalogs introduced in Section 3.2.3, $\mathtt{MG}_{1.8}$ and $\mathtt{MG}_{0.6}$, producing the one-dimensional posterior, for both Ξ_0 and

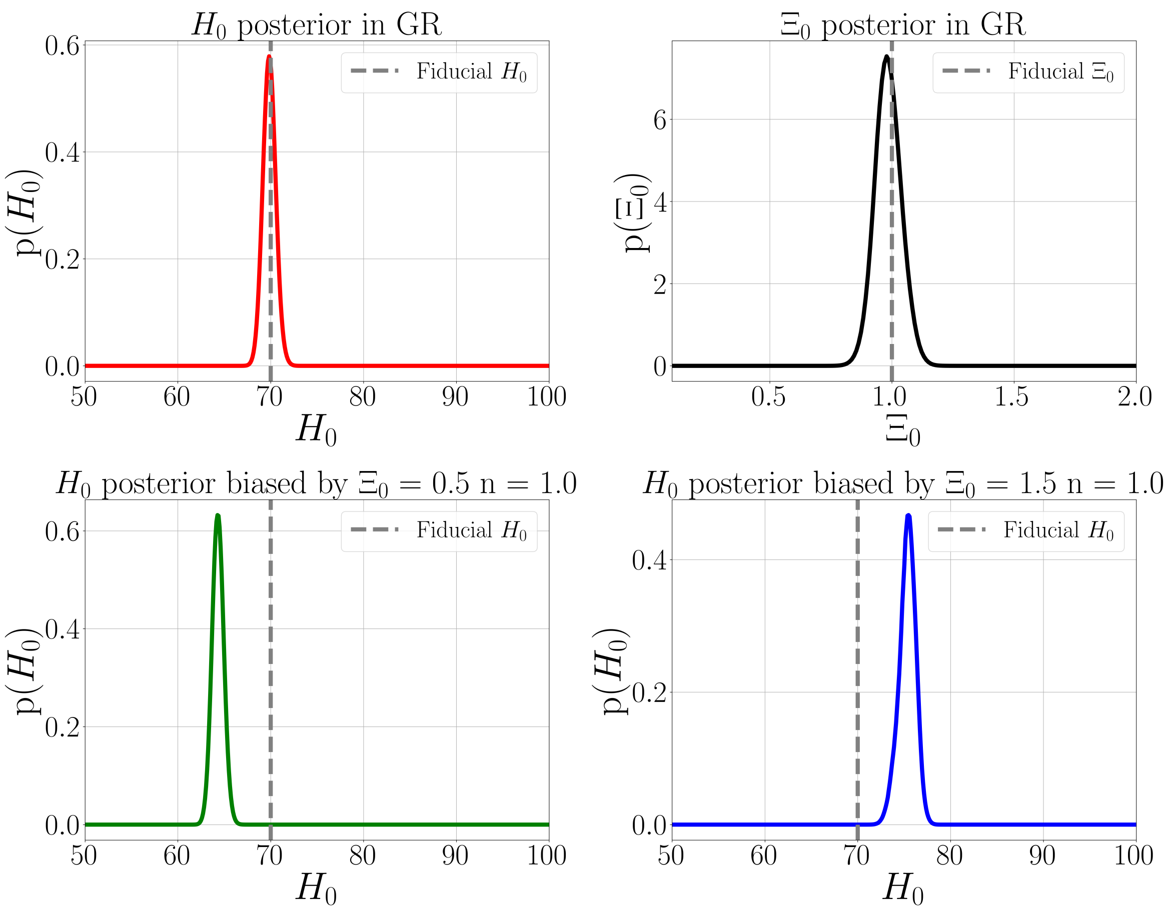

Figure 4.1: One dimensional posteriors on cosmological parameters for the `GR` catalog. *Upper panels*: Constraints on H_0 and Ξ_0 when assuming the correct cosmology. In this case, we recover unbiased values. *Lower panels*: Constraints on H_0 assuming wrong values for Ξ_0. A significant bias on H_0 is observed due to the positive correlation between H_0 and Ξ_0.

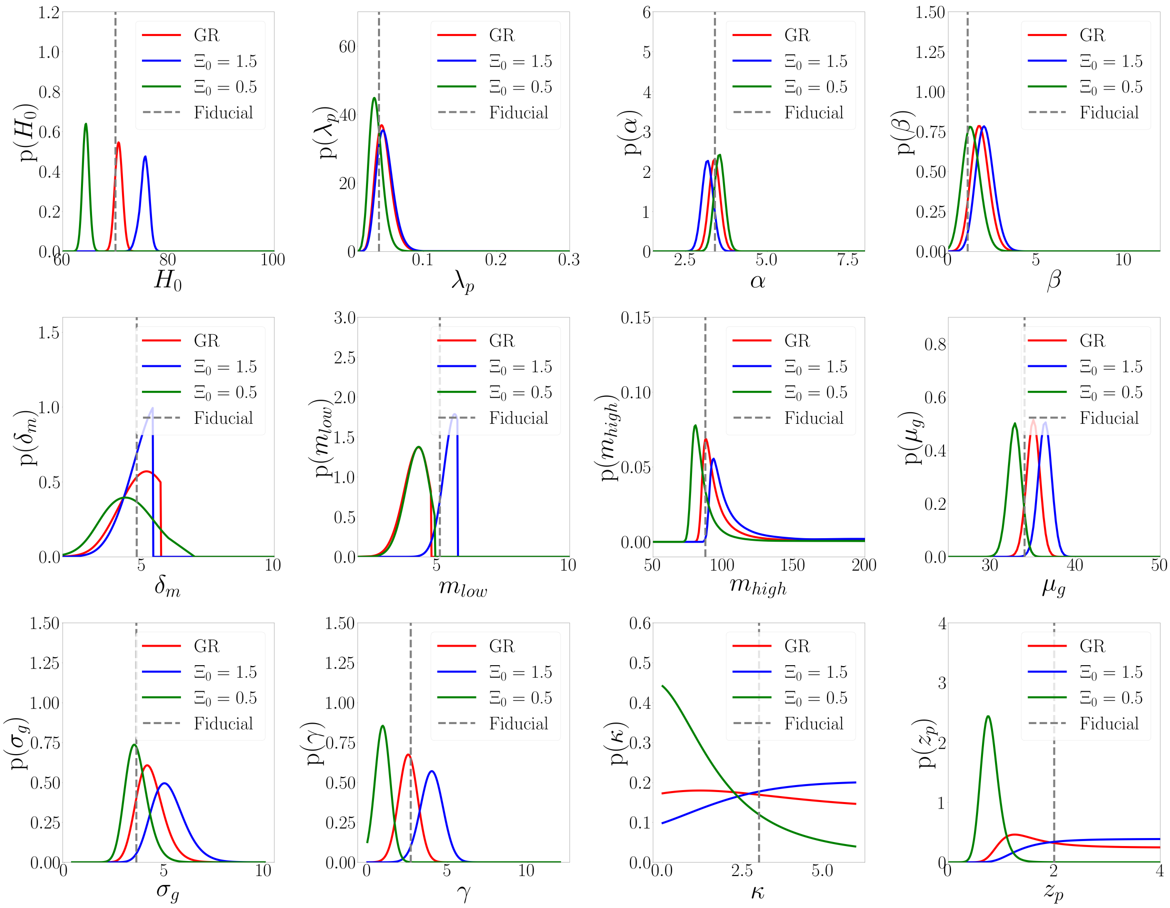

Figure 4.2: Multiple parameters posteriors obtained by considering spectroscopic error on galaxy redshifts' and calculated with three different values of Ξ_0, in red GR ($\Xi_0 = 1$), while in blue and green Ξ_0 is changed respectively to a 1.5 and 0.5. These two cases result in biased posteriors in all the parameters, again because of wrongly giving Ξ_0 values different from the fiducials of `GR` case.

H_0, fixing the parameters accordingly to the respective fiducials as defined in Tab.3.1. They are employed in order to test if considering modified GW propagation scenarios the cosmological parameters can be constrained. Fig.4.3 reveals H_0 and Ξ_0 posteriors for the different GW catalogs, showing that these parameters can be recovered by fixing the rest of the parameters to the correct simulated model. In the top row, H_0 and Ξ_0 values are recovered for a modified GW propagation model $\mathtt{MG}_{1.8}$ assuming correct fiducial values. This proves that also for $\mathtt{MG}_{1.8}$ model the values of H_0 and Ξ_0 can be constraint, finding $H_0 = 70$ with a relative error of $\sim 3\%$ while $\Xi_0 = 1.77$ with relative error of $\sim 10\%$. This can be compared once more with the findings of Leyde et al. 2022, who provided forecasts for O5 using the spectral siren method with an MCMC approach, reporting a relative error of approximately $\sim 20\%$. It is important to note, however, that the methodologies differ, as our analysis generates one-dimensional posteriors and incorporates a comprehensive galaxy catalog with spectroscopic redshifts. Despite these differences, the approaches are complementary and yield comparable results.

In the bottom row, the results for the $\mathtt{MG}_{0.6}$ model are presented. Here, H_0 and Ξ_0 can also be constrained, providing new predictions for their uncertainties within this specific modified GW scenario. By fixing all other parameters to their fiducial values, we obtain $H_0 = 70$ with an uncertainty of approximately $\sim 4\%$, while the relative error on Ξ_0 is around $\sim 10\%$. These results indicate that the constraints on H_0 are triple compared to the GR model scenario, while Ξ_0 has similar uncertainties. This highly suggests performing a full MCMC analysis approach, where the currently fixed parameters are allowed to vary, to explore more H_0 and Ξ_0 degeneracy and respective uncertainties.

Full population parameters in modified GW propagation

The second part of the one-dimensional analysis involves generating one-dimensional posteriors for all parameters, considering the new GW catalogs $\mathtt{MG}_{1.8}$ and $\mathtt{MG}_{0.6}$ introduced as in Sec.3.2.3. These analyses will be conducted using three distinct methods: dark sirens with redshift measurements from two galaxy catalogs, one incorporating spectroscopic uncertainties and the other photometric uncertainties, and the spectral sirens method for scenarios with empty galaxy catalog. Until now, with the exception of the work on spectral sirens by Leyde et al. 2022, the impact of modified GW propagation has not been extensively explored, especially in scenarios involving a full galaxy catalog with both spectroscopic and photometric redshifts. For this reason, results involving modified GW propagation with galaxy catalogs in an O5 scenario are both innovative and significant to explore. In Figs. 4.4 and 4.5 the posteriors on all parameters are shown. The

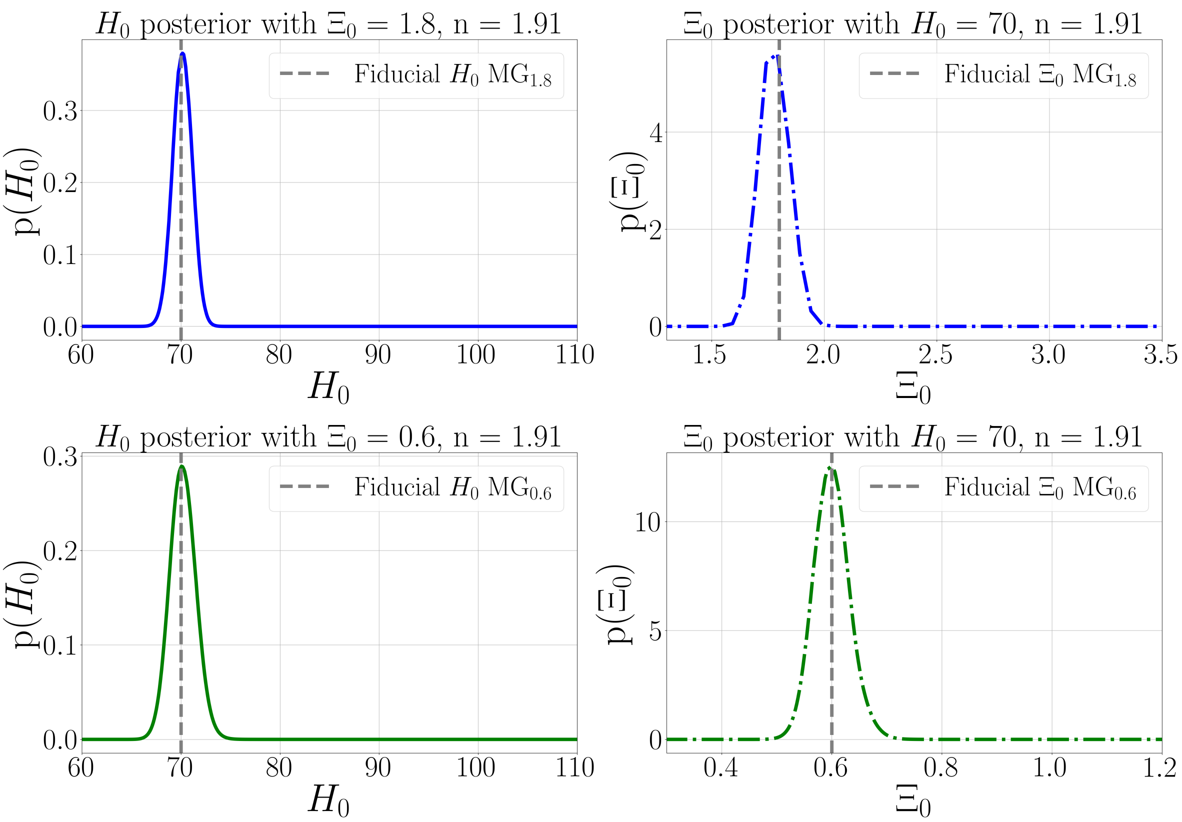

Figure 4.3: One dimensional posteriors on cosmological parameters for the $\mathtt{MG}_{1.8}$ and $\mathtt{MG}_{0.6}$ catalogs. *Upper panels*: Constraints on H_0 and Ξ_0 for the simulated $\mathtt{MG}_{1.8}$ model, obtained by fixing $\Xi_0 = 1.8$ to constrain H_0 and fixing $H_0 = 70$ to retrieve Ξ_0. *Lower panels*: Similar constraints for the $\mathtt{MG}_{0.6}$ model, with H_0 constrained by fixing $\Xi_0 = 0.6$ and Ξ_0 retrieved by fixing $H_0 = 70$. In both cases, the correct values are recovered without bias, offering a preliminary indication of the potential to constrain H_0 and Ξ_0 in modified GW propagation models. Final MCMC runs will further refine these results.

first figure depicts the ones for $\Xi_0 = 1.8$ and $n = 1.91$, while the second for $\Xi_0 = 0.6$ and $n = 1.91$. Both show that the spectroscopic case is the best one, with posteriors centered on the fiducial value (carefully noting that in this modified scenatio the fiducial for Ξ_0 and n are different than `GR`'s, as defined in Tab. 3.1). It is clear that the cosmological parameter's posteriors for the three different galaxy catalogs are centering the fiducial, with just a small deviation close to 1σ. This shows that no bias is found in any of the three cases and reports that the spectroscopic galaxy catalog has the lowest errors on the parameters.

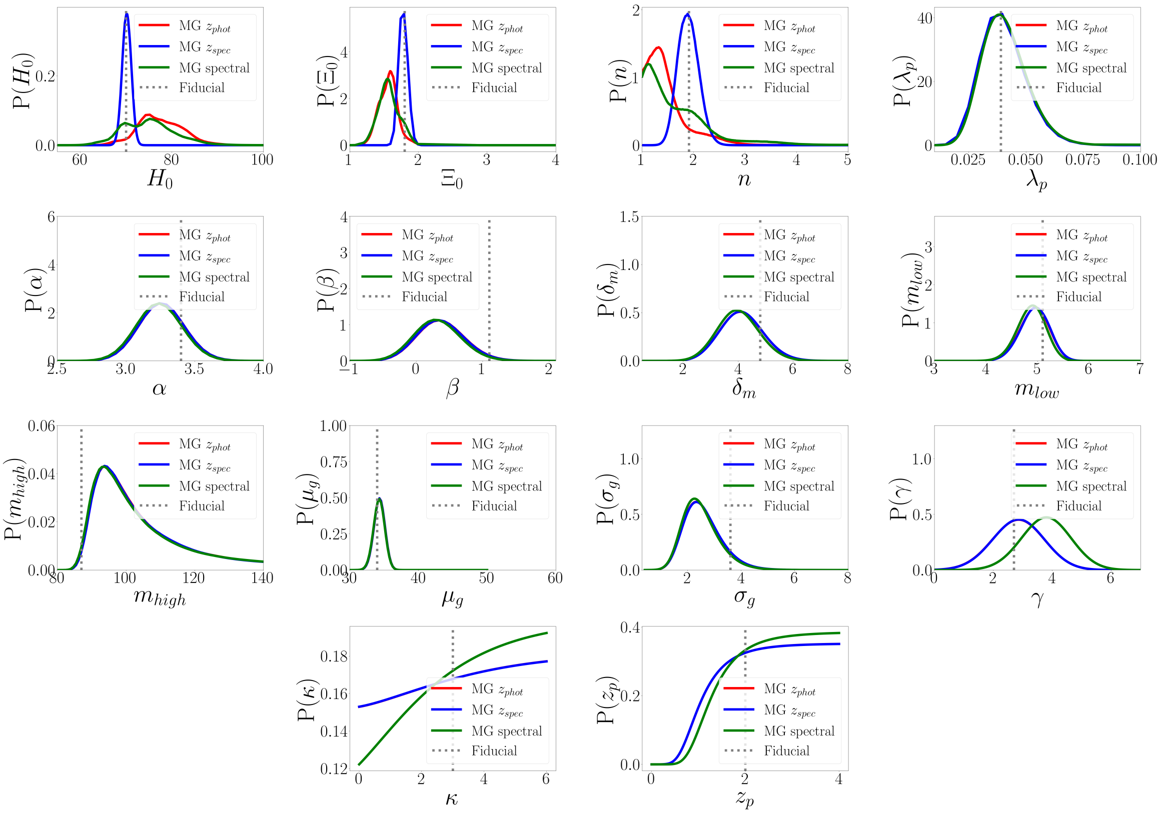

Figure 4.4: Multiple parameters for GW catalog with $\Xi_0 = 1.8$ and $n = 1.91$ with different sensitivities. In blue posteriors for z_{spec} uncertainty. In red posteriors with z_{phot} uncertainty. In green posteriors in the spectral sirens case.

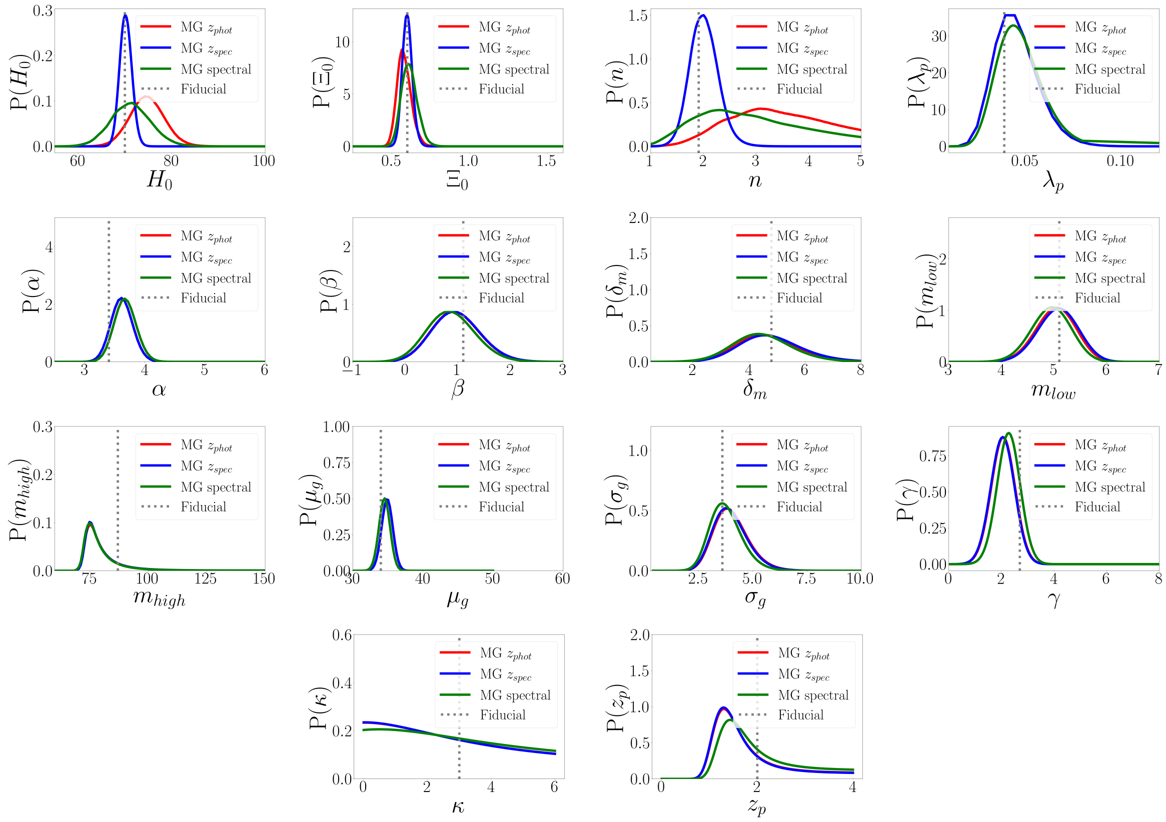

Figure 4.5: Multiple parameters for GW catalog with $\Xi_0 = 0.6$ and $n = 1.91$ with different sensitivities. In blue posteriors for z_{spec} uncertainty. In red posteriors with z_{phot} uncertainty. In green posteriors in the spectral sirens case.

4.2 MCMC analysis

The previous section provided a preliminary study aimed at two objectives. First, to demonstrate that posterior distributions are significantly biased if the fixed hyper-parameters differ from those used for generating the GW catalog. Second, to identify the optimal redshift uncertainty case to use. The one-dimensional posteriors are computed by fixing all the other parameters to the fiducial values except one which is left free. They represent optimal tools for visualizing biases and interpreting constraints on individual parameters, although locking specific values loses information by breaking the degeneracy among the parameters simplifying the interpretation of the results. They can still show some correlation, for example Ξ_0 biases H_0 and this propagates to other quantities, however it loses information on the correlation among other parameters. This leads to the motivation for this section. As shown in Tab.3.2, there is considerable uncertainty in the prior knowledge of all parameters, so to explore correlations and degeneracy it is logical to adopt a method that allows for all parameters to vary freely when computing the likelihood. While a brute-force approach is possible, it is computationally expensive. Instead, for this work the employment of MCMC sampling method is done.

To achieve this, MCMC sampling was performed on the OPH-DIFA cluster at the University of Bologna. The sampling in a 14-dimensional parameter space is performed to estimate the expected values of each hyper-parameter in both `GR` and modified GW propagation scenarios ($\texttt{MG}_{1.8}$ and $\texttt{MG}_{0.6}$) for future O5 runs. The MCMC chains were computed using the python package `emcee` Foreman-Mackey et al. 2013, an efficient sampler compatible with the `CHIMERA` code and considering the initial settings for the hyper-likelihood consistently with those used for the one-dimensional case, with the fiducial values in Tab.3.1 and priors in Tab3.2. The MCMC has specific initializing settings which have to be described in order to understand the work-flow to obtain the final constraints:

- Walkers: Individual points that explore the parameter space to construct the posterior distribution moving through the space according to the rules of the MCMC algorithm. The collective movement of all walkers approximate the probability distribution. The number of walkers was set to 52 determined by the following criterion: $N_{walkers} \in [2 \times N_{param}, 10 \times N_{param}]$, which ensures adequate sampling of the parameter space. Here, $N_{walkers} = 4 \times N_{param}$ was chosen.

- Burn-in phase: During this initial phase, the walkers explore the parameter space randomly and usually away from the stationary distribution. Only after this burn-in phase the walkers start to sample accurately the final posterior. So the points in the burn-in phase need to be removed. For this study the burn-in was relatively short, typically requiring around 200 points to be discarded but a conservative limit of 1000 points was used to exclude any outliers.

- Convergence: In this work, convergence was assessed using the auto-correlation time test, which measures how efficiently the chain "forgets" its previous states. Ensuring that the sampling process is effective. All results presented in this thesis are based on MCMCs that meet the convergence criteria.

4.2.1 Results for `GR` catalog

This section aims to finalize the constrained value in a joint analysis of `GR` catalog and galaxy catalog with both spectroscopic and photometric uncertainty. This is to prove that the methods and results are scientifically accurate, showing no biases and retrieving accurate forecasts for O5. This motivates the next part of this work for which the same analysis can be performed for different catalogs taking in consideration a modified GW propagation. Table 4.1 shows for each catalog, the parameters constraints resulting from all the MCMCs considering the median as central value and as errors the 16th and 84th-percentiles. The motivation is for statistical reasons. For Gaussian distributions, the mean and median yield similar results. However, GW analyses often involve non-Gaussian distributions, making the median a better choice for two reasons:

- If an initial flat distribution with some asymmetry is given, the median provides a more accurate estimate of the peak value, as it reflects the central value of the prior

- If bi-modal distributions are given, the mean may lie in a low-probability region between peaks, leading to misleading results.

Using the median and percentiles allows for robust parameter estimation, even for parameters that are poorly constrained. This is especially relevant for n, κ, and z_p. The first result is depicted in figure 4.6 done with the GW events catalog in `GR` case. What was expected matched the results, clearly there is a lower accuracy in constraining the parameters in the photometric case compared to the spectroscopic one. For H_0 the constrain in the z_{spec} case is $H_0 = 67.7^{+2.3}_{-2.18}$ while for z_{phot} the accuracy deteriorates to $H_0 = 81.3^{+24.2}_{-14.7}$. The reason for this comes from fact that considering higher uncertainty on redshift, the probability of galaxy hosting the event are worse, so less informative catalog results in worsened constraints. Regarding the value of Ξ_0 in the z_{spec} case $\Xi_0 = 0.905^{+0.094}_{-0.092}$, while for z_{phot} $\Xi_0 = 1.20^{+0.67}_{-0.37}$ which is in agreement with GR for both redshift cases, being at 1σ from the fiducial. The next image Fig.4.8, shows very intriguing results, it contains two contour plots considering the same catalogs in `GR` case (borrowed from Borghi et al. 2024). Although one is generated by fixing the values of $\Xi_0 = 1$ and $n = 0$, the other loosens this condition. These results were done to describe what happens to the uncertainties on the constraints when fixing some parameters and so investigating what occurs on the contours when the degeneracies are broken.

It clearly demonstrates that leaving Ξ_0 free to vary during the likelihood sampling worsens the constraints on H_0 making its constraints wider. This happens because during the MCMC when Ξ_0 is free, the likelihood value obtained for different H_0, Ξ_0 pairs results the same. This is a clear statement of the degeneracy between the two parameters. However by fixing $\Xi_0 = 1$ the degeneracy is completely broken and the constraint will result narrower. Resulting in $H_0 = 70.5^{+0.74}_{-0.73}$ with a constraining error of $\sim 1\%$ in the fixed case.

Another peculiar characteristic present in both figures4.6 and 4.8 is a small shift of the constrained value for Ξ_0. To better investigate the nature of this, a new MCMC is run by fixing H_0 to the fiducial value. Results are in Fig.4.7. The constrained value in this scenario is $\Xi_0 = 0.97 \pm 0.03$, which is just on the limits of 1σ from the fiducial Ξ_0. This is not due to bias because of wrongly fixing H_0 to 70 but it is related to the initial distribution generated when the GW catalog was built; it is probably of statistical nature. This work is simulating the best 100 dark sirens for 1 year of observation but it might be a too low number of events, so some small deviation from a precise value of $\Xi_0 = 1$ are expected, additionally since they are selected from a bigger population, the cut might take events that prefer a slightly smaller Ξ_0. This means that if the final goal was to test modified GW propagation, it is clear that LVK collaboration detectors need more than 100 events with SNR>25 and better observation on the cosmic expansion in order to accurately constrain Ξ_0. In this work only the 100 best events are chosen for the analysis, although more events with smaller SNR are expected, in Section 3.3 the number of events just with an 20 <SNR< 25 in a GR scenario are revealed to be ~ 8000 which means that a lot can be constrained with those and strong constraints are expected from future O5 runs.

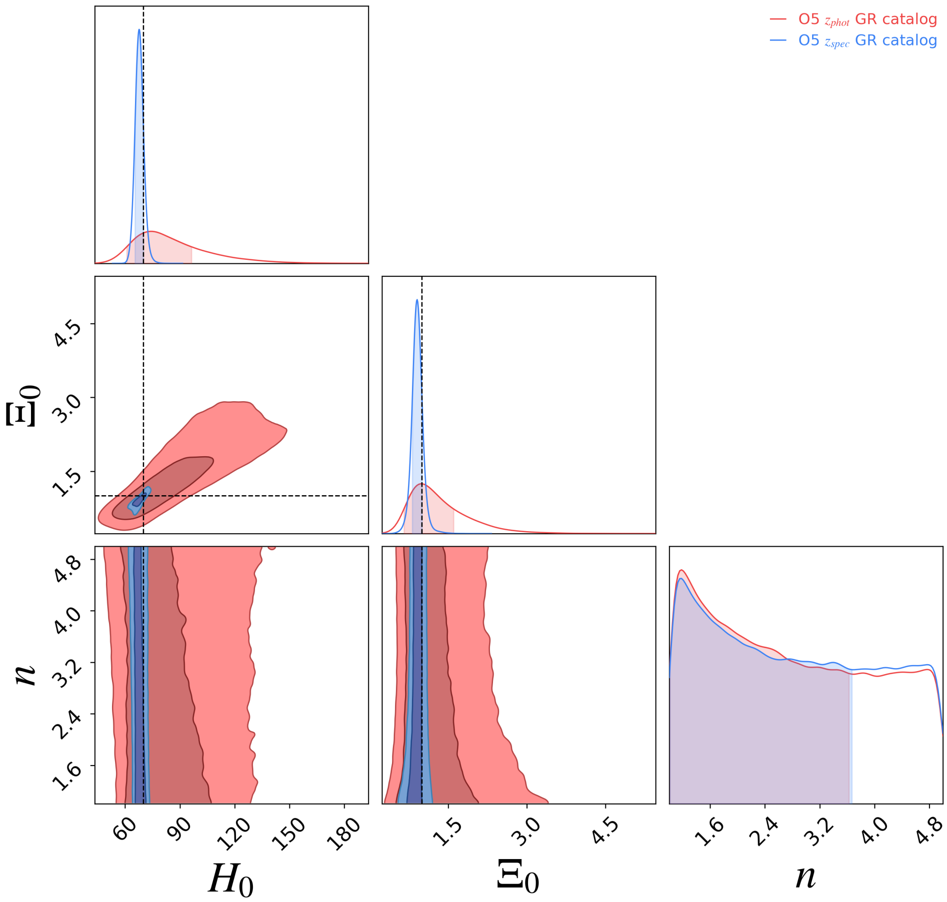

Figure 4.6: Contours plot for the λ_c, both in spectroscopic (blue) and photometric (red) cases.

Parameter	z_{spec} GR	z_{spec} GR $\Xi_0 = 1$ fixed	z_{phot} GR	z_{phot} GR $H_0 = 70$ fixed	z_{spec} GR $H_0 = 70$ fixed	z_{spec} MG$_{1.8}$	z_{spec} MG$_{1.8}$ Ξ_0 fixed	z_{spec} $MG_{0.6}$	z_{spec} $MG_{0.6}$ Ξ_0 fixed
H_0	$67.7^{+2.28}_{-2.18}$	$70.50^{+0.74}_{-0.73}$	$81.32^{+24.17}_{-14.66}$	70	70	$72.26^{+4.14}_{-5.00}$	$70.18^{+0.88}_{-0.88}$	$67.62^{+4.87}_{-4.58}$	$70.18^{+1.42}_{-1.42}$
Ξ_0	$0.905^{+0.094}_{-0.092}$	1	$1.20^{+0.67}_{-0.37}$	$0.92^{+0.13}_{-0.12}$	$0.97^{+0.03}_{-0.03}$	$1.78^{+0.25}_{-0.39}$	1.80	$0.60^{+0.13}_{-0.13}$	0.60
n	$2.74^{+1.53}_{-1.30}$	0	$2.67^{+1.59}_{-1.25}$	$2.67^{+1.54}_{-1.24}$	$2.39^{+1.62}_{-1.38}$	$2.63^{+1.53}_{-1.28}$	1.91	$2.53^{+1.49}_{-0.50}$	1.91
λ_{peak}	$0.066^{+0.037}_{-0.028}$	$0.066^{+0.036}_{-0.028}$	$0.074^{+0.038}_{-0.030}$	$0.069^{+0.037}_{-0.029}$	$0.065^{+0.037}_{-0.027}$	$0.068^{+0.031}_{-0.027}$	$0.068^{+0.031}_{-0.029}$	$0.072^{+0.041}_{-0.033}$	$0.075^{+0.042}_{-0.043}$
α	$3.25^{+0.27}_{-0.26}$	$3.25^{+0.27}_{-0.27}$	$3.24^{+0.27}_{-0.26}$	$3.24^{+0.27}_{-0.26}$	$3.25^{+0.27}_{-0.26}$	$3.11^{+0.24}_{-0.26}$	$3.11^{+0.25}_{-0.25}$	$3.53^{+0.36}_{-0.36}$	$3.51^{+0.37}_{-0.37}$
β	$1.92^{+0.56}_{-0.52}$	$1.91^{+0.55}_{-0.52}$	$1.91^{+0.57}_{-0.52}$	$1.92^{+0.55}_{-0.51}$	$1.92^{+0.56}_{-0.44}$	$0.24^{+0.42}_{-0.40}$	$0.24^{+0.41}_{-0.39}$	$1.18^{+0.49}_{-0.51}$	$1.15^{+0.50}_{-0.50}$
δ_m	$2.7^{+2.1}_{-2.2}$	$3.17^{+2.21}_{-1.81}$	$2.33^{+2.04}_{-1.46}$	$2.84^{+2.34}_{-1.77}$	$3.20^{+2.17}_{-1.66}$	$1.94^{+2.40}_{-1.55}$	$1.97^{+2.43}_{-1.54}$	$2.33^{+2.83}_{-1.99}$	$2.20^{+2.73}_{-1.73}$
m_{low}	$5.65^{+0.77}_{-1.00}$	$5.64^{+0.72}_{-0.96}$	$5.89^{+0.66}_{-0.91}$	$5.75^{+0.74}_{-1.00}$	$5.61^{+0.74}_{-0.86}$	$5.97^{+0.58}_{-0.42}$	$5.93^{+0.59}_{-0.41}$	$6.25^{+0.72}_{-0.30}$	$6.32^{+0.66}_{-0.33}$
m_{high}	$93.34^{+34.15}_{-7.32}$	$93.84^{+32.27}_{-7.11}$	$94.06^{+28.80}_{-8.05}$	$93.06^{+32.56}_{-8.11}$	$93.45^{+31.02}_{-8.98}$	$97.47^{+17.86}_{-18.14}$	$97.47^{+17.95}_{-17.93}$	$85.77^{+64.81}_{-10.81}$	$85.42^{+65.66}_{-10.66}$
μ_{mass}	$34.64^{+0.95}_{-1.00}$	$34.77^{+0.93}_{-1.00}$	$34.47^{+1.21}_{-1.26}$	$34.37^{+1.18}_{-1.24}$	$34.70^{+1.00}_{-1.07}$	$34.62^{+0.69}_{-0.32}$	$34.57^{+0.64}_{-0.35}$	$34.80^{+0.53}_{-0.20}$	$34.87^{+0.53}_{-0.06}$
σ_{mass}	$4.10^{+0.82}_{-0.67}$	$4.16^{+0.82}_{-0.68}$	$4.16^{+0.85}_{-0.70}$	$4.08^{+0.82}_{-0.66}$	$4.15^{+0.81}_{-0.63}$	$2.44^{+0.78}_{-0.22}$	$2.44^{+0.79}_{-0.21}$	$4.19^{+1.65}_{-0.35}$	$4.13^{+1.55}_{-0.45}$
γ	$1.97^{+2.46}_{-1.11}$	$2.28^{+2.49}_{-1.15}$	$2.97^{+3.12}_{-1.70}$	$2.06^{+2.50}_{-1.15}$	$2.25^{+2.60}_{-1.39}$	$2.69^{+1.47}_{-0.53}$	$2.76^{+1.32}_{-0.68}$	$2.05^{+1.21}_{-0.79}$	$2.00^{+1.22}_{-0.78}$
κ	$2.63^{+2.26}_{-1.86}$	$2.75^{+2.18}_{-1.96}$	$2.70^{+2.19}_{-1.90}$	$2.60^{+2.24}_{-1.85}$	$2.65^{+2.24}_{-1.79}$	$2.88^{+2.13}_{-1.87}$	$2.83^{+2.14}_{-1.86}$	$2.60^{+2.29}_{-1.73}$	$2.57^{+2.21}_{-1.99}$
z_p	$1.31^{+1.74}_{-0.86}$	$1.23^{+1.76}_{-0.75}$	$1.14^{+1.80}_{-0.65}$	$1.31^{+1.73}_{-0.86}$	$1.19^{+1.77}_{-0.80}$	$2.37^{+1.12}_{-0.88}$	$2.37^{+1.12}_{-0.88}$	$2.05^{+1.33}_{-0.67}$	$1.95^{+1.37}_{-0.63}$

Table 4.1: Table with all the parameters constrained for the different models. The parameter constraints are given as the median values with the 16th and 84th percentiles.

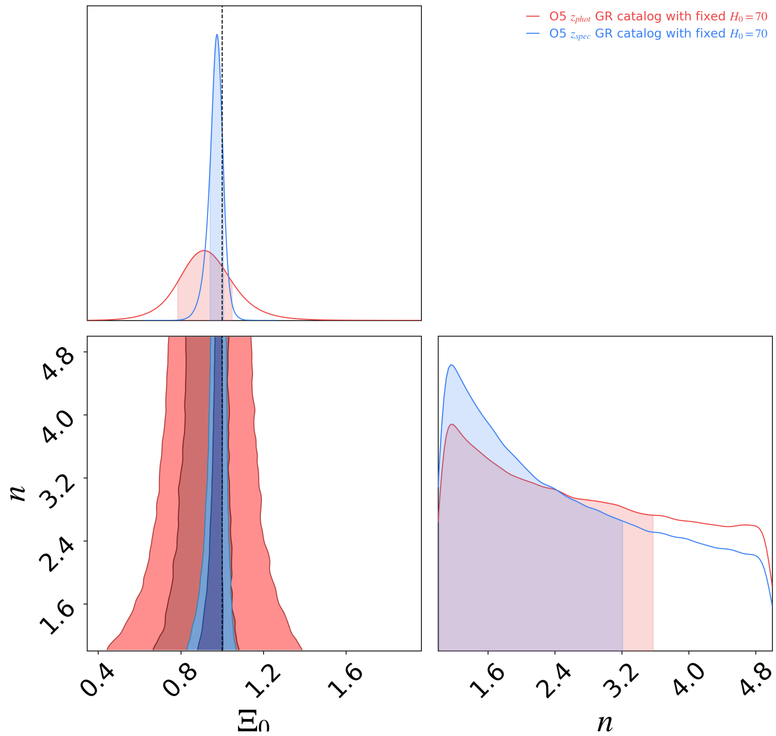

Figure 4.7: Contours of parameters fixing H_0 to 70, both in spectroscopic (blue) and photometric (red) cases.

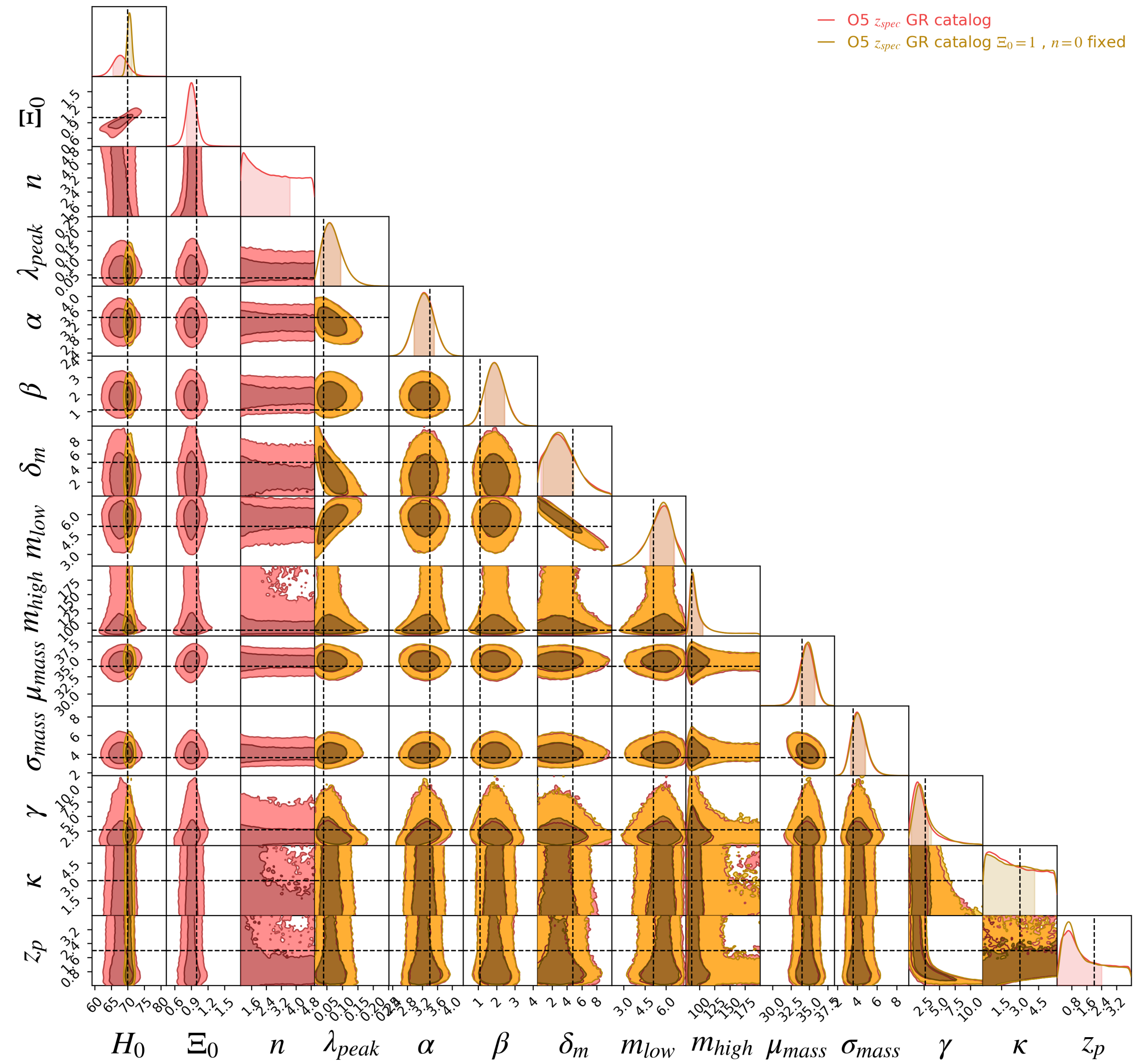

Figure 4.8: Contours of parameters in the case of spectroscopic redshift showing the comparison of two cases, ΛCDM with no initialized Ξ_0 and n and modified GW propagation case.

4.2.2 Results for MG catalogs

This section focuses on the new generated catalogs built as described in Chapter 3, with the settings found in 3.1, initialized with $\Xi_0 = 1.8$, 0.6 and $n = 1.91$. The choice of the galaxy catalog uncertainty was made after the preemptive analyses described above, so spectroscopic redshift was chosen. These catalogs will be analyzed as the previous `GR` catalog with a major focus on the changes in the parameter constraints for these two new cases. Lastly, by considering all these modifications, the final alteration of the uncertainty levels will be shown, to conclusively define the constraining power of O5 for these two types of cosmological scenarios. To analyze these scenarios, two MCMCs were obtained by considering all 14 parameters, and then by fixing Ξ_0 and n to values corresponding to the correct catalog to avoid biases. This is generated with the final purpose to reveal the differences of constraining H_0 with and without prior accurate constraints on the modified GW propagation. The respective errors for all parameters are reported in the last four columns of Table 4.1 for these scenarios. However, this discussion will specifically focus on Ξ_0 and H_0. In Figs.4.9 and 4.10 the contour plot for $\texttt{MG}_{1.8}$ and $\texttt{MG}_{0.6}$ catalogs are depicted. The first observation is that again, as in the `GR` case, both the figures and the contours with and without fixing Ξ_0 are well centered on the fiducial of $H_0 = 70$. However, the constraints found here are a little weaker than the `GR` case. Indeed the uncertainty on H_0 increases for the free Ξ_0 case finding $H_0 = 72.3^{+4.14}_{-5,2}$ for $\texttt{MG}_{1.8}$ and $H_0 = 67.6^{+4.87}_{4.58}$ for $\texttt{MG}_{0.6}$. Instead, by fixing the MG parameters and breaking the degeneracy between H_0 and Ξ_0, the cosmic expansion rate results in $H_0 = 70.2^{+0.88}_{-0.88}$ for $\texttt{MG}_{1.8}$ and $H_0 = 70.2^{+1.42}_{1.42}$ for $\texttt{MG}_{0.6}$. This indicates that the measurement becomes less uncertain when the degeneracy is broken, although the resulting constraints found, say that in a universe that intrinsically has $\Xi_0 > 1$ (as in $\texttt{MG}_{1.8}$), will measure H_0 more accurately than a universe with $\Xi_0 < 1$ (as in $\texttt{MG}_{0.6}$). However, both constraints remain weaker in comparison with `GR`. Regarding Ξ_0, the constraints in these cases are $\Xi_0 = 1.78^{+0.39}_{-0.31}$ for $\texttt{MG}_{1.8}$ and $\Xi_0 = 0.6^{+0.13}_{-0.13}$ for $\texttt{MG}_{0.6}$, which, compared to the `GR` case given in the previous section, provide an interesting outcome. The error on constraining Ξ_0 is indeed the worst for a catalog with $\Xi_0 > 1$, slightly better for a catalog with $\Xi_0 < 1$, and the best in the `GR` case. For n it seems that in these modified GW scenarios a small peak at low values of the prior has appeared but it is still too flat for constraints.

After discussing the final contour plots for new scenarios for modified GW propagation ($\texttt{MG}_{1.8}$, $\texttt{MG}_{0.6}$), it was clear that their overall uncertainty on H_0 and Ξ_0 was worsened concerning the GR case. Therefore final results of this work are revealed in Fig.4.11

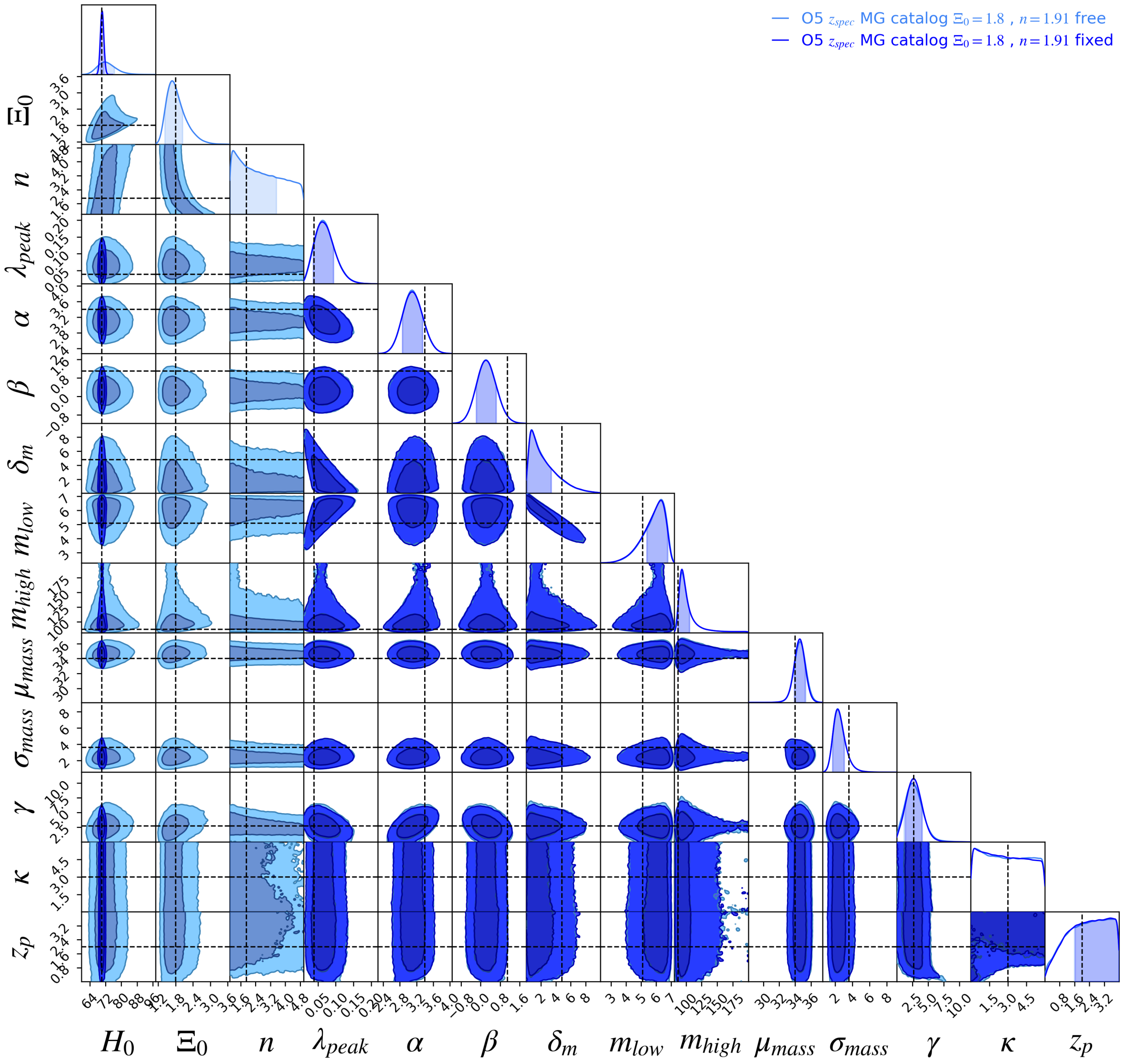

Figure 4.9: Double contours for catalog initialized with $\Xi_0 = 1.8$ and $n = 1.91$, in light blue the chain that ran with all parameters free, while in dark blue with fixed MG parameters

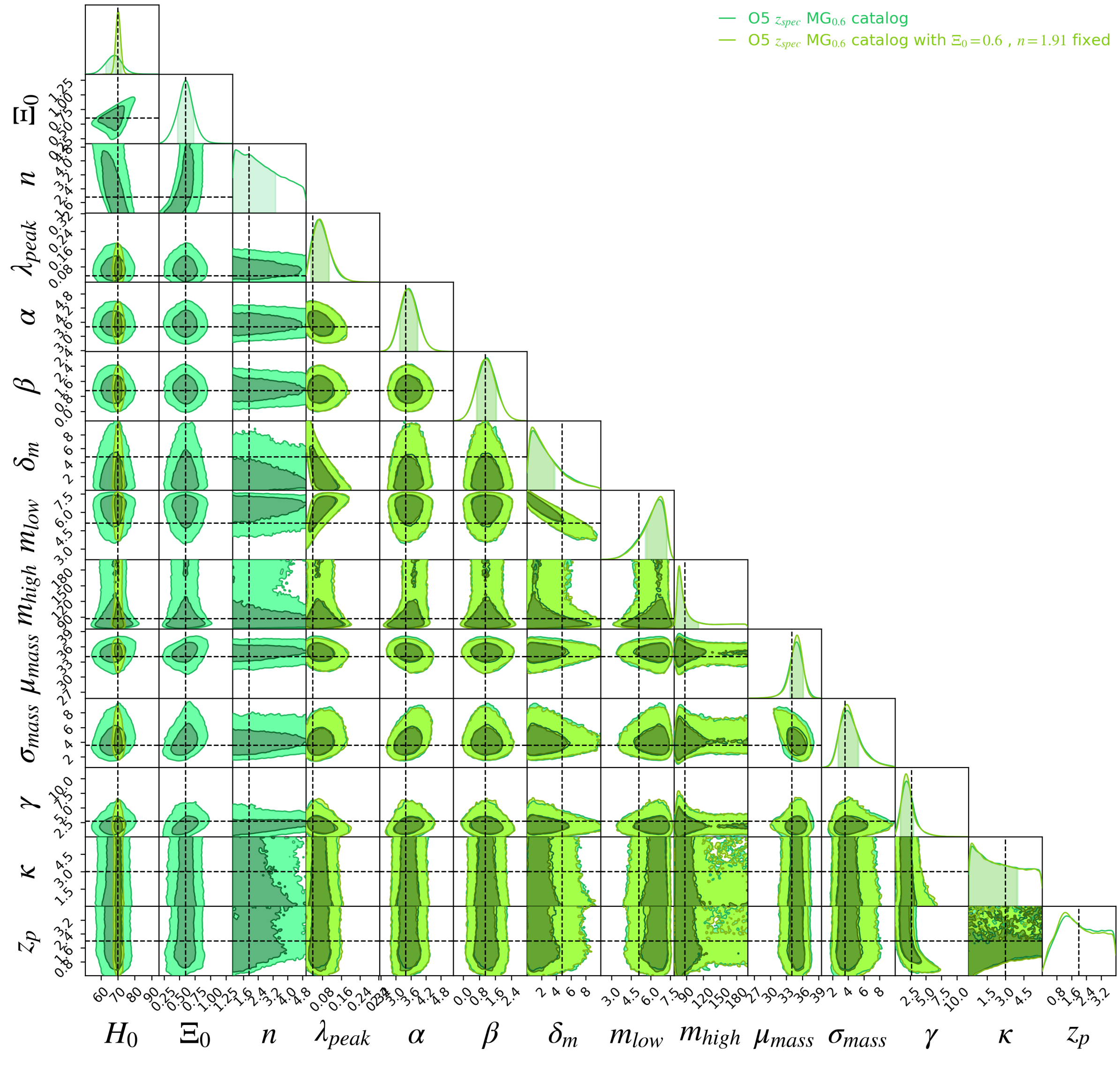

Figure 4.10: Double contours for catalog initialized with $\Xi_0 = 0.6$ and $n = 1.91$, in dark green the chain that ran with all parameters free, while in lime green the chain with fixed MG parameters

to visualize the variation of relative errors on H_0 either locking or freeing Ξ_0, obtained through the 16th-percentile and 84th-percentile of H_0 and dividing it by the median of H_0. Additionally Figs.4.12,4.13 are shown to compare standard and relative errors on Ξ_0 and H_0. Quantitatively, these figures' results can be summarized as follows. The errors for H_0 are:

- In `GR` scenario H_0 results as $\sim 1\%$ when fixing $\Xi_0 = 1$ in line with the findings of Borghi et al. 2024 for a fixed `GR` Universe. Meanwhile if left free the relative error for H_0 is $\sim 2.3\%$.
- In $\mathtt{MG}_{1.8}$ scenario the uncertainty is $\sim 1.2\%$, when fixing $\Xi_0 = 1.8$ as the fiducial for the simulated catalog, and $\sim 6\%$ when everything is left free.
- In $\mathtt{MG}_{0.6}$ scenario the uncertainty is $\sim 2\%$, when fixing $\Xi_0 = 0.6$ to the fiducial for the simulated catalog and $\sim 7\%$ when everything is left free.

The results for Ξ_0 are:

- In `GR`, $\Xi_0 = 0.91$ with relative error of $\sim 10\%$.
- In $\mathtt{MG}_{1.8}$, $\Xi_0 = 1.78$ with relative error of $\sim 17\%$.
- In $\mathtt{MG}_{0.6}$, $\Xi_0 = 0.6$ with relative error of $\sim 20\%$.

The first natural statement that comes through is that the constraint for $H_0 = 70$ is found with an uncertainty that is lower when Ξ_0 is locked, which means that if Ξ_0 will be measured with percentage level accuracy, the uncertainty on H_0 will decrease. Moreover, in the left side of Figs.4.13 and 4.12 an opposite trend on the standard error is found in the two modified GW propagation scenarios. For $\mathtt{MG}_{1.8}$ the error on Ξ_0 is higher while for $\mathtt{MG}_{0.6}$ the error is lower; it is also true that H_0 in $\mathtt{MG}_{1.8}$ has slightly wider errors than in $\mathtt{MG}_{0.6}$: this again results from the correlation and impact that these quantities have on the luminosity distance. In fact, as previously said, d_L^{GW} is positively correlated with Ξ_0 (since a higher value of Ξ_0 increases luminosity distance) and negatively correlated with H_0 (since a higher value of H_0 decreases luminosity distance). Their uncertainties then will be influenced by their mutual degeneracies, and these differences are well explained by their correlation with luminosity distance.

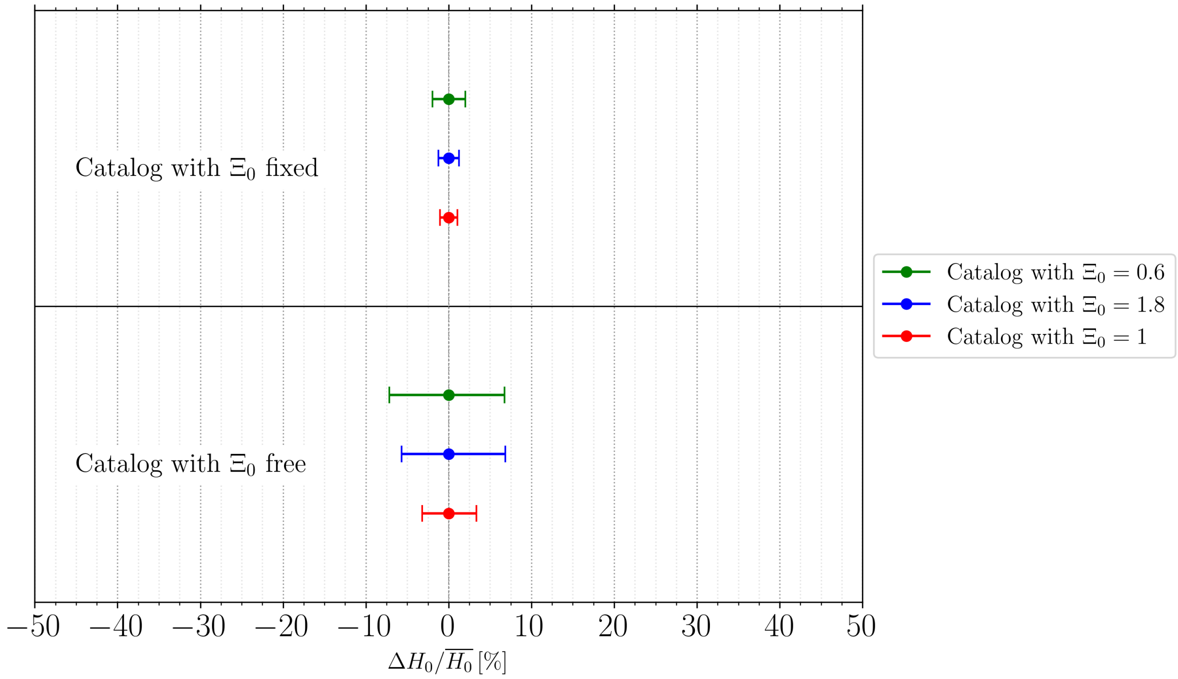

Figure 4.11: Here the percentage errors on possible H_0 measurement from an O5 run with dark sirens with a z_{spec} uncertainty, are presented. In red the GR case is displayed, while blue and green are the two different modified GW propagation cases.

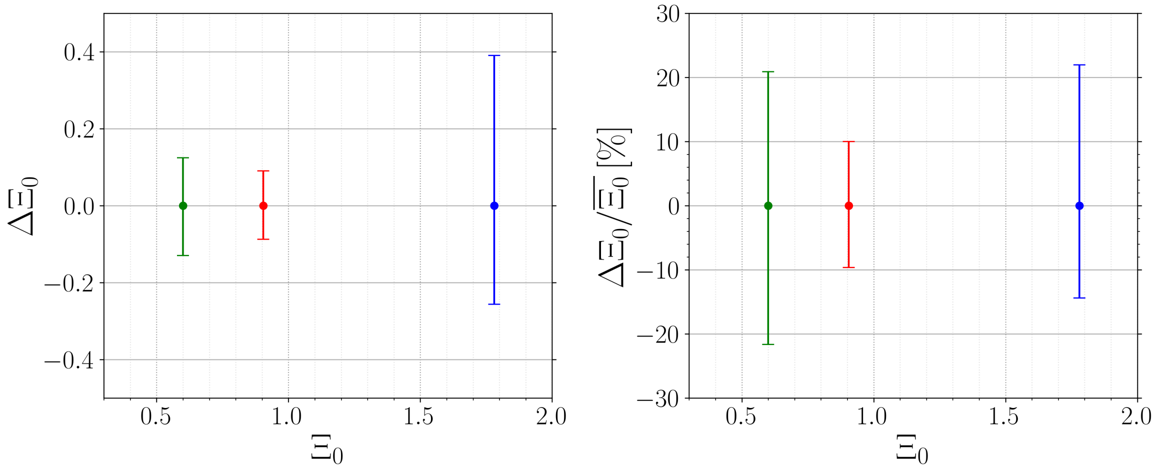

Figure 4.12: Error-bars for Ξ_0 vs. Ξ_0 for all three catalogs leaving Ξ_0 free with a spectroscopic redshift galaxy catalog. Left: Error values from 16th-percentile and 84th-percentile for Ξ_0 vs. Ξ_0 free for each GW catalog. Right: % Errors of Ξ_0 vs. Ξ_0.

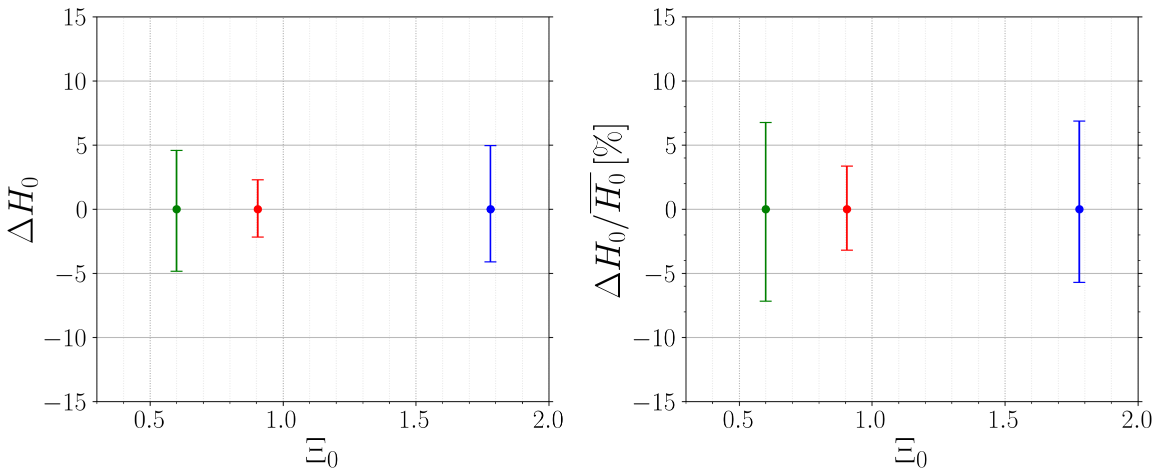

Figure 4.13: Error-bars for H_0 vs. Ξ_0 for all three catalogs leaving Ξ_0 free with a spectroscopic redshift galaxy catalog. Left: Error values from 16th-percentile and 84th-percentile for H_0 vs. Ξ_0 free for each GW catalog. Right: % Errors of H_0 vs. Ξ_0.

4.3 Beyond a spectroscopic galaxy catalog

In the thesis the main scientific mission was to recover the constraining power for future O5 runs in order to understand how future detectors with their expected capabilities and sensitivities are able to constraint Ξ_0 and H_0 in a GR scenario and extend it to other types of universes in which the propagation of GWs is modified. Given the results and what was analyzed, there are some interesting open questions to explore in the future. Throughout this work, $\Omega_{0,m}$ was kept fixed, as it has only a mild impact on d_L^{GW} at lower redshifts. However, at higher redshifts, it is expected to exert a stronger influence, making it an intriguing parameter to investigate. As a cosmological parameter, $\Omega_{0,m}$ could easily be left free, potentially revealing correlations and degeneracies with other parameters. This presents an opportunity for future work to explore whether this parameter, despite its limited effect on modified GW propagation, can still be constrained within these altered GR scenarios. Moreover, during the workflow, certain challenges arose in analyzing O5 prospects using spectral sirens. While spectral sirens are a valuable tool for analysis, their results did not align with those obtained using spectroscopic and photometric redshift error methods. Multiple attempts were made to identify the root of the issue; although the problem remains unresolved, it will be further investigated in the future. Details of these attempts are provided in Appendix A.

Chapter 5

Conclusions

The ΛCDM model, which describes a Universe dominated by cold dark matter and dark energy (Peebles and Ratra 2003 , Dodelson and Schmidt 2020) has been remarkably successful in explaining a wide range of phenomena, from the cosmic microwave background to galaxy clustering. However, its reliance on two enigmatic components, dark energy and dark matter, leaves important questions unanswered, particularly as neither has been directly detected (Sahni 2004). These open points, alongside issues such as the Hubble tension, suggest that ΛCDM might not provide the complete picture. In recent years, gravitational waves have emerged as powerful tools for cosmology (B. P. Abbott 2017a). Since their first detection in 2015 (B. P. Abbott 2016), GWs have not only opened a new observational window but have also been recognized as "standard sirens", powerful distance indicators (Holz and Hughes 2005 Chen, Maya Fishbach, and Holz 2018) that do not rely on any distance ladder calibration. Analogous to electromagnetic "standard candles", standard sirens measure the luminosity distance directly from the GW signal, offering an independent way to probe the Universe's expansion. This is possible only by breaking the degeneracy between mass and redshift which imposes a dependency on the redshifts of the observable quantities obtained by GWs that needs to be resolved.

To overcome this issue, multiple approaches have been proposed to inform the GW posterior with information about the redshift of the potential hosts, ranging from direct detection of the electromagnetic counterpart ("bright sirens") to statistically obtaining the redshift information from a galaxy catalog ("dark sirens") to taking advantage of information in the distribution of astrophysical parameters of the merging population ("spectral sirens").

However, due to the limited number of detected GW events, the current constraints that can be obtained on cosmology are weak. So far, the LIGO-Virgo-KAGRA (LVK) network have detected only ∼100 BBH events up to the last publicly available Observing run (O3, R. Abbott et al. 2023), and the current observing run is currently ongoing (O4, B. P. Abbott et al. 2020). The next observing run (O5, B. P. Abbott et al. 2020, Kiendrebeogo et al. 2023) is expected to improve in terms of sensitivity, range of distances probed, and number of detected events, and it is therefore important to assess the science cases enabled by this new data.

In parallel to cosmological constraints, gravitational waves and standard sirens have been useful to provide a new avenue also to test General Relativity (GR) (Yunes, Yagi, and Pretorius 2016, B. Abbott et al. 2016, B. P. Abbott 2017a, Goldstein et al. 2017, Savchenko et al. 2017). Many Modified Gravity theories (Belgacem et al. 2018a, Dvali, Gabadadze, and Porrati 2000) predict deviations in the propagation of GWs with respect to the one of electromagnetic radiation. These deviations, encoded in parameters like Ξ_0 and n (Mancarella, Finke, et al. 2022) in the parametrization used in this Thesis, offer a new way to test physics beyond GR. The results obtained so far tested these parameters only assuming a fixed cosmology (H_0), and no test was performed using dark sirens in a scenario with a joint inference of astrophysical, cosmological, and modified gravity parameters Ξ_0 and n. Only recently, new codes have been developed to perform this joint analysis (`CHIMERA` Borghi et al. 2024, `icarogw` Simone Mastrogiovanni et al. 2023, `gwcosmo` Gray et al. 2023), but so far they are not including the MG parameters in their analysis.

In this Thesis work, we aim to carry out a full analysis of MG parameters, integrating in a self-consistent way their parametrization in the analysis code, and providing forecasts on their detectability with future GW observations. To this end, the work focuses on understanding how parameters that model modified GW propagation affect the GW luminosity distance (d_L^{GW}) by simulating realistic GW catalogs including these modified GW propagation scenarios; the capabilities of improved detectors on constraining deviation from GR were evaluated and their potential systematics on cosmological measurements like H_0 were tested. In the following, I present the methods and data used for this study and the main results obtained.

Extending the analysis to account for modified GW propagation

To perform these analyses, the required components are a simulated galaxy catalog, its corresponding GW events catalog, and the `CHIMERA` code. To adapt those to the science case of a MG scenario, both the code and the GW catalogs needed to be further developed.

The main problem was that `CHIMERA` did not initially include modules to handle modified GW propagation, and for this Thesis a new module was developed and validated (MG_FLRW) in the `CHIMERA` pipeline. This module incorporates MG effects into the computation of d_L^{GW} as in Eq.2.49 and its derivative, enabling the analysis of GW propagation under modified GW propagation scenarios. Modifying the luminosity distance required also redefining the methods used to calculate the likelihood. A new adaptive redshift grid is introduced, based on the new definitions.

These updates allowed us to study the impact of the new parameters on the luminosity distance, and to explore the dependencies and relation with other cosmological parameters. Considering a redshift $z = 1$, it was found that, while a 10% increase in H_0 results in a $\sim 10\%$ decrease in d_L^{GW}, a 10% increase in Ξ_0 leads to a 5% increase in the luminosity distance, showing the clear and direct anticorrelation among these parameters. On the other hand, the impact of other parameters is significantly less relevant, and as an example a 10% increase in $\Omega_{0,m}$ causes a modest 1.8% variation, while the parameter n, which only affects d_L^{GW} when $\Xi_0 \neq 1$, shows that for $n = 1.5$ the relative increase is just 1%. These results demonstrate a mutual degeneracy between Ξ_0 and H_0, suggesting how future measurements of H_0 could be crucially influenced by variations in Ξ_0.

Simulating GW Event Catalogs in MG scenarios

Simulating GW catalogs represented the backbone of this analysis. Nowadays there are no accurate mock catalogs that reveal information on galaxy hosts and related GW events in a modified GW propagation scenario, but to simulate these GW mock catalogs, it is necessary to introduce modifications in existing codes.

Two new realistic GW simulated catalogs were generated for an O5 LVK detectors network using `GWFAST` (Iacovelli et al. 2022a), a code that uses Fisher matrices to generate simulated posteriors of GW events. These new catalogs are created within two extreme scenarios with $\Xi_0 = 1.8$, $n = 1.91$ ($\mathtt{MG}_{1.8}$) and $\Xi_0 = 0.6$, $n = 1.91$ ($\mathtt{MG}_{0.6}$). These values have been chosen to be compliant with recent measurements on GWTC-3 events, that obtained $\Xi_0 = 1.2 \pm 0.7$ and $n = 1.91$ (Leyde et al. 2022). These are chosen to study two different regimes $\Xi_0 > 1$ which expects a lower number of detected GWs and $\Xi_0 < 1$ which expects the opposite. These were compared to a GR scenario mock event catalog borrowed from Borghi et al. 2024.

To create these catalogs, `GWFAST` also needed to be modified in order to allow to include modified GW luminosity distance.

Forecasts on the detectability of MG propagation parameters with future data

Applying all the aforementioned tools, it is possible to derive the constraining power for future GW observations even in modified GW propagation.

Two different analyses are performed. Firstly, a brute-force sampling of the posterior is done on single parameters considering all the other fixed, in order to validate all the previous steps and have a first assessment of the results. No bias was found when the cosmological and astrophysical parameters were fixed to their fiducial values, yielding an H_0 constraint of 70 km/s/Mpc with a relative error of 1% and a constraint on $\Xi_0 \sim 1$ with a relative uncertainty of $\sim 10\%$. These findings suggest that future O5 observations could achieve H_0 constraints with $\leq 1\%$ accuracy, offering new insights into the Hubble tension. Additionally, Ξ_0 was constrained for the first time using dark sirens, achieving an improved uncertainty of $\sim 10\%$, compared to the 16% uncertainty found with current real O3 data by Leyde et al. 2022 using the spectral sirens approach. However, when Ξ_0 is incorrectly fixed to a value different from the fiducial one, the H_0 measured is biased, with a 9% offset with respect to the correct one when Ξ_0 is 50% higher or lower than the fiducial value of 1.

Next, we extended our analysis by performing a full MCMC sampling of the posterior for all the scenarios available. The main results can be summarized as follows:

- Using a GW catalog within a GR model, we investigated how varying redshift accuracies in galaxy catalogs affect parameter constraints. Specifically, when the MG parameters are also included in the analysis, the accuracy on H_0 worsens from $< 1\%$ to $\sim 3\%$ with a spectroscopic catalog and ranges from $\sim 9\%$ to 24% with a photometric catalog. These results are significant as both H_0 and Ξ_0 impact the luminosity distance, meaning that constraining one parameter helps break their mutual degeneracy. By fixing $H_0 = 70$ km/s/Mpc, an improved constraint on Ξ_0 is obtained. For a spectroscopic redshift catalog, Ξ_0 is constrained to ~ 0.97 with an uncertainty of $\sim 3\%$, while for a photometric redshift catalog, Ξ_0 was constrained to 0.92 with an uncertainty of $\sim 14\%$.

- In the `GR` case, it was found that H_0 can be retrieved unbiased with slightly worse accuracy due to the degeneracy between H_0 and Ξ_0.

- We then explored the constraints that can be obtained within MG scenarios, focusing the analysis on the results that can be obtained with a spectroscopic catalog (which was providing the best detections). Once again, no bias in Ξ_0 or H_0 was confirmed in these perturbed cosmological models, allowing for reliable constraints even in universes that incorporate modified GW propagation. In these cases, for the $\texttt{MG}_{1.8}$ universe, Ξ_0 was constrained to 1.78 with a relative error of 17%, while for the $\texttt{MG}_{0.6}$ universe, Ξ_0 was constrained to 0.6 with an uncertainty of 20%. These results were obtained while allowing all the parameters to vary freely.

- Finally, the impact of different cosmologies on the precision of H_0 constraints was analyzed. For the $\texttt{MG}_{1.8}$ universe, the uncertainty on H_0 was $\sim 6\%$, while for $\texttt{MG}_{0.6}$, H_0 was constrained with an uncertainty of $\sim 7\%$, both obtained while allowing Ξ_0 to vary freely. These findings show that the accuracy in scenarios with modified GW propagation is reduced compared to a `GR` universe. However, an exciting result emerged: if the type of universe were known specifically, i.e. if the value of Ξ_0 was precisely known and fixed, the uncertainties on H_0 would improve to $\sim 1.2\%$ for $\texttt{MG}_{1.8}$ and $\sim 2\%$ for $\texttt{MG}_{0.6}$. This highlights that while future O5 runs may see a deterioration in H_0 accuracy when $\Xi_0 \neq 1$, a constraint of Ξ_0 would still enable H_0 to be determined with exceptional precision in both universes, and also the modified GW propagation parameters could be determined with higher accuracy with respect to current ones.

In conclusion, this Thesis demonstrated the potential of gravitational waves for testing Modified Gravity theories forecasting on future observing runs to refine our understanding of the cosmological model. Extending the `CHIMERA` pipeline, simulating future GW catalogs, and analyzing future detectors' observations lays the groundwork for future investigations into deviations from GR. As detector sensitivities continue to improve, the insights gained here will play a crucial role in revealing news about understanding the Universe's expansion rate in altered GR scenarios and finally exploring the nature of diverse gravitational wave propagation.

5.1 Future Prospects

The Thesis work has described a framework in which the joint analysis for both cosmological and astrophysical parameters inference is possible through the `CHIMERA` pipeline, although it has not touched on some specific details that might be interesting to investigate. The future prospects will encompass a series of analyses that will consider the same framework as this Thesis, cross-correlating the same galaxy catalog and the mock GW event catalogs modified GW propagation scenarios, focusing on the following matters:

- The possibility of using spectral sirens to retrieve information on Ξ_0 and n.
- The effects of unlocking $\Omega_{0,m}$ as a cosmological parameter on forecasting the constraining power for LVK.

The first point has been partially explored during this Thesis work although revealing a series of issues in the computation of the posteriors that have compromised the employment of spectral sirens methods for modified GW propagation catalogs. By not fixing Ξ_0 and n a huge bias on H_0 is found, biasing H_0 to 20.5. After investigating the possible obstacles, the issue was pinpointed as a problem during the catalog generation that needs to be looked into further.

The second prospect comes in light of the fact that the quantity $\Omega_{0,m}$ was fixed to 0.25 (the value assumed by the mock galaxy catalog) because of its mild influence on luminosity distance. However, from the analysis, its effects seemed to increase for higher redshifts; for this reason, it would be interesting to perform a joint cosmological and astrophysical parameter inference freeing $\Omega_{0,m}$ to recover degeneracies with the other parameters and constrain its value in a modified GW propagation scenario.

Appendix A

The spectral siren problem

Spectral sirens are a specific case of dark sirens when the catalog is considered empty, which means that the respective co-moving volume in which the GW event is detected, does not have galaxies in it. Spectral sirens are an interesting tool to study cosmology, the redshift derivation as explained in the previous sections happens with specific relations, like the merging rate and the mass population distribution of binaries, so it is in need of some assumptions and modeling from prior knowledge on galaxies evolution. For these reasons there were not big expectation for improved constrain of the cosmological parameters with O5, however, it would have to be in agreement with the past measurements done with spectral sirens in past O3-O4 runs. As seen in Borghi et al. 2024, spectral sirens in a ΛCDM model, depicted worse results than dark sirens but still in 1σ from the fiducial, which for this work was not the case. From the MCMC in figure A.1, the green contours are the posteriors computed with spectral sirens catalog and as it can be seen, the walkers favoured points with H_0 value of ~ 20.5 which is much less than what expected. Beside that, also Ξ_0 and all the astrophysical parameters are distant from the fiducial value, symptom of degeneration of the parameters through the cosmology dependency. A first hypothesis for these issues would be that the GW injections used for the selection bias were not covering the correct redshift range, biasing the results. Injections have to cover the entirety of the redshift-mass distribution space, because when `CHIMERA` weights on the populations, if the event is outside, the code biases the value of the posterior.

One possibility considered was whether a significant number of events in the entire catalog fall outside the redshift range of injections, $z \sim [0, 1.3]$. However, comparisons revealed that only a few events fall outside this range, ruling out this as the cause of the large bias. This conclusion is further supported by the fact that, if selection bias were not accounted for, Fig.A.2, which shows the same analysis with H_0 fixed at 70, would also exhibit a bias. However, no such bias was observed in that case.

After ruling out selection bias as the issue, the likelihood function was analyzed with a focus on the primary parameters H_0, Ξ_0, and n. Figure A.3 was created by zooming in on Figure A.1 for these parameters and applying a color map to the logarithm of the likelihood to filter out the values with the lowest probabilities.

The figure clearly shows that the walkers are directed toward the likelihood maxima. As detailed in Tab.A.1, the difference in probability between $H_0 = 20.5$ and $H_0 \sim 70$ is minimal, although $H_0 = 20.5$ corresponds to a higher probability. Consequently, the walkers cluster around these values. This demonstrates that the issue is not related to `CHIMERA` itself, as the likelihood is being computed correctly.

The underlying cause may be intrinsic to the catalog used, whose generation characteristics are either unknown or not yet fully understood. Therefore, a potential avenue for future work is to investigate this issue further, aiming to understand why spectral sirens constrained by modified GW propagation exhibit such a strong bias.

Log_{prob}	H_0	Ξ_0	n	λ_p	α	β	δ_m	m_{low}	m_{high}	μ_m	σ_m	γ	κ	ζ_p
-9870.3	22.3	3.03	4.87	0.06	3.21	1.91	3.46	6.46	135.9	43.6	7.74	11.4	3.16	2.76
-9876.4	20.9	3.15	3.68	0.03	2.89	1.33	7.05	4.7	134.9	43.8	7.84	11.2	2.31	3.16
-9900	24.6	2.39	3.11	0.04	3.47	2.45	2.24	6.57	141.4	43.4	5.74	9.73	0.74	2.3
-9932.9	70	1	0	0.039	3.4	1.1	4.8	5.1	87	34	3.6	2.7	3	2

Table A.1: Table of the log-likelihood and values of all the parameters in the spectral sirens case

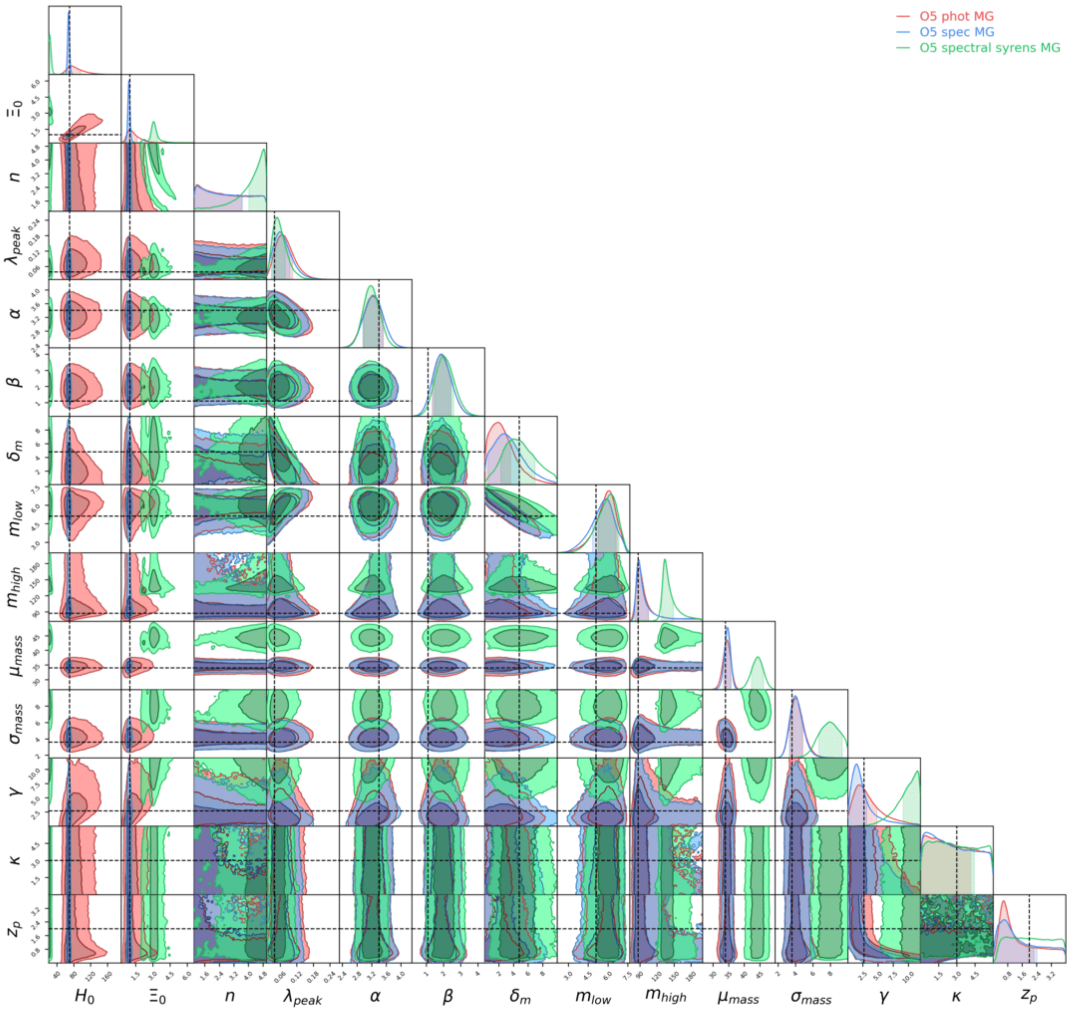

Figure A.1: MCMC contours in three different cases. Red: photometric galaxy catalog, Blue: Spectroscopic galaxy catalog Green: Spectral Sirens. The spectral sirens case shows a huge problem in the parameter estimation with $H_0 \sim 20.5$.

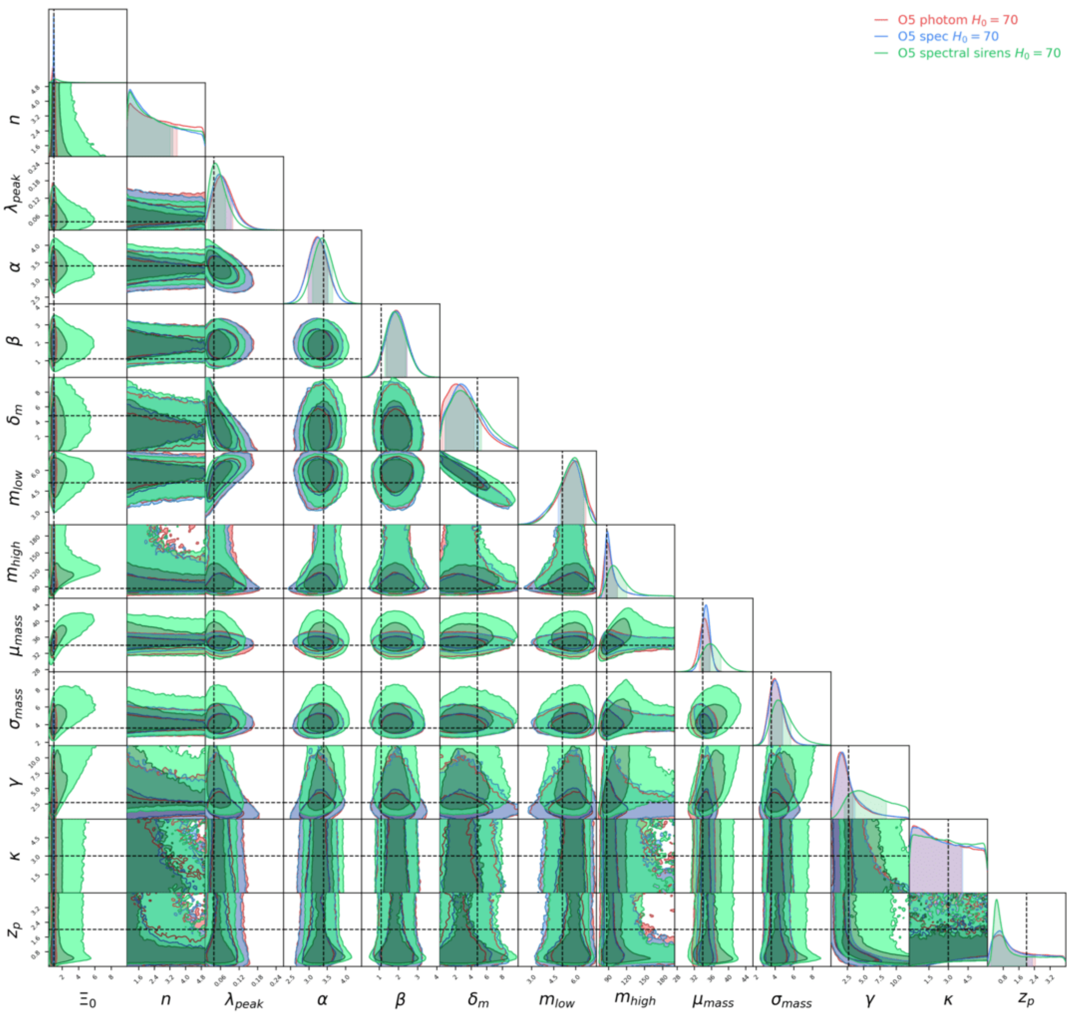

Figure A.2: Contour plot obtained reducing the H_0 prior to [50, 90]

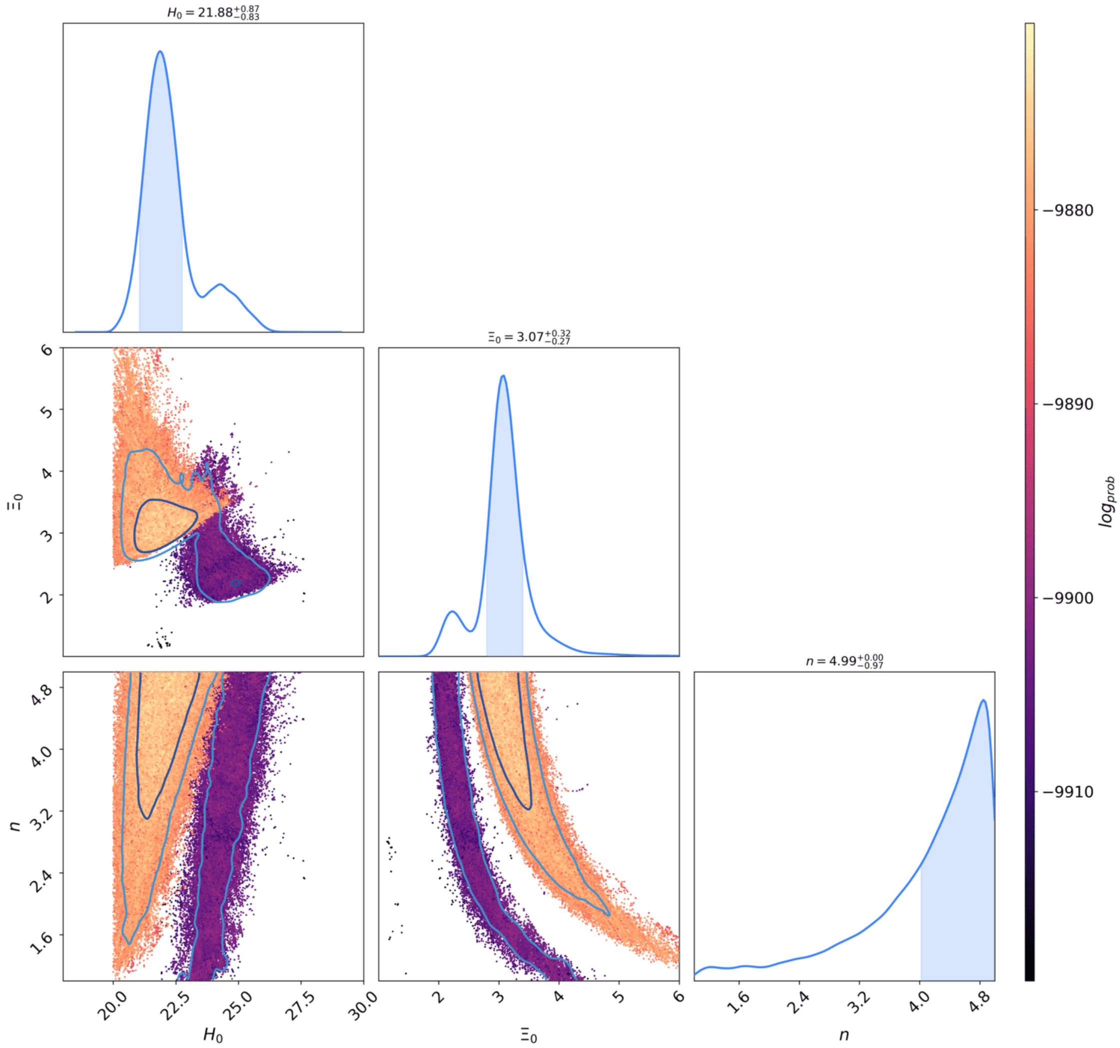

Figure A.3: Contours of parameters in the case of spectroscopic redshift fixing H_0 to 70 and varying all the other parameters

Bibliography

Abbott, B. P. (Feb. 2016). "GW17O817: Observation of Gravitational Waves from a Binary Black Hole Merger". In: *Phys. Rev. Lett.* 116 (6), p. 061102. DOI: 10.1103/PhysRevLett.116.061102. URL: https://link.aps.org/doi/10.1103/PhysRevLett.116.061102.

— (Oct. 2017a). "A gravitational-wave standard siren measurement of the Hubble constant". In: *Nature* 551.7678, pp. 85–88. ISSN: 1476-4687. DOI: 10.1038/nature24471. URL: http://dx.doi.org/10.1038/nature24471.

— (Oct. 2017b). "GW170817: Observation of Gravitational Waves from a Binary Neutron Star Inspiral". In: *Physical Review Letters* 119.16. ISSN: 1079-7114. DOI: 10.1103/physrevlett.119.161101. URL: http://dx.doi.org/10.1103/PhysRevLett.119.161101.

— (Sept. 2018). "Prospects for observing and localizing gravitational-wave transients with Advanced LIGO, Advanced Virgo and KAGRA". In: *Living Reviews in Relativity* 23.1. ISSN: 1433-8351. DOI: 10.1007/s41114-020-00026-9. URL: http://dx.doi.org/10.1007/s41114-020-00026-9.

— (Jan. 2019). "Properties of the Binary Neutron Star Merger GW170817". In: *Physical Review X* 9.1. ISSN: 2160-3308. DOI: 10.1103/physrevx.9.011001. URL: http://dx.doi.org/10.1103/PhysRevX.9.011001.

— (June 2023). "Constraints on the Cosmic Expansion History from GWTC–3". In: *The Astrophysical Journal* 949.2, p. 76. ISSN: 1538-4357. DOI: 10.3847/1538-4357/ac74bb. URL: http://dx.doi.org/10.3847/1538-4357/ac74bb.

Abbott, B. P. et al. (Sept. 2020). "Prospects for observing and localizing gravitational-wave transients with Advanced LIGO, Advanced Virgo and KAGRA". In: *Living Reviews in Relativity* 23.1. ISSN: 1433-8351. DOI: 10.1007/s41114-020-00026-9. URL: http://dx.doi.org/10.1007/s41114-020-00026-9.

Abbott, B.P. et al. (Mar. 2016). "GW150914: The Advanced LIGO Detectors in the Era of First Discoveries". In: *Physical Review Letters* 116.13. ISSN: 1079-7114. DOI: 10.1103/physrevlett.116.131103. URL: http://dx.doi.org/10.1103/PhysRevLett.116.131103.

Abbott B. P., LIGO Scientific Collaboration et al. (Oct. 2017). "Gravitational Waves and Gamma-Rays from a Binary Neutron Star Merger: GW170817 and GRB 170817A". In:

The Astrophysical Journal Letters 848.2, p. L13. DOI: 10.3847/2041-8213/aa920c. URL: https://dx.doi.org/10.3847/2041-8213/aa920c.

Abbott, R. et al. (Dec. 2023). "GWTC-3: Compact Binary Coalescences Observed by LIGO and Virgo during the Second Part of the Third Observing Run". In: *Phys. Rev. X* 13 (4), p. 041039. DOI: 10.1103/PhysRevX.13.041039. URL: https://link.aps.org/doi/10.1103/PhysRevX.13.041039.

Abdalla, Elcio et al. (June 2022). "Cosmology intertwined: A review of the particle physics, astrophysics, and cosmology associated with the cosmological tensions and anomalies". In: *Journal of High Energy Astrophysics* 34, pp. 49–211. DOI: 10.1016/j.jheap.2022.04.002. arXiv: 2203.06142 [astro-ph.CO].

Adams, Matthew R., Neil J. Cornish, and Tyson B. Littenberg (Dec. 2012). "Astrophysical model selection in gravitational wave astronomy". In: *Physical Review D* 86.12. ISSN: 1550-2368. DOI: 10.1103/physrevd.86.124032. URL: http://dx.doi.org/10.1103/PhysRevD.86.124032.

Aghanim, N. et al. (Sept. 2020). "Planck2018 results: VI. Cosmological parameters". In: *Astronomy & amp; Astrophysics* 641, A6. ISSN: 1432-0746. DOI: 10.1051/0004-6361/201833910. URL: http://dx.doi.org/10.1051/0004-6361/201833910.

Amarasinghe, Asanka et al. (Apr. 2022). "Boundary conditions and proof of the scalar, vector, tensor decomposition theorem in cosmological perturbation theory". In: APS Meeting Abstracts 2022, T15.005, T15.005.

Artale, M. Celeste et al. (Jan. 2020). "Mass and star formation rate of the host galaxies of compact binary mergers across cosmic time". In: *Monthly Notices of the Royal Astronomical Society* 491.3, pp. 3419–3434. DOI: 10.1093/mnras/stz3190. arXiv: 1910.04890 [astro-ph.GA].

Belgacem, Enis et al. (May 2018a). "Gravitational-wave luminosity distance in modified gravity theories". In: *Phys. Rev. D* 97 (10), p. 104066. DOI: 10.1103/PhysRevD.97.104066. URL: https://link.aps.org/doi/10.1103/PhysRevD.97.104066.

— (May 2018b). "Gravitational-wave luminosity distance in modified gravity theories". In: *Phys. Rev. D* 97 (10), p. 104066. DOI: 10.1103/PhysRevD.97.104066. URL: https://link.aps.org/doi/10.1103/PhysRevD.97.104066.

Bera, Sayantani et al. (Oct. 2020). "Incompleteness Matters Not: Inference of H0 from Binary Black Hole–Galaxy Cross-correlations". In: *The Astrophysical Journal* 902.1, p. 79. ISSN: 1538-4357. DOI: 10.3847/1538-4357/abb4e0. URL: http://dx.doi.org/10.3847/1538-4357/abb4e0.

Borghi, Nicola et al. (Mar. 2024). "Cosmology and Astrophysics with Standard Sirens and Galaxy Catalogs in View of Future Gravitational Wave Observations". In: *The Astrophysical Journal* 964.2, p. 191. ISSN: 1538-4357. DOI: 10.3847/1538-4357/ad20eb. URL: http://dx.doi.org/10.3847/1538-4357/ad20eb.

Brandenburg, Axel et al. (June 2021). "The scalar, vector, and tensor modes in gravitational wave turbulence simulations". In: *Classical and Quantum Gravity* 38.14, p. 145002. ISSN: 1361-6382. DOI: 10.1088/1361-6382/ac011c. URL: http://dx.doi.org/10.1088/1361-6382/ac011c.

Cahillane, Craig and Georgia Mansell (Feb. 2022). "Review of the Advanced LIGO Gravitational Wave Observatories Leading to Observing Run Four". In: *Galaxies* 10.1, p. 36. ISSN: 2075-4434. DOI: 10.3390/galaxies10010036. URL: http://dx.doi.org/10.3390/galaxies10010036.

Chen, Hsin-Yu, Maya Fishbach, and Daniel E. Holz (Oct. 2018). "A two per cent Hubble constant measurement from standard sirens within five years". In: *Nature* 562.7728, pp. 545–547. ISSN: 1476-4687. DOI: 10.1038/s41586-018-0606-0. URL: http://dx.doi.org/10.1038/s41586-018-0606-0.

Chernoff, David F. and Lee S. Finn (July 1993). "Gravitational radiation, inspiraling binaries, and cosmology". In: *The Astrophysical Journal* 411, p. L5. ISSN: 1538-4357. DOI: 10.1086/186898. URL: http://dx.doi.org/10.1086/186898.

Coles, P.P. and P.F. Lucchin (2003). *Cosmology: The Origin and Evolution of Cosmic Structure*. Wiley. ISBN: 9780470852996. URL: https://books.google.it/books?id=BGYcivB1EtMC.

Collaboration, DESI et al. (2016). *The DESI Experiment Part I: Science,Targeting, and Survey Design*. arXiv: 1611.00036 [astro-ph.IM]. URL: https://arxiv.org/abs/1611.00036.

Dalal, Neal et al. (Sept. 2006). "Short GRB and binary black hole standard sirens as a probe of dark energy". In: *Phys. Rev. D* 74 (6), p. 063006. DOI: 10.1103/PhysRevD.74.063006. URL: https://link.aps.org/doi/10.1103/PhysRevD.74.063006.

Deffayet, Cédric and Kristen Menou (Oct. 2007). "Probing Gravity with Spacetime Sirens". In: *The Astrophysical Journal* 668.2, p. L143. DOI: 10.1086/522931. URL: https://dx.doi.org/10.1086/522931.

Del Pozzo, Walter (Aug. 2012). "Inference of cosmological parameters from gravitational waves: Applications to second generation interferometers". In: *Phys. Rev. D* 86 (4), p. 043011. DOI: 10.1103/PhysRevD.86.043011. URL: https://link.aps.org/doi/10.1103/PhysRevD.86.043011.

Desprez, G. et al. (Nov. 2020). "Euclidpreparation: X. TheEuclidphotometric-redshift challenge". In: *Astronomy & Astrophysics* 644, A31. ISSN: 1432-0746. DOI: 10.1051/0004-6361/202039403. URL: http://dx.doi.org/10.1051/0004-6361/202039403.

Dodelson, S. and F. Schmidt (2020). *Modern Cosmology*. Elsevier Science. ISBN: 9780128159484. URL: https://books.google.it/books?id=GGjfywEACAAJ.

Dvali, Gia, Gregory Gabadadze, and Massimo Porrati (2000). "4D gravity on a brane in 5D Minkowski space". In: *Physics Letters B* 485.1, pp. 208–214. ISSN: 0370-2693. DOI: https://doi.org/10.1016/S0370-2693(00)00669-9. URL: https://www.sciencedirect.com/science/article/pii/S0370269300006699.

Ezquiaga, Jose María and Daniel E. Holz (Aug. 2022). "Spectral Sirens: Cosmology from the Full Mass Distribution of Compact Binaries". In: *Physical Review Letters* 129.6. ISSN: 1079-7114. DOI: 10.1103/physrevlett.129.061102. URL: http://dx.doi.org/10.1103/PhysRevLett.129.061102.

Farr, Will M. et al. (Oct. 2019). "A Future Percent-level Measurement of the Hubble Expansion at Redshift 0.8 with Advanced LIGO". In: *The Astrophysical Journal Letters* 883.2, p. L42. ISSN: 2041-8213. DOI: 10.3847/2041-8213/ab4284. URL: http://dx.doi.org/10.3847/2041-8213/ab4284.

Finke, Andreas et al. (Aug. 2021). "Cosmology with LIGO/Virgo dark sirens: Hubble parameter and modified gravitational wave propagation". In: *Journal of Cosmology and Astroparticle Physics* 2021.08, p. 026. ISSN: 1475-7516. DOI: 10.1088/1475-7516/2021/08/026. URL: http://dx.doi.org/10.1088/1475-7516/2021/08/026.

Fishbach, M. et al. (Jan. 2019). "A Standard Siren Measurement of the Hubble Constant from GW170817 without the Electromagnetic Counterpart". In: *The Astrophysical Journal Letters* 871.1, p. L13. ISSN: 2041-8213. DOI: 10.3847/2041-8213/aaf96e. URL: http://dx.doi.org/10.3847/2041-8213/aaf96e.

Foreman-Mackey, Daniel et al. (Mar. 2013). "emcee: The MCMC Hammer". In: *pasp* 125.925, p. 306. DOI: 10.1086/670067. arXiv: 1202.3665 [astro-ph.IM].

Gair, Jonathan R. et al. (June 2023). "The Hitchhiker's Guide to the Galaxy Catalog Approach for Dark Siren Gravitational-wave Cosmology". In: *The Astronomical Journal* 166.1, p. 22. DOI: 10.3847/1538-3881/acca78. URL: https://dx.doi.org/10.3847/1538-3881/acca78.

Goldstein, A. et al. (Oct. 2017). "An Ordinary Short Gamma-Ray Burst with Extraordinary Implications: Fermi-GBM Detection of GRB 170817A". In: *The Astrophysical Journal Letters* 848.2, p. L14. DOI: 10.3847/2041-8213/aa8f41. URL: https://dx.doi.org/10.3847/2041-8213/aa8f41.

Gray, Rachel et al. (2023). *Joint cosmological and gravitational-wave population inference using dark sirens and galaxy catalogues.* arXiv: 2308.02281 [astro-ph.CO]. URL: https://arxiv.org/abs/2308.02281.

Hobson, M.P., G.P. Efstathiou, and A.N. Lasenby (2006). *General Relativity: An Introduction for Physicists.* General Relativity: An Introduction for Physicists. Cambridge University Press. ISBN: 9780521829519. URL: https://books.google.it/books?id=5dryXCWR7EIC.

Holz, Daniel E. and Scott A. Hughes (Aug. 2005). "Using Gravitational-Wave Standard Sirens". In: *The Astrophysical Journal* 629.1, pp. 15–22. ISSN: 1538-4357. DOI: 10.1086/431341. URL: http://dx.doi.org/10.1086/431341.

Husa, Sascha et al. (Feb. 2016). "Frequency-domain gravitational waves from nonprecessing black-hole binaries. I. New numerical waveforms and anatomy of the signal". In: *Physical*

Review D 93.4, 044006, p. 044006. DOI: 10.1103/PhysRevD.93.044006. arXiv: 1508.07250 [gr-qc].

Iacovelli, Francesco et al. (Dec. 2022a). "Forecasting the Detection Capabilities of Third-generation Gravitational-wave Detectors Using GWFAST". In: *The Astrophysical Journal* 941.2, p. 208. DOI: 10.3847/1538-4357/ac9cd4. URL: https://dx.doi.org/10.3847/1538-4357/ac9cd4.

— (Oct. 2022b). "GWFAST: A Fisher Information Matrix Python Code for Third-generation Gravitational-wave Detectors". In: *The Astrophysical Journal Supplement Series* 263.1, p. 2. DOI: 10.3847/1538-4365/ac9129. URL: https://dx.doi.org/10.3847/1538-4365/ac9129.

Khan, Sebastian et al. (Feb. 2016). "Frequency-domain gravitational waves from nonprecessing black-hole binaries. II. A phenomenological model for the advanced detector era". In: *Physical Review D* 93.4, 044007, p. 044007. DOI: 10.1103/PhysRevD.93.044007. arXiv: 1508.07253 [gr-qc].

Kiendrebeogo, R. Weizmann et al. (Nov. 2023). "Updated Observing Scenarios and Multimessenger Implications for the International Gravitational-wave Networks O4 and O5". In: *The Astrophysical Journal* 958.2, p. 158. ISSN: 1538-4357. DOI: 10.3847/1538-4357/acfcb1. URL: http://dx.doi.org/10.3847/1538-4357/acfcb1.

Leyde, Konstantin et al. (2022). *Current and future constraints on cosmology and modified gravitational wave friction from binary black holes*. arXiv: 2203.11680 [gr-qc].

Lombriser, Lucas and Andy Taylor (Mar. 2016). "Breaking a dark degeneracy with gravitational waves". In: *Journal of Cosmology and Astroparticle Physics* 2016.03, p. 031. DOI: 10.1088/1475-7516/2016/03/031. URL: https://dx.doi.org/10.1088/1475-7516/2016/03/031.

MacLeod, Chelsea L. and Craig J. Hogan (Feb. 2008). "Precision of Hubble constant derived using black hole binary absolute distances and statistical redshift information". In: *Phys. Rev. D* 77 (4), p. 043512. DOI: 10.1103/PhysRevD.77.043512. URL: https://link.aps.org/doi/10.1103/PhysRevD.77.043512.

Madau, Piero and Mark Dickinson (Aug. 2014). "Cosmic Star-Formation History". In: *Annual Review of Astronomy and Astrophysics* 52.1, pp. 415–486. ISSN: 1545-4282. DOI: 10.1146/annurev-astro-081811-125615. URL: http://dx.doi.org/10.1146/annurev-astro-081811-125615.

Maggiore, M. (2008). *Gravitational Waves: Volume 1: Theory and Experiments*. Gravitational Waves. OUP Oxford. ISBN: 9780198570745. URL: https://books.google.it/books?id=mk-1DAAAQBAJ.

Mancarella, Michele, Andreas Finke, et al. (2022). *Cosmology and modified gravity with dark sirens from GWTC-3*. arXiv: 2203.09238 [gr-qc]. URL: https://arxiv.org/abs/2203.09238.

Mancarella, Michele, Edwin Genoud-Prachex, and Michele Maggiore (Mar. 2022). "Cosmology and modified gravitational wave propagation from binary black hole population models". In: *Physical Review D* 105.6. ISSN: 2470-0029. DOI: 10.1103/physrevd.105.064030. URL: http://dx.doi.org/10.1103/PhysRevD.105.064030.

Mandel, Ilya, Will M Farr, and Jonathan R Gair (Mar. 2019). "Extracting distribution parameters from multiple uncertain observations with selection biases". In: *Monthly Notices of the Royal Astronomical Society* 486.1, pp. 1086–1093. ISSN: 1365-2966. DOI: 10.1093/mnras/stz896. URL: http://dx.doi.org/10.1093/mnras/stz896.

Mastrogiovanni, S. et al. (Sept. 2021). "On the importance of source population models for gravitational-wave cosmology". In: *Physical Review D* 104.6. ISSN: 2470-0029. DOI: 10.1103/physrevd.104.062009. URL: http://dx.doi.org/10.1103/PhysRevD.104.062009.

Mastrogiovanni, Simone et al. (2023). *ICAROGW: A python package for inference of astrophysical population properties of noisy, heterogeneous and incomplete observations*. arXiv: 2305.17973 [astro-ph.CO]. URL: https://arxiv.org/abs/2305.17973.

Moresco, Michele et al. (Dec. 2022). "Unveiling the Universe with emerging cosmological probes". In: *Living Reviews in Relativity* 25.1. ISSN: 1433-8351. DOI: 10.1007/s41114-022-00040-z. URL: http://dx.doi.org/10.1007/s41114-022-00040-z.

Mortlock, Daniel J. et al. (Nov. 2019). "Unbiased Hubble constant estimation from binary neutron star mergers". In: *Physical Review D* 100.10. ISSN: 2470-0029. DOI: 10.1103/physrevd.100.103523. URL: http://dx.doi.org/10.1103/PhysRevD.100.103523.

Mukherjee, Suvodip and Benjamin D. Wandelt (2018). *Beyond the classical distance-redshift test: cross-correlating redshift-free standard candles and sirens with redshift surveys*. arXiv: 1808.06615 [astro-ph.CO]. URL: https://arxiv.org/abs/1808.06615.

Mukherjee, Suvodip, Benjamin D. Wandelt, et al. (Feb. 2021). "Accurate precision cosmology with redshift unknown gravitational wave sources". In: *Phys. Rev. D* 103 (4), p. 043520. DOI: 10.1103/PhysRevD.103.043520. URL: https://link.aps.org/doi/10.1103/PhysRevD.103.043520.

Oguri, Masamune (Apr. 2016). "Measuring the distance-redshift relation with the cross-correlation of gravitational wave standard sirens and galaxies". In: *Physical Review D* 93.8. ISSN: 2470-0029. DOI: 10.1103/physrevd.93.083511. URL: http://dx.doi.org/10.1103/PhysRevD.93.083511.

Palmese, A. et al. (Sept. 2020). "A Statistical Standard Siren Measurement of the Hubble Constant from the LIGO/Virgo Gravitational Wave Compact Object Merger GW190814 and Dark Energy Survey Galaxies". In: *The Astrophysical Journal Letters* 900.2, p. L33. ISSN: 2041-8213. DOI: 10.3847/2041-8213/abaeff. URL: http://dx.doi.org/10.3847/2041-8213/abaeff.

Peebles, P. J. E. and Bharat Ratra (Apr. 2003). "The cosmological constant and dark energy". In: *Rev. Mod. Phys.* 75 (2), pp. 559–606. DOI: 10.1103/RevModPhys.75.559. URL: https://link.aps.org/doi/10.1103/RevModPhys.75.559.

Perlmutter, S. et al. (June 1999). "Measurements of Ω and Λ from 42 High-Redshift Supernovae". In: *The Astrophysical Journal* 517.2, pp. 565–586. ISSN: 1538-4357. DOI: 10.1086/307221. URL: http://dx.doi.org/10.1086/307221.

Riess, Adam G., Stefano Casertano, et al. (May 2019). "Large Magellanic Cloud Cepheid Standards Provide a 1% Foundation for the Determination of the Hubble Constant and Stronger Evidence for Physics beyond ΛCDM". In: *The Astrophysical Journal* 876.1, p. 85. ISSN: 1538-4357. DOI: 10.3847/1538-4357/ab1422. URL: http://dx.doi.org/10.3847/1538-4357/ab1422.

Riess, Adam G., Alexei V. Filippenko, et al. (Sept. 1998). "Observational Evidence from Supernovae for an Accelerating Universe and a Cosmological Constant". In: *The Astronomical Journal* 116.3, pp. 1009–1038. ISSN: 0004-6256. DOI: 10.1086/300499. URL: http://dx.doi.org/10.1086/300499.

Sahni, Varun (Dec. 2004). "5 Dark Matter and Dark Energy". In: *The Physics of the Early Universe.* Springer Berlin Heidelberg, pp. 141–179. ISBN: 9783540315353. DOI: 10.1007/978-3-540-31535-3_5. URL: http://dx.doi.org/10.1007/978-3-540-31535-3_5.

Saltas, Ippocratis D. et al. (Nov. 2014). "Anisotropic Stress as a Signature of Nonstandard Propagation of Gravitational Waves". In: *Physical Review Letters* 113.19. ISSN: 1079-7114. DOI: 10.1103/physrevlett.113.191101. URL: http://dx.doi.org/10.1103/PhysRevLett.113.191101.

Savchenko, V. et al. (Oct. 2017). "INTEGRAL Detection of the First Prompt Gamma-Ray Signal Coincident with the Gravitational-wave Event GW170817". In: *The Astrophysical Journal Letters* 848.2, p. L15. DOI: 10.3847/2041-8213/aa8f94. URL: https://dx.doi.org/10.3847/2041-8213/aa8f94.

Schirmer, M. et al. (June 2022). "Euclidpreparation: XVIII. The NISP photometric system". In: *Astronomy & Astrophysics* 662, A92. ISSN: 1432-0746. DOI: 10.1051/0004-6361/202142897. URL: http://dx.doi.org/10.1051/0004-6361/202142897.

Schutz, B. F. (Sept. 1986). "Determining the Hubble constant from gravitational wave observations". In: *Nature* 323.6086, pp. 310–311. DOI: 10.1038/323310a0.

Talbot, Colm and Eric Thrane (Apr. 2018). "Measuring the Binary Black Hole Mass Spectrum with an Astrophysically Motivated Parameterization". In: *The Astrophysical Journal* 856.2, p. 173. ISSN: 1538-4357. DOI: 10.3847/1538-4357/aab34c. URL: http://dx.doi.org/10.3847/1538-4357/aab34c.

Taylor, Stephen R. and Jonathan R. Gair (July 2012). "Cosmology with the lights off: Standard sirens in the Einstein Telescope era". In: *Physical Review D* 86.2. ISSN: 1550-2368. DOI: 10.1103/physrevd.86.023502. URL: http://dx.doi.org/10.1103/PhysRevD.86.023502.

Thrane, Eric and Colm Talbot (2019). “An introduction to Bayesian inference in gravitational-wave astronomy: Parameter estimation, model selection, and hierarchical models”. In: *Publications of the Astronomical Society of Australia* 36. ISSN: 1448-6083. DOI: 10.1017/pasa.2019.2. URL: http://dx.doi.org/10.1017/pasa.2019.2.

Tiwari, Vaibhav (June 2018). “Estimation of the sensitive volume for gravitational-wave source populations using weighted Monte Carlo integration”. In: *Classical and Quantum Gravity* 35.14, p. 145009. ISSN: 1361-6382. DOI: 10.1088/1361-6382/aac89d. URL: http://dx.doi.org/10.1088/1361-6382/aac89d.

Vijaykumar, Aditya et al. (Nov. 2023). “Probing the large scale structure using gravitational-wave observations of binary black holes”. In: *Physical Review D* 108.10. ISSN: 2470-0029. DOI: 10.1103/physrevd.108.103017. URL: http://dx.doi.org/10.1103/PhysRevD.108.103017.

Weinberg, S. (1976). *Gravitation and Cosmology: Principles and Applications of the General Theory of Relativity*. John Wiley & Sons. URL: https://books.google.it/books?id=ftoazQEACAAJ.

Wong, Kenneth C et al. (Sept. 2019). “H0LiCOW – XIII. A 2.4 per cent measurement of H0 from lensed quasars: 5.3σ tension between early- and late-Universe probes”. In: *Monthly Notices of the Royal Astronomical Society* 498.1, pp. 1420–1439. ISSN: 1365-2966. DOI: 10.1093/mnras/stz3094. URL: http://dx.doi.org/10.1093/mnras/stz3094.

Yunes, Nicolás, Kent Yagi, and Frans Pretorius (Oct. 2016). “Theoretical physics implications of the binary black-hole mergers GW150914 and GW151226”. In: *Physical Review D* 94.8. ISSN: 2470-0029. DOI: 10.1103/physrevd.94.084002. URL: http://dx.doi.org/10.1103/PhysRevD.94.084002.